Towards Establishing Methods of Synthesis, Purification, and Structural Determination for Human Fibrinogen

By

Nicholas Carter Kirby

May, 2023

Director of Thesis: Dr. Nathan E. Hudson, Dr. Adam R. Offenbacher

Major Department: Chemistry

Abstract

Fibrinogen is a prevalent blood-based glycoprotein. In its polymerizable form, fibrin, it serves as the structural component of blood clots and helps to incorporate red blood cells, macrophages, and fibroblasts to the wound-site. Fibrinogen plays important roles in inflammation and tissue regeneration, regulating growth factor receptor pathway activation, scar formation, and immune response, yet many questions remain about fibrinogen's structure-function link in these various pathophysiological states. Studies focused on improving expression systems for recombinant fibrinogen, and developing more rapid and robust techniques for purifying fibrinogen from complex media would provide a means by which to progress mutational studies of fibrinogen. Similarly, developing methods for high-resolution imaging of fibrinogen in its native, aqueous-based environment is necessary to establish proper structure-function relationships encompassing this complex 340 kDa glycoprotein. The work described in this thesis produced advancements in each of these crucial areas of fibrinogen research. Herein, chapter 2 reports, to our knowledge, the first methodology of transient recombinant human fibrinogen expression using suspension HEK Expi293^{TM} cells. A highly selective and robust affinity-based approach was also developed for the rapid isolation of fibrinogen from a variety of

complex media. Chapter 3 describes cryogenic electron microscopy and our process of obtaining a high-resolution, in-solution structure of human fibrinogen's D region. This structure is currently the highest resolution structure of any fibrinogen domain obtained in the native, solution state and further supports evidence for fibrinogen's intrinsic flexibility, expanding the textbook representations of fibrinogen as a rigid, rod-like structure. Lastly, future directions outlining fibrinogen's role during pregnancy and unique fibrinogen-specific protofibril-like structures are discussed. In an appendix, I have included figures from an illustrated review journal article, which I participated in as a co-first author.

Towards Establishing Methods of Synthesis, Purification, and Structural Determination for Human Fibrinogen

A Thesis

Presented to the Department of Chemistry

East Carolina University

In Partial Fulfillment of the Requirements for the Degree

Master of Science in Chemistry

By

Nicholas Carter Kirby

May, 2023

Director of Thesis: Adam R. Offenbacher, PhD
Thesis Committee Members:
Nathan E. Hudson, PhD
Adam R. Offenbacher, PhD
Robert M. Hughes, PhD

Dedicated to my wife, family, and friends for loving me beyond comprehension

ACKNOWLEDGMENTS

It is with great honor that I acknowledge both Dr. Nathan Hudson, and Dr. Adam Offenbacher for their extraordinary mentorship throughout my time at East Carolina University. Their intellectual brilliance and exceptional ability to inspire have been instrumental in shaping my academic and professional growth, for which I am deeply grateful. Overall, Dr. Hudson and Dr. Offenbacher have been a source of constant inspiration and motivation in my life, and I feel privileged to have had the opportunity to learn from and be mentored by them. Their impact on my life is immeasurable, and I will be forever grateful for their guidance, wisdom, and friendship.

Additionally, I would like to thank my thesis committee and East Carolina University's Department of Chemistry for their help throughout my Master's program.

Outside of my work I would like to thank my wonderful family for their unwavering love, support, and encouragement. Their sacrifices, belief in me, and constant motivation have been the driving force behind my success. To my outstanding wife, I am beyond thankful for your love, patience, and selflessness, which have been my anchor throughout my academic pursuits. Lastly, I extend my gratitude to East Carolina University's rock-climbing club for allowing me to represent the university and providing me with a place to meet lifelong friends.

TABLE OF CONTENTS

LIST OF TABLES

LIST OF FIGURES

LIST OF SYMBOLS OR ABBREVIATIONS

PREFACE

Preface A

Work from Chapter 2 has been published in "Popovic, G.; Kirby, N. C.; Dement, T. C.; Peterson, K. M.; Daub, C. E.; Belcher, H. A.; Guthold, M.; Offenbacher, A. R.; Hudson, N. E., Development of Transient Recombinant Expression and Affinity Chromatography Systems for Human Fibrinogen. *International Journal of Molecular Sciences* **2022,** *23* (3), 1054." of which copyright is retained, and therefore no permission was needed.

Preface B

Work from the appendix has been published in "Risman, R. A.; Kirby, N. C.; Bannish, B. E.; Hudson, N. E.; Tutwiler, V., Fibrinolysis: an illustabletrated review. *Research and Practice in Thrombosis and Haemostasis* **2023,** *7* (2)." of which copyright is retained, and therefore no permission was needed.

Chapter 1

Introduction

1.1 Fibrinogen and Fibrin: A Brief History and Significance

Fibrinogen as it is known today originated in Malpighi's 1666 *De Polypo Cordis*[1], where he vaguely highlights the structure of a "Polyp" (thrombi) and discusses the presence of a "fibrous texture, and a network of nerve-like threads." This was further classified by Antoine Fourcroy in 1788[2, 3],where he conceived the term "fibrin". Finally, Virchow and Denis each independently invented the name "fibrinogen" from their discoveries of a clottable substance in plasma distinct from fibrin[4]. Fibrinogen has since been classified as a soluble 340 kDa multimeric glycoprotein present in human blood plasma at concentrations ranging from 1.5-4.2 g/L[5], and is essential for hemostasis, wound healing, inflammation, angiogenesis, and many other physiological functions.

In response to vascular injury, hemostasis (blood flow termination) culminates in the creation of a platelet-fibrin clot to prevent blood loss, where fibrin serves as a bridge between activated platelets and incorporates red blood cells (RBCs), macrophages, and fibroblasts to the wound-site[5]. Alterations to fibrinogen by fluctuation of its concentration in blood plasma, modifications to its structure, genetic polymorphisms, or spatial variability throughout the body can lead to the onset of disease (Figure 1.1)[6]. Notably, it has been shown that fibrinogen plasma concentration represents a powerful biomarker in assessing risk of cardiovascular disease (CVD), the number one worldwide cause of morbidity and mortality[7]. Qualitative changes to fibrinogen's structure will have downstream effects on fibrin polymerization, and the overall structure and mechanical properties of the formed fibrin scaffold, which can enhance the risk of myocardial infarction, ischemic stroke, or other bleeding disorders[8]. Functionally altered clots are also evident from congenital fibrinogen mutations, such as afibrinogenemia and hypofibrinogenemia which involve

a quantitative absence or lowering of fibrinogen (Type I), or dysfibrinogenemia and hypo-dysfibrinogenemia whereby fibrinogen quality is compromised (Type II) [9].

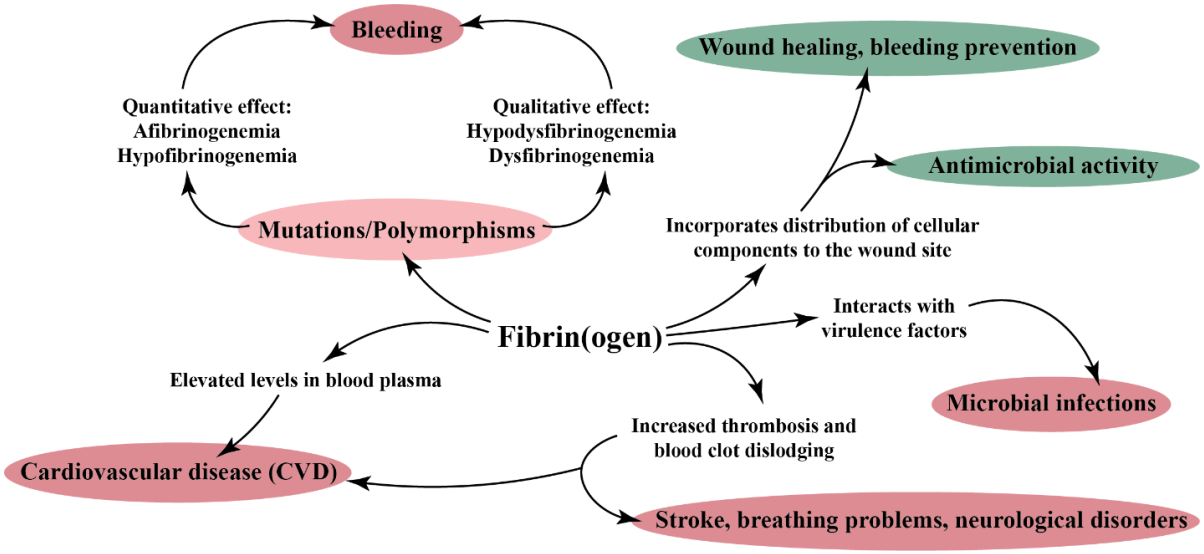

Figure 1.1: Summarization of fibrin(ogen)'s advantageous (green) and disadvantageous (red) roles in various human diseases. Figure adapted and modified from doi:10.3324/haematol.2019.236901[6].

In addition to fibrin(ogen)'s utility as a biomarker for disease, a connection between coagulation and inflammation has been implicated during the early stages of infection[10]. Fibrinogen derived peptides stimulate neutrophil and monocyte movement to the wound site, where fibrinogen can then interact with the integrins and TLR4 of these immune cells to elicit an inflammatory response (Figure 1.1)[10]. A direct link to innate immunity has also been shown through fibrinogen's antimicrobial activity in eliminating bacteria from a host environment before it can adapt[10]. However, it has also been shown that fibrinogen recruitment to microbial surfaces can lead to enhanced bacterial survival[6]. Namely, fibrinogen interacts with virulence factors that aid in bacterial entry into a host while also protecting the microorganisms from pharmaceutical treatments (Figure 1.1). The pro- and anti-contributions of fibrinogen in

pathological settings can be more easily determined with a better understanding of the structural qualities of fibrinogen and the effect modifications have on its function.

Fibrinogen serves as the starting platform for what will become a fibrin fiber. The macroscopic mechanical properties of formed fibers highlight potential biomaterial applications. With similar stretching properties compared to rubber, fibrin fibers can stretch more than three times their natural length before rupturing[11]. However, maintaining proper balance between hemostasis and thrombosis requires fibers to remain strong as well as elastic in order to effectively capture coagulants while avoiding rupture from stretching[12, 13]. Fibers must also contain a degree of permeability to allow for the incorporation of lytic enzymes for the decomposition/lysis of fiber networks. This permeability in conjunction with fiber extensibility affords a mechanistic stability for clots in dynamic environments (epidermal injuries that require stretching during healing, or clot retraction via platelet pulling). Research focused on better understanding fibrinogen's structural characteristics and the effects of its modifications on the function of formed fibers thus has high clinical significance and biomaterial utility for practices of regenerative medicine and the creation of robust medical sealants[14, 15].

1.2 **Fibrin(ogen) Structure: Anatomy of a Complex Protein and its Derivatives**

1.2.1 *Fibrinogen to Fibrin Degradation Products: From Polymerization to Digestion*

Balancing the processes of coagulation (prevention of bleeding) and fibrinolysis (clot dissolution) is imperative for proper wound healing. Coagulation is initiated upon thrombin's cleavage of fibrinopeptides A and B (FpA/FpB)[16], forming insoluble fibrin from its soluble precursor fibrinogen (Figure 1.2A/B). Enzymatic cleavage of both FpA and FpB exposes knobs 'A' and 'B' of the central E region, leading to complementary, "half-staggered" binding to adjacent fibrin monomer holes 'a' and 'b' of the distal D regions to form protofibrils (Figure

1.2C)[17]. Lateral aggregation continues, and these two-stranded protofibrils bundle together with the use of two dynamic αC regions into fibrin fibers that serve as the building blocks to highly integrated three-dimensional fiber networks (Figure 1.2D)[18]. While protofibril formation is initiated by 'A:a' knob-hole intermolecular interactions, 'B:b' knob-hole interactions have been shown to promote lateral aggregation of protofibrils due to the co-release of FpB and the αC region from the central E region upon thrombin's conversion of fibrinogen to fibrin[18, 19]. Thrombin is also responsible for the catalytic activation of FXIII into FXIIIa, a transglutaminase involved in covalently cross-linking fibrin monomers and protofibrils to form γ-γ dimers and α polymers for enhanced clot stability (Figure 1.2C)[20].

The coagulation cascade terminates with the formation of a stable blood clot; hemostasis is achieved, the wound is healed, and the processes of fibrinolysis are then needed to aid in clot dissolution. Protofibril formation initiates the complexation of numerous fibrinolysis activator and inhibitor enzymes with fibrin (the fibrinolytic system), which are used to regulate fiber network breakdown[17]. Although fibrinogen and fibrin share some of these binding partners, some proteins, such as plasminogen and tissue-type plasminogen activator (tPA), solely interact with one or the other. This suggests some important structural differences between the two despite their nearly identical amino acid sequences, and highlights how fibrinogen's and fibrin's structural changes and dynamics affect function. One such difference is the formation of the DDE complex in fibrin (Figure 1.2C), whereby the E region of one fibrin molecule noncovalently binds to the dimeric D-D fragments of adjacent fibrin molecules. It has been suggested that this complexation process involves a conformational change within the D regions of the D-D fragments, exposing known plasminogen and tPA binding sites[21]. Evidence for the conformational change of the β-nodule lies in the exposure of plasminogen's (Aα148-160) and

tPA's (γ312-324) binding sites on fibrin upon its conversion from fibrinogen (Figure 1.2C). The binding event relaxes plasminogen into its open conformation, allowing for plasminogen conversion into plasmin by plasminogen activators. Plasmin-mediated fibrinolysis then results in the sequential creation of fibrin degradation products (FDPs). Initial degradation of the αC region by plasmin cleavage at αK206 and αK230 generates fragment "*X*" (Figure 1.2E)[17]. Lysis continues within the coiled coils between the E and D regions, where cleavage of one side produces either "*Y*" or "*Y'* " fragments and oppositely D region fragments. Further cleavage of the Y fragments yields an isolated E region fragment.

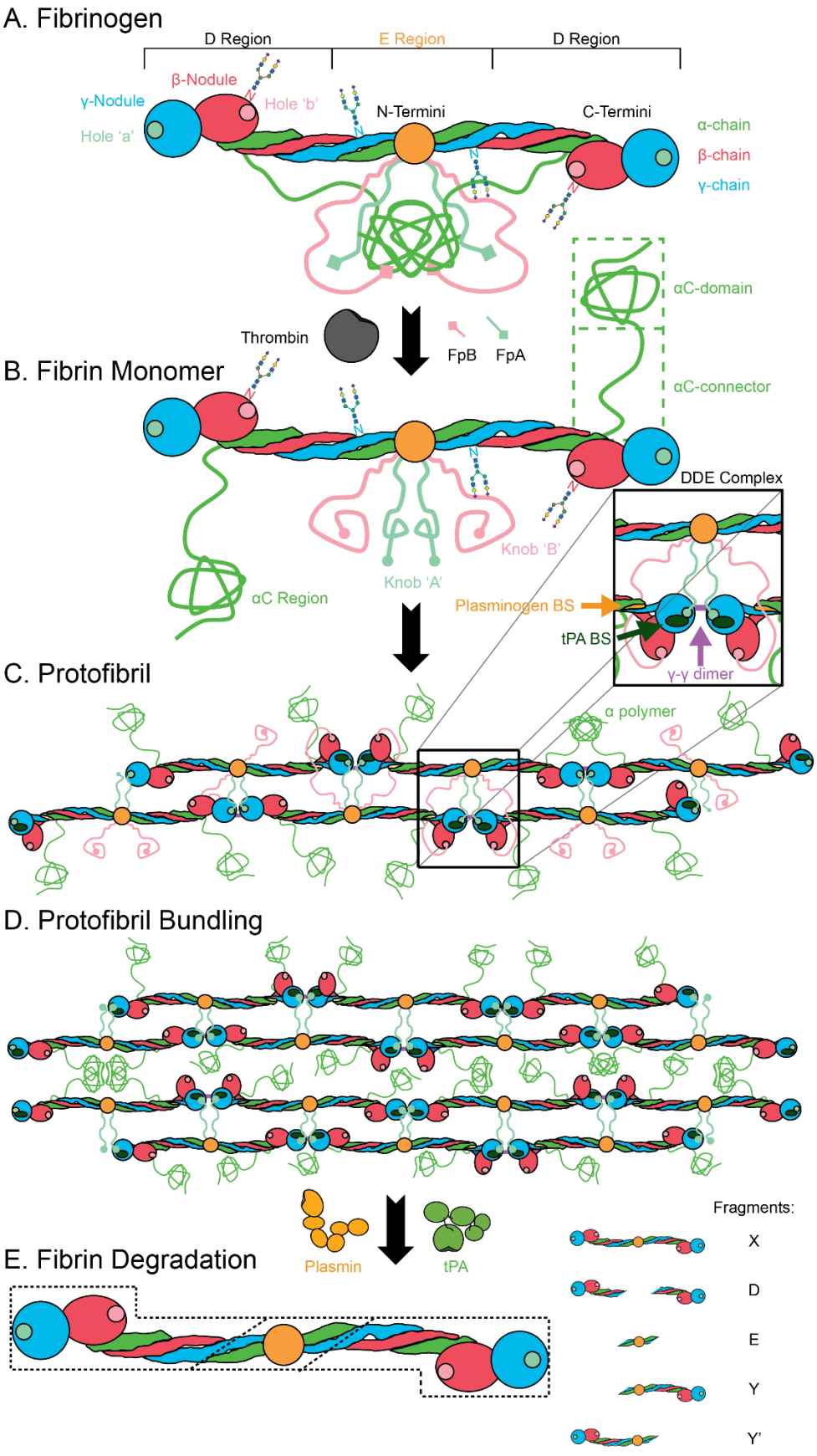
A. Fibrinogen
D Region
E Region
D Region
β-Nodule
γ-Nodule
Hole 'b'
Hole 'a'
N-Termini
C-Termini
α-chain
β-chain
γ-chain
αC-domain
Thrombin
FpB
FpA
B. Fibrin Monomer
αC-connector
DDE Complex
Knob 'B'
Knob 'A'
αC Region
Plasminogen BS
tPA BS
γ-γ dimer
C. Protofibril
α polymer
D. Protofibril Bundling
Plasmin
tPA
E. Fibrin Degradation
Fragments:
X
D
E
Y
Y'

Figure 1.2: Fiber network formation and dissolution. (A) The fibrinogen molecule is divided into three regions: two distal D regions containing C-termini β- and γ-nodules with their respective holes 'b' and 'a', and one central E region containing the N-termini of all six polypeptide chains $(A\alpha B\beta\gamma)_2$. (B) Thrombin cleaves fibrinopeptides A and B (FpA/FpB) to convert insoluble fibrinogen into soluble fibrin, revealing knobs 'A' and 'B', as well as releasing the αC region. (C) Knob:hole interactions lead to half-staggered, lateral aggregation of fibrin monomers into a protofibril after proposed conformational change of the β-nodule upon formation of the DDE complex. Fiber integrity is maintained through α-α polymerization and γ-γ dimerization. (D) Two-stranded protofibrils interact with adjacent protofibrils through α polymers and allow for the preliminary bundling of protofibrils before fibrin fibers are formed. (E) Fibrin degradation begins with the conversion of plasminogen into plasmin from a trimeric complex with tPA and fibrin, to yield fibrin degradation products (FDPs) such as fragments X, D, E, and Y/Y.'

1.2.2 *A More In-Depth Look into Fibrin(ogen)'s Structural Features: Regions and Domains*

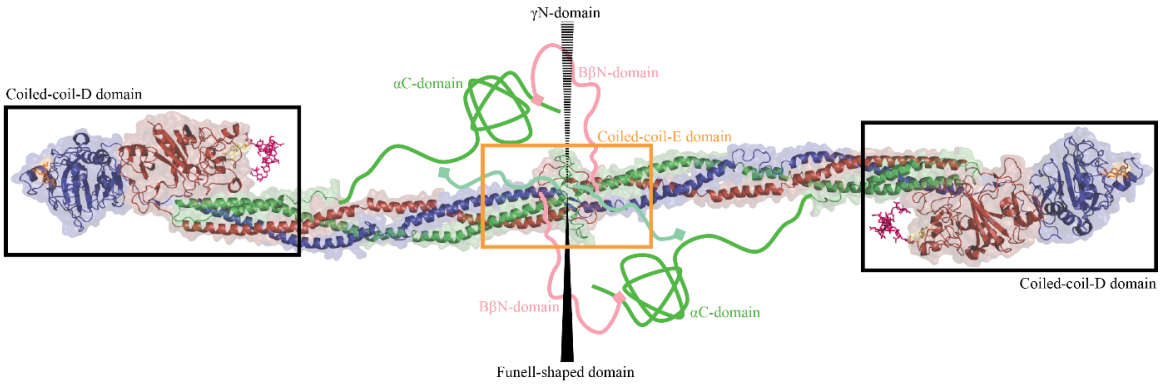

Figure 1.3: Fibrinogen's domains (PDB 3GHG and illustrations for missing structures). Located in the central E region, the N-termini of fibrinogen form a coiled-coil-E domain (orange). From here, the Aα and Bβ N-termini project out of the page (solid wedge) and form a funnel-shaped domain, whereas the γN-termini project into the page (dashed wedge) to form a γN-domain. Also centrally placed in fibrinogen is the αC-domain, which is bound by FpB (green). Upon conversion to fibrin, FpB is released, and a proposed BβN-domain is formed (pink). The ends of fibrinogen are comprised of coiled-coil-D domains (left and right) that are discussed in more detail in Figure 1.4.

Located in a cluster on chromosome 4, the *FGA*, *FGB*, and *FGG* genes are responsible for producing the pair of three nonidentical polypeptide chains $(A\alpha B\beta\gamma)_2$ making up the homodimer, glycoprotein fibrinogen[22]. Held together by 29 disulfide bonds, this protein has 7 distinct regions (one E region, two BβN regions, two D regions, and two αC regions; Figure 1.3) and 21 structural domains (one coiled-coil-E domain, one funnel-shaped domain, one γN-domain, two BβN-domains, two coiled-coil-D domains, two αC-domains, and four A-,B-, and P-domains; Figure 1.4)[16]. All six polypeptide chains coalesce with their N-termini located in the central E region and are connected by 5 disulfide bonds. Within the E region the γ chains (residues 1-20)

join into one asymmetric domain (γN-domain; Figure 1.3), while the Aα (residues 35-49) and Bβ chains (64-84) form their own domain on the opposing side (funnel shaped domain; Figure 1.3) and are thought to contain most of the binding sites for thrombin (AαW33, F35, D38, and E39; BβA68, and N69)[23,24]. Thrombin binding initiates cleavage of FpAs (residues 1-16) at the AαR16-G17 bond, exposing knobs 'A' with the known αG17-P18-R19 (GPR) motif[5]. Each Bβ chain protrudes from the central E domain into separate regions (BβN regions) composed of their own domains (BβN-domains; Figure 1.3). The N-terminal ends of the BβN regions contain the FpBs (residues 1-14) which are cleaved at the BβR14-G15 bond, exposing knobs 'B' with the known βG15-H16-R17 (GHR) motif. Extending outwards from each side of the central nodule, the α-helical portions of the three chains form a coiled-coil structure (coiled-coil-E domain; Figure 1.3). The C-terminal portions of the molecule then expand outwards into the coiled-coil-D domains (Figure 1.3) where the beginnings of the highly dynamic αC regions (Aα221-610) reverse direction around AαSer166 to form a fourth α-helical strand prior to fibrin conversion. From here, a flexible unstructured tether (αC-connector; Aα221–391) connects to a globular domain (αC-domain; Aα392-610) by which clot structure and stability are significantly influenced[18].

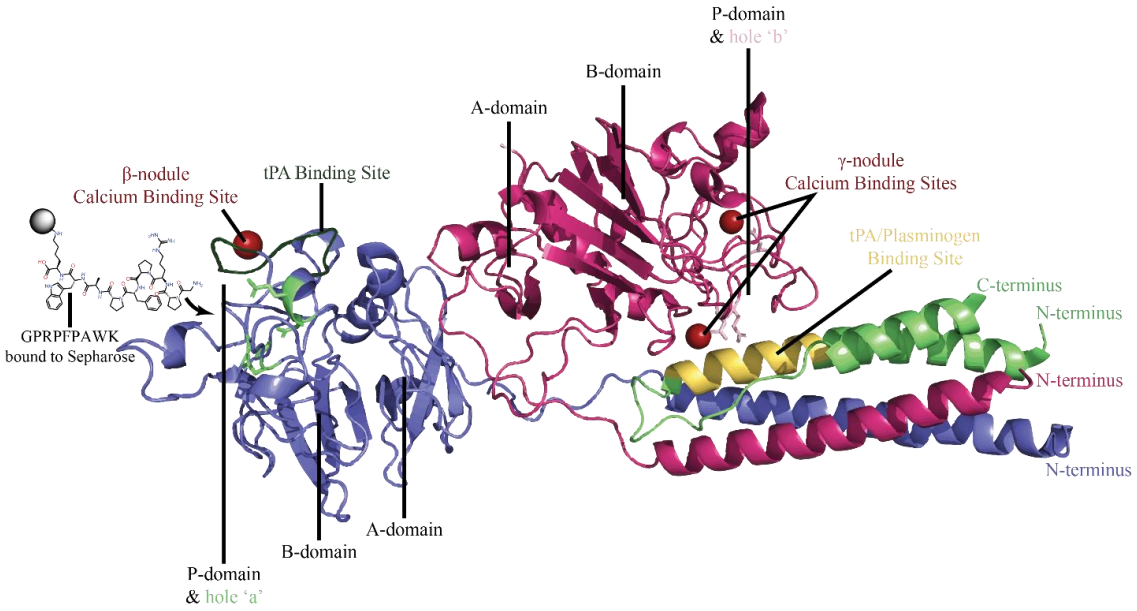

Figure 1.4: Fibrinogen's D region (PDB 1LT9). The D region is made up of three polypeptide chains: Aα (light green), Bβ (pink), and γ (blue). The Aα chain C-terminal segment approaches the Bβ and γ chain C-terminal nodules before folding back over to make up a fourth helical segment of the coiled-coil region, and also contains a known tPA/plasminogen binding site for fibrin (Aα148-160; yellow). The Bβ- and γ-nodules each contain a polymerization pocket, termed hole 'b' (residues BβE397, BβD398, and BβD432) and hole 'a' (residues γD364,γD330, γQ329, and γH340), respectively. The γ-nodule contains a known tPA-specific binding site (γ312-324; dark green) very close to a known calcium (red spheres) binding region. Next to hole 'a' is a knob 'A'-mimic with enhanced affinity for the polymerization pocket that was designed for capture of fibrinogen from complex media (to be discussed in further detail in Chapter 2).

At the opposing end of the coiled-coil-D domain, the Bβ and γ chains form the β- and γ-nodules, respectively. Each of the homologous Bβ- and γ-chain C-terminal nodules are made up of a N- and C-terminal subdomain (A and P domains, respectively; Figure 1.4), as well as a 5-stranded antiparallel β-sheet central domain (B domain; Figure 1.4)[25]. Each C-terminal subdomain contains a ligand-binding cavity composed of three extended loops shown to bind

calcium, with the γ chain binding cavity showing more electronegativity than its Bβ chain homolog. Research conducted by the Lord lab has even proposed that these calcium binding sites might act as potential anchors for the β-nodule to the coiled coil region, preventing their initial conformational change to interact with an adjacent knob 'b'[26]. On the opposing side of the γ-nodule's calcium binding site are known residues involved in γ-γ crosslinking by FXIIIa (γGln397 on one molecule and γLys406 on the linking partner), where two molecules are connected end-to-end (longitudinally) as opposed to side-by-side (transversely)[25].

1.2.3 *Exploring the Unknown: Insights into Fibrinogen's in-Solution Structure*

Fibrinogen structural determination has an extensive history involving a variety of methods. The initial trinodular structure of fibrinogen first confirmed by electron microscopy (EM)[27] has been greatly enhanced, from individual x-ray crystallographic refinement of a C-terminal γ chain fragment[28] to the whole fibrinogen Fragment X equivalent (PDB 3GHG; missing αC region)[29]. These crystallographic structures have provided a static perspective of fibrinogen, whereby a longitudinally straight E region and slightly bent coiled-coil connector between E and D regions produces an overall planar-sigmoidal shape. However, a variety of techniques and sample preparations have highlighted fibrinogen's ability to adopt different conformations and show a higher degree of intrinsic flexibility[30, 31]. Though such atomic-force microscopy (AFM) and EM methods indicate flexing of fibrinogen about the E region, both rely on protein adsorption to a surface which potentially introduces biases towards the observed structures. To mitigate the impact of such methods, solution-based techniques have been utilized to explore the native conformation(s) of soluble fibrinogen. One study looking into the hydrodynamic character of fibrinogen at a range of concentrations (0.3-60 mg/mL) and temperatures (5-42°C) found that the in-solution structure favored sigmoidal and bent conformations over the rod-shaped straight

static structure[32]. This is further suggested by molecular dynamics (MD) simulations that indicate extraordinary flexibility of fibrinogen's coiled-coil connector[33]. Our lab has since utilized temperature-dependent hydrogen deuterium exchange mass spectrometry (TD-HDXMS) and negative stain EM studies for the assessment of human fibrinogen's "*conformational dynamism*" in solution (Figure 1.5). Representative TD-HDXMS traces of the exchange properties for fibrinogen-derived peptides allowed for classification into three categories (Figure 1.5A). The three classes were then displayed onto a fibrinogen model (Figure 1.5B), which highlights the temperature-dependent exchange properties across fibrinogen's structure. These experiments and corroborating negative stain EM classifications collectively supported a more conformationally heterogenic in-solution fibrinogen structure with the central regions of the coiled-coils as well as the homodimeric interface of the E region displaying high flexibility or bending (Figure 1.5C). Flexion along fibrinogen's structure has similarly been allocated to multiple "flexible hinge sites" thought to elicit fibrin gel compressibility and extensibility[29]. These include the nonhelical components of the otherwise stiff α-helices of the coiled-coil regions, the connecting region between coiled coils and β-nodules for exposure of plasminogen/tPA binding sites (Aα148-160) following predicted conformational changes from fibrinogen to fibrin, and the interface between β- and γ-nodules for similar uncovering of tissue-type plasminogen activator (tPA)-specific binding sites (γ312-324)[34]. Of the disordered regions of fibrinogen, the most notable is the intrinsically disordered C-terminal segment of the Aα chain that shows considerable mobility due to the αC-connector linking its globular αC-domain to fibrinogen's main structure[18]. Additionally, the C-termini regions of the Bβ (residues 459-461) and γ chains (residues 394-411), as well as the N-termini of all three chains (residues 1-26, 1-57,

and 1-13 of the Aα, Bβ, and γ chains, respectively) display a level of disorder likely causing them to remain undetermined crystallographically[5].

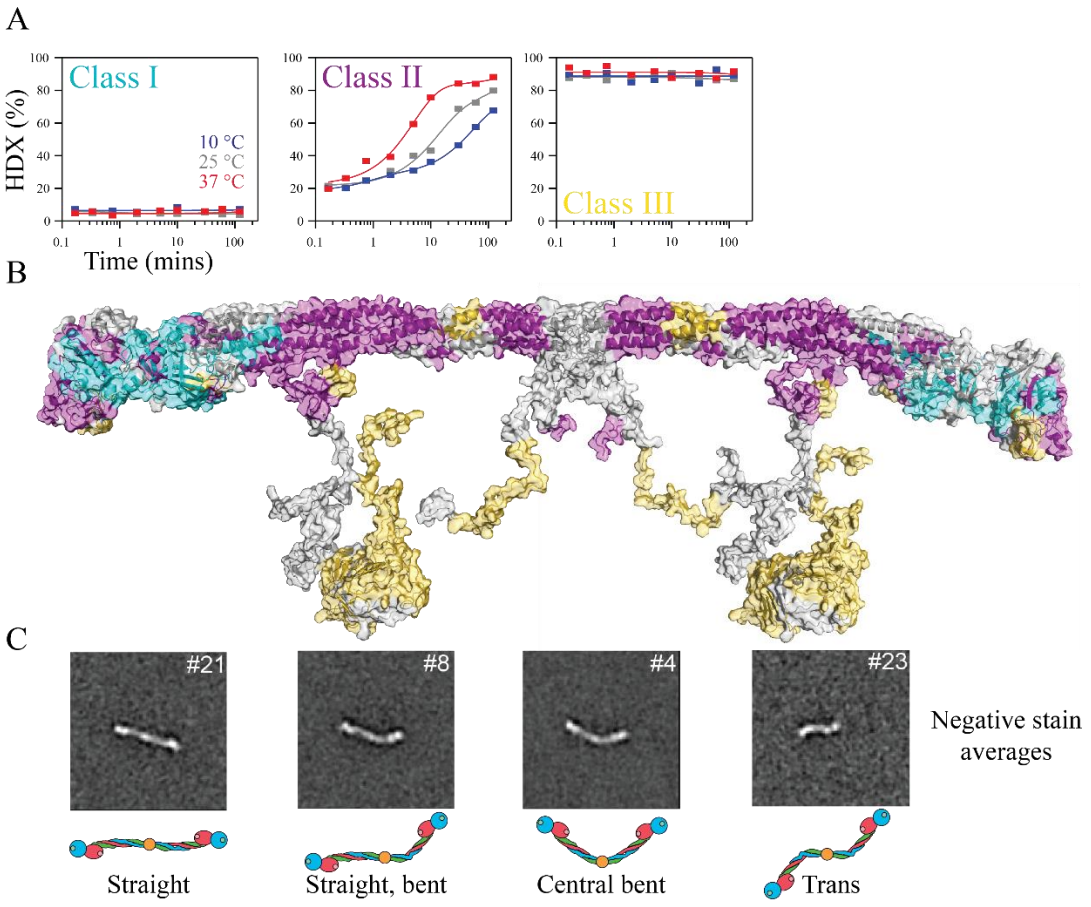

Figure 1.5: Insights into fibrinogen's in-solution structure. (A) TD-HDXMS traces highlight the correlation of exchange properties for fibrinogen-derived peptides at three temperatures (10°C=blue; 25°C=grey; 37°C=red) into three classes: low, temperature-independent exchange (Class I), moderate, temperature-dependent exchange (Class II), and moderate-to-elevated, temperature-independent exchange (Class III). (B) Structural mapping of all three classes onto the whole fibrinogen molecule (uncovered regions in grey). (C) Negative stain electron micrograph averages of fibrinogen conformations into four major classes: straight, straight-bent, central bent, and trans.

While there is evidence emerging to indicate flexibility for fibrinogen, the view is overall of a lower spatial resolution with limited high-resolution information. One such high resolution structural determination method for multiple conformation/flexible proteins is cryogenic electron microscopy (cryo-EM). Cryo-EM imaging has obvious advantages over conventional structural methods (NMR and x-ray crystallography): less sample consumption, more biological relevance from natural state imaging in solution, and no requirement of crystallization (lower risk of sample degradation and bias towards certain conformations due to crystal contacts)[35, 36]. This high-resolution structure resolving method greatly complements our less spatially resolved methods of TD-HDXMS and negative stain EM mentioned above, and will aid in uncovering the conformational dynamism of fibrinogen's in-solution structure.

1.2.4 *Structural and Functional Implications of Fibrinogen's N-linked Glycosylations*

In addition to its primary protein scaffold, fibrinogen in healthy patients contains four N-linked glycosylation sites (2 at BβN364 and 2 at γN52), that are occupied by biantennary, 11 sugar residue carbohydrates[29]. There are several other predicted O-linked glycosylation sites in fibrinogen, but the occupancy of the glycosylation at these sites is substoichiometric (1-13% glycosylation for O-linked sites)[37]. Appended to the ends of the N-linked carbohydrates are sialic acid residues, with an average of 6 mol of sialic acid per mole of fibrinogen[38]. Altering the content or presence/absence of fibrinogen's glycans can have downstream effects on clot formation/dissolution. For example, in *in vitro* isolated fibrinogen studies, the complete removal of the N-linked glycans (i.e., deglycosylation) by use of PNGaseF to convert Asn into Asp and causes the acceleration of fibrin polymerization along with the formation of thicker, more porous fiber networks from increased lateral aggregation upon treatment with thrombin[39]. Oppositely, polymerization is delayed for patients suffering from hepatoma-associated dysfibrinogenemia, a

condition characterized by abnormal fibrinogen by way of increased carbohydrate content[40]. Decreases in the sialic acid content of fibrinogen, such as with asialofibrinogen (sialic acid deficient fibrinogen), displays a similar marked decrease in polymerization rates with thicker fiber formation. A noticeable decrease in the sialic acid content of adult fibrinogen has been suggested to occur during certain states of pregnancy (5.0±0.07 mol sialic acid per mol fibrinogen vs. 5.3±0.06 mol/mol control during the third trimester), which may help explain the hypercoagulable state that increases the risk of thrombosis throughout gestation[38]. Contrary to this, neonatal fibrinogen displays increased sialic acid content (5.88±1.08 μg/mL) compared to adult fibrinogen (3.07±0.09 μg/mL) with less dense fiber networks, likely derived from enhanced 'B:b' knob:hole interactions that affect the structural and mechanical properties of neonatal fibrin matrices[41]. These results overall display how lateral aggregation and fiber thickness are affected by fibrinogen's carbohydrate moieties, and it has been hypothesized that 'B;b' knob:hole interactions may be affected by the tethering of knob 'B' by the γ chain carbohydrates, the obstruction of hole 'b' by the β chain carbohydrates, or some combination of both[5].

1.3 **Synthesis and Purification of Fibrinogen**

The development of robust systems for fibrinogen synthesis and purification are needed to develop a better understanding of this dynamic protein's structural characteristics. Assessing the link between protein structure and function via establishment of a mutant library generally utilizes recombinant expression systems[42]. However, traditional expression systems using bacteria are unable to reproduce the complex glycan structures of proteins, like those mentioned above for fibrinogen's Bβ and γ chains. Instead, mammalian expression systems using human embryonic kidney (HEK) or Chinese hamster ovarian (CHO) mammalian cells are used for transfections (insertion of nucleic acids into eukaryotic cells) to produce fibrinogen. There are

only a select number of examples with successful preparations of recombinant fibrinogen in academic laboratories[43], of which all rely heavily upon the use of stable transfections (complete insertion into the cell's nuclear genome). Creation of each stable cell line using these procedures can take several months, and the typical fibrinogen expression yields were reported in the range of 2-8 mg/L of media, which make structure-function studies challenging and commercial scale expression unlikely[44]. More recently, commercial companies have developed higher-yield stable cell lines for wild-type recombinant fibrinogen[45, 46]. While successful, the process of developing and isolating high-yield clones utilized cell lines, including PER.C6 and CHO DG44, that are cost prohibitive for most academic laboratories and are also time intensive. These strategies are time and cost prohibitive for building a library of mutations to assess structure-function analyses. In addition, there are a lack of comparative and analytical expression studies performed within the same laboratory to test the effectiveness of each recombinant system for a series of conditions. In this study, we provide a proof-of-concept expression of recombinant human fibrinogen using transiently transfected mammalian HEK cells.

Expression systems for complex proteins must be coupled with highly-selective purification practices for the attainment of pure, and fully-functional protein. Methods for fibrinogen purification from complex media currently involve either precipitation of affinity-based approaches, both of which can be time-intensive and run the risk of degradation or contamination[47-49]. In order to surpass previous purification methods, this thesis will discuss a novel purification method using an affinity chromatography approach with a stable, highly-selective, and reusable GPRP-based peptide coupled resin column, which is demonstrated to purify fully-functional fibrinogen from complex media (such as blood plasma) in a single rapid step with high recovery[50].

Scope of Thesis

Chapter 2 describes the first successful transient transfection system for human fibrinogen expression in suspension HEK Expi293^{TM} mammalian cells for more rapid and cost-effective protein production. Additionally, the development of a rapid, reusable, and highly-selective affinity chromatography column utilizing a high affinity knob 'A'-mimic peptide (Fmoc-GPRPFPAWK) coupled to NHS-activated Sepharose beads for the successful capture of fully functional fibrinogen from complex media will be discussed.

Chapter 3 introduces the highest resolved D region cryo-EM structure of fibrinogen to date utilizing cryoSPARC, along with some insight into the possible role of fibrinogen's intrinsic flexibility on the processes of polymerization and fibrinolysis.

Conclusions and Future Directions explains the potential next steps for the work presented in Chapters 2 and 3.

Appendix presents my contributions towards the publication of an illustrated review on fibrinolysis of which I am a co-first author.

References

1. Forrester, J. M., Malpighi's De polypo cordis: an annotated translation. *Medical history* **1995,** *39* (4), 477-492.

2. Fourcroy, A. F., *Analyse chimique de l'eau sulfureuse d'Enghien: pour servir a l'histoire des eaux sulfureuses en général*. Chez Cuchet: 1788.

3. Weisel, J. W.; Litvinov, R. I., Visualizing thrombosis to improve thrombus resolution. *Research and Practice in Thrombosis and Haemostasis* **2021,** *5* (1), 38-50.

4. Costa-Filho, R.; Hochleitner, G.; Wendt, M.; Teruya, A.; Spahn, D. R., Over 50 years of fibrinogen concentrate. *Clinical and Applied Thrombosis/Hemostasis* **2016,** *22* (2), 109-114.

5. Weisel, J. W.; Litvinov, R. I., Fibrin formation, structure and properties. *Fibrous proteins: structures and mechanisms* **2017**, 405-456.

6. Vilar, R.; Fish, R. J.; Casini, A.; Neerman-Arbez, M., Fibrin (ogen) in human disease: both friend and foe. *Haematologica* **2020,** *105* (2), 284.

7. Surma, S.; Banach, M., Fibrinogen and Atherosclerotic Cardiovascular Diseases—Review of the Literature and Clinical Studies. *International Journal of Molecular Sciences* **2021,** *23* (1), 193.

8. Weisel, J. W.; Litvinov, R. I., Mechanisms of fibrin polymerization and clinical implications. *Blood, The Journal of the American Society of Hematology* **2013,** *121* (10), 1712-1719.

9. Asselta, R.; Duga, S.; Tenchini, M. L., The molecular basis of quantitative fibrinogen disorders. *Journal of Thrombosis and Haemostasis* **2006,** *4* (10), 2115-2129.

10. Påhlman, L. I.; Mörgelin, M.; Kasetty, G.; Olin, A. I.; Schmidtchen, A.; Herwald, H., Antimicrobial activity of fibrinogen and fibrinogen-derived peptides–a novel link between coagulation and innate immunity. *Thrombosis and haemostasis* **2013,** *109* (05), 930-939.

11. Houser, J. R.; Hudson, N. E.; Ping, L.; O'Brien, E. T.; Superfine, R.; Lord, S. T.; Falvo, M. R., Evidence that αC region is origin of low modulus, high extensibility, and strain stiffening in fibrin fibers. *Biophysical journal* **2010,** *99* (9), 3038-3047.

12. Brown, A. E.; Litvinov, R. I.; Discher, D. E.; Purohit, P. K.; Weisel, J. W., Multiscale mechanics of fibrin polymer: gel stretching with protein unfolding and loss of water. *science* **2009,** *325* (5941), 741-744.

13. Liu, W.; Jawerth, L.; Sparks, E.; Falvo, M.; Hantgan, R.; Superfine, R.; Lord, S.; Guthold, M., Fibrin fibers have extraordinary extensibility and elasticity. *Science* **2006,** *313* (5787), 634-634.

14. Xu, W.; Wang, X.; Yan, Y.; Zheng, W.; Xiong, Z.; Lin, F.; Wu, R.; Zhang, R., Rapid prototyping three-dimensional cell/gelatin/fibrinogen constructs for medical regeneration. *Journal of bioactive and compatible polymers* **2007,** *22* (4), 363-377.

15. Elvin, C.; Danon, S.; Brownlee, A.; White, J.; Hickey, M.; Liyou, N.; Edwards, G.; Ramshaw, J.; Werkmeister, J., Evaluation of photo-crosslinked fibrinogen as a rapid and strong tissue adhesive. *Journal of Biomedical Materials Research Part A: An Official Journal of The Society for Biomaterials, The Japanese Society for Biomaterials, and The Australian Society for Biomaterials and the Korean Society for Biomaterials* **2010,** *93* (2), 687-695.

16. Medved, L.; Weisel, J., Recommendations for nomenclature on fibrinogen and fibrin. *Journal of Thrombosis and Haemostasis* **2009,** *7* (2), 355.

17. Hudson, N. E., Biophysical mechanisms mediating fibrin fiber lysis. *BioMed research international* **2017,** *2017*.

18. McPherson, H. R.; Duval, C.; Baker, S. R.; Hindle, M. S.; Cheah, L. T.; Asquith, N. L.; Domingues, M. M.; Ridger, V. C.; Connell, S. D.; Naseem, K. M., Fibrinogen αC-subregions critically contribute blood clot fibre growth, mechanical stability, and resistance to fibrinolysis. *Elife* **2021,** *10*, e68761.

19. Kononova, O.; Litvinov, R. I.; Zhmurov, A.; Alekseenko, A.; Cheng, C. H.; Agarwal, S.; Marx, K. A.; Weisel, J. W.; Barsegov, V., Molecular mechanisms, thermodynamics, and dissociation kinetics of knob-hole interactions in fibrin. *Journal of Biological Chemistry* **2013,** *288* (31), 22681-22692.

20. Alshehri, F. S.; Whyte, C. S.; Mutch, N. J., Factor XIII-A: An Indispensable "Factor" in Haemostasis and Wound Healing. *International Journal of Molecular Sciences* **2021,** *22* (6), 3055.

21. Yakovlev, S.; Makogonenko, E.; Kurochkina, N.; Nieuwenhuizen, W.; Ingham, K.; Medved, L., Conversion of fibrinogen to fibrin: mechanism of exposure of tPA-and plasminogen-binding sites. *Biochemistry* **2000,** *39* (51), 15730-15741.

22. Kant, J. A.; Fornace Jr, A. J.; Saxe, D.; Simon, M. I.; McBride, O. W.; Crabtree, G. R., Evolution and organization of the fibrinogen locus on chromosome 4: gene duplication accompanied by transposition and inversion. *Proceedings of the National Academy of Sciences* **1985,** *82* (8), 2344-2348.

23. Madrazo, J.; Brown, J. H.; Litvinovich, S.; Dominguez, R.; Yakovlev, S.; Medved, L.; Cohen, C., Crystal structure of the central region of bovine fibrinogen (E5 fragment) at 1.4-Å resolution. *Proceedings of the National Academy of Sciences* **2001,** *98* (21), 11967-11972.

24. Pechik, I.; Madrazo, J.; Mosesson, M. W.; Hernandez, I.; Gilliland, G. L.; Medved, L., Crystal structure of the complex between thrombin and the central "E" region of fibrin. *Proceedings of the National Academy of Sciences* **2004,** *101* (9), 2718-2723.

25. Spraggon, G.; Everse, S. J.; Doolittle, R. F., Crystal structures of fragment D from human fibrinogen and its crosslinked counterpart from fibrin. *Nature* **1997,** *389* (6650), 455-462.

26. Kostelansky, M. S.; Betts, L.; Gorkun, O. V.; Lord, S. T., 2.8 Å crystal structures of recombinant fibrinogen fragment D with and without two peptide ligands: GHRP binding to the "b" site disrupts its nearby calcium-binding site. *Biochemistry* **2002,** *41* (40), 12124-12132.

27. Hall, C., Electron microscopy of fibrinogen and fibrin. *Journal of Biological Chemistry* **1949,** *179* (2), 857-864.

28. Yee, V. C.; Pratt, K. P.; Côté, H. C.; Le Trong, I.; Chung, D. W.; Davie, E. W.; Stenkamp, R. E.; Teller, D. C., Crystal structure of a 30 kDa C-terminal fragment from the γ chain of human fibrinogen. *Structure* **1997,** *5* (1), 125-138.

29. Kollman, J. M.; Pandi, L.; Sawaya, M. R.; Riley, M.; Doolittle, R. F., Crystal structure of human fibrinogen. *Biochemistry* **2009,** *48* (18), 3877-3886.

30. Sit, P. S.; Marchant, R. E., Surface-dependent conformations of human fibrinogen observed by atomic force microscopy under aqueous conditions. *Thrombosis and haemostasis* **1999,** *82* (09), 1053-1060.

31. Beijbom, L.; Larsson, U.; Kavéus, U.; Hebert, H., Structure analysis of fibrinogen by electron microscopy and image processing. *Journal of ultrastructure and molecular structure research* **1988,** *98* (3), 312-319.

32. Zuev, Y. F.; Litvinov, R. I.; Sitnitsky, A. E.; Idiyatullin, B. Z.; Bakirova, D. R.; Galanakis, D. K.; Zhmurov, A.; Barsegov, V.; Weisel, J. W., Conformational flexibility and

self-association of fibrinogen in concentrated solutions. *The Journal of Physical Chemistry B* **2017,** *121* (33), 7833-7843.

33. Köhler, S.; Schmid, F.; Settanni, G., The internal dynamics of fibrinogen and its implications for coagulation and adsorption. *PLoS computational biology* **2015,** *11* (9), e1004346.

34. Mican, J.; Toul, M.; Bednar, D.; Damborsky, J., Structural biology and protein engineering of thrombolytics. *Computational and structural biotechnology journal* **2019,** *17*, 917-938.

35. Bai, X.-C.; McMullan, G.; Scheres, S. H., How cryo-EM is revolutionizing structural biology. *Trends in biochemical sciences* **2015,** *40* (1), 49-57.

36. Scapin, G.; Potter, C. S.; Carragher, B., Cryo-EM for small molecules discovery, design, understanding, and application. *Cell chemical biology* **2018,** *25* (11), 1318-1325.

37. Zauner, G.; Hoffmann, M.; Rapp, E.; Koeleman, C. A.; Dragan, I.; Deelder, A. M.; Wuhrer, M.; Hensbergen, P. J., Glycoproteomic analysis of human fibrinogen reveals novel regions of O-glycosylation. *Journal of proteome research* **2012,** *11* (12), 5804-5814.

38. Maghzal, G. J.; Brennan, S. O.; George, P. M., The sialic acid content of fibrinogen decreases during pregnancy and increases in response to fibrate therapy. *Thrombosis research* **2005,** *115* (4), 293-299.

39. Langer, B.; Weisel, J.; Dinauer, P. A.; Nagaswami, C.; Bell, W. R., Deglycosylation of fibrinogen accelerates polymerization and increases lateral aggregation of fibrin fibers. *Journal of Biological Chemistry* **1988,** *263* (29), 15056-15063.

40. Gralnick, H. R.; Givelber, H.; Abrams, E., Dysfibrinogenemia associated with hepatoma: increased carbohydrate content of the fibrinogen molecule. *New England Journal of Medicine* **1978,** *299* (5), 221-226.

41. Nellenbach, K.; Kyu, A.; Guzzetta, N.; Brown, A. C., Differential sialic acid content in adult and neonatal fibrinogen mediates differences in clot polymerization dynamics. *Blood Advances* **2021,** *5* (23), 5202-5214.

42. Assenberg, R.; Wan, P. T.; Geisse, S.; Mayr, L. M., Advances in recombinant protein expression for use in pharmaceutical research. *Current opinion in structural biology* **2013,** *23* (3), 393-402.

43. Gorkun, O. V.; Veklich, Y. I.; Weisel, J. W.; Lord, S. T., The conversion of fibrinogen to fibrin: recombinant fibrinogen typifies plasma fibrinogen. *Blood, The Journal of the American Society of Hematology* **1997,** *89* (12), 4407-4414.

44. Binnie, C. G.; Hettasch, J. M.; Strickland, E.; Lord, S. T., Characterization of purified recombinant fibrinogen: partial phosphorylation of fibrinopeptide A. *Biochemistry* **1993,** *32* (1), 107-113.

45. Piechocka, I.; Kurniawan, N.; Grimbergen, J.; Koopman, J.; Koenderink, G., Recombinant fibrinogen reveals the differential roles of α-and γ-chain cross-linking and molecular heterogeneity in fibrin clot strain-stiffening. *Journal of Thrombosis and Haemostasis* **2017,** *15* (5), 938-949.

46. Hirashima, M.; Imamura, T.; Yano, K.; Kawamura, R.; Meta, A.; Tokieda, Y.; Nakashima, T., High-level expression and preparation of recombinant human fibrinogen as biopharmaceuticals. *The Journal of Biochemistry* **2016,** *159* (2), 261-270.

47. Brennan, M., Fibrin glue. *Blood reviews* **1991,** *5* (4), 240-244.

48. Liu, C.-Z.; Cheng, H.-J.; Chang, L.-Y., A new feasible method for fibrinogen purification based on the affinity of Staphylococcus aureus clumping factor A to fibrinogen. *Protein expression and purification* **2008,** *61* (1), 31-35.

49. Kuyas, C.; Haeberli, A.; Walder, P.; Straub, P., Isolation of human fibrinogen and its derivatives by affinity chromatography on Gly-Pro-Arg-Pro-Lys-Fractogel. *Thrombosis and haemostasis* **1990,** *63* (03), 439-444.

50. Popovic, G.; Kirby, N. C.; Dement, T. C.; Peterson, K. M.; Daub, C. E.; Belcher, H. A.; Guthold, M.; Offenbacher, A. R.; Hudson, N. E., Development of Transient Recombinant Expression and Affinity Chromatography Systems for Human Fibrinogen. *International Journal of Molecular Sciences* **2022,** *23* (3), 1054.

Chapter 2

Synthesis and Purification of Human Fibrinogen

2.1 **Introduction**

2.1.1 *Recombinant Expression Systems for Human Fibrinogen*

Although there has been much exploration of fibrin(ogen)'s structural elements, few studies have focused on the etiology involved with posttranslational modifications or polymorphisms of fibrinogen. Structure-function assessment through protein mutational modifications has been previously determined by creating recombinant expression systems, allowing for quantifiable protein production with high success rates[2]. Large, eukaryotic proteins with complex structures involving glycans, such as fibrinogen, require cell culturing beyond traditional *E. coli* or bacterial expression systems. For this reason, researchers employ mammalian systems such as human embryonic kidney 293 (HEK293), or Chinese hamster ovarian (CHO) mammalian cells in a transient or stable manner. Both methods utilize the process of transfection, where an expression vector (ex: plasmid) is inserted into the nucleus of a mammalian cell and either becomes fully integrated into the host's nuclear genome (stable), or only remains in the cell temporarily/until cellular replication (transient). However, fibrinogen's complexity has challenged traditional expression system viability, and only a select number of recombinant fibrinogen systems have been developed utilizing stable transfection systems[3, 4]. The first successful stable cell fibrinogen expression system was optimized by Susan T. Lord's lab, which employed adherent CHO cells grown in roller bottles expressing recombinant fibrinogen over several months[3]. The procedure followed a co-transfection of an Aα and γ chain combined expression vector with a pRSVneo selection vector and secondary co-transfection of a Bβ expression vector with a pMSVhis selection vector with subsequent cell selection steps between

co-transfections. By using this two-step, two plasmid system, the lab achieved 2-4 mg/L protein expression. With these results, several companies have pushed for elevated fibrinogen production at commercial levels. Combining all three fibrinogen chains into a single plasmid ($A\alpha B\beta\gamma_2$, double γ for its limited transfection efficacy), the Chemo-Sero-Therapeutic Research Institute established a fibrinogen expression system with stably transfected CHO DG44 cells[4]. Optimization of the expression vector and cell culturing conditions garnered high level expression of recombinant fibrinogen (1.3 g/L or higher) with characteristics synonymous to plasma purified fibrinogen, as justified by chain-specific antibody western blots, polymerization evaluating turbidity assays, and scanning electron microscopy (SEM) images. Despite achieving elevated protein production, successful development of these stable cell expression systems presents a cost and time prohibitive strategy for structure-function analysis via mutational studies. As such, this thesis will highlight our efforts towards the creation of a transient transfection system for human fibrinogen expression in HEK Expi293™ mammalian cells for more rapid and cost-effective protein production compared to current expression strategies[1].

In recent years, novel transient expression systems have been developed with the potential for high expression yields and much shorter lead times, but, to our knowledge, no transient expression system has yet been reported for producing fibrinogen. In this study, we test the recombinant expression of fibrinogen in the HEK Expi293™ line (ThermoFisher, Waltham, MA, USA) using a transient cell expression strategy. We report on a series of expression conditions using both a single and complex plasmid encoding all three fibrinogen chains (Combined Single Plasmid or CSP; Figure 2.1) and a three-plasmid system (3P) with each plasmid encoding a single fibrinogen chain, comparable to a previously reported expression strategy[3]. The CSP contains cDNA's for all three fibrinogen chains, and two copies of the fibrinogen γ chain in

accordance with the design by the Chemo-Sero-Therapeutic Research Institute[4]. The CSP deviates from the previous plasmid at several important points. While the original design used the same promoter/poly-A tail for all four genes[4], the CSP contains four different promoters in order to avoid repetitive sequences[5]. For similar reasons, and to limit the size of the plasmid, the ARS insulator sequence[6] was not included in the CSP. Promoters were all selected for their relatively high expression levels in mammalian cells and include the cytomegalovirus (CMV)[5], CMV early enhancer/chicken beta-actin (CAG)[7], eukaryotic translation elongation factor 1α (EF-1α)[8], and simian vacuolating virus 40 (SV40)[9] (Figure 2.1). In addition, each gene is proceeded by a Kozak sequence, which has been shown to facilitate the initial binding of mRNA to the ribosome (Figure 2.1)[10, 11]. The second γ chain gene was codon optimized by Genscript to enable site-specific mutation validation in future studies.

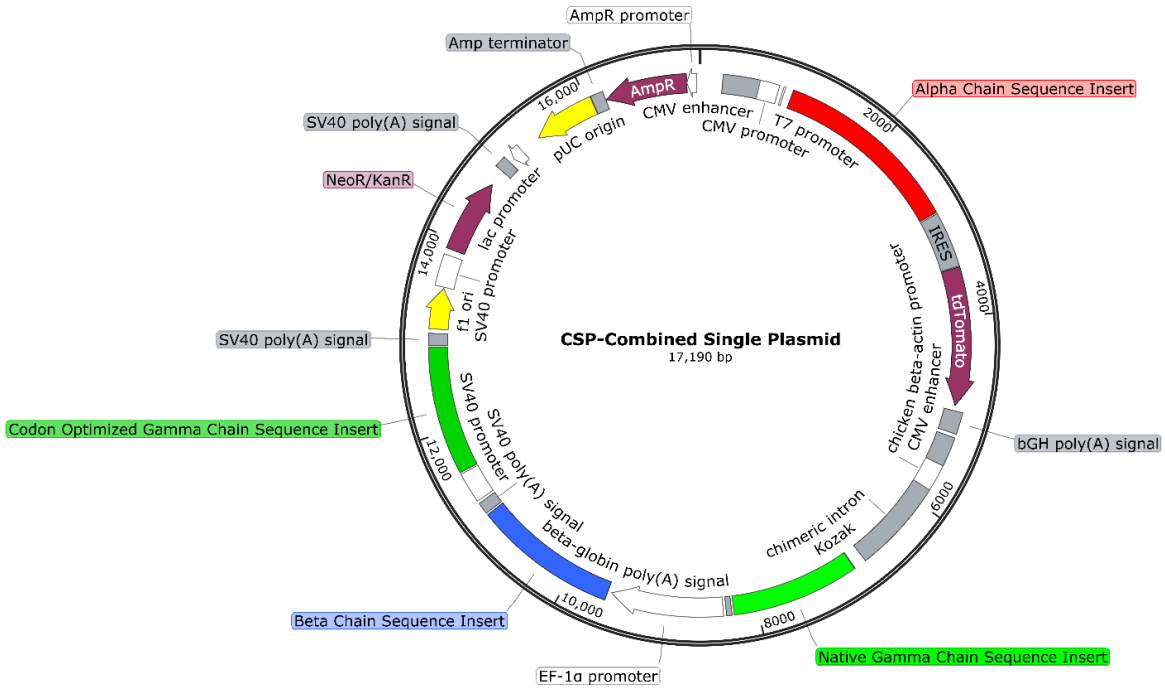

Figure 2.1: Map of Combined Single Plasmid. Plasmid map showing the locations of the main elements of the CSP, including promoters, genes, and poly (A) signals.

2.1.2 *Strategies for Fibrinogen Purification from Complex Media*

Development of any expression system must be coupled with highly-selective purification practices. Current methods for fibrinogen isolation from complex media involve either precipitation or affinity chromatography purification. Precipitation techniques often involve the use of various agents (ammonium sulphate, ethanol, polyethylene glycol) and multiple time-consuming centrifugation steps, with the possibility of sample degradation or contamination[12]. Affinity approaches instead utilize fibrinogen-specific interactions with either immobilized proteins or peptides[13, 14]. Clumping factor A (clfA) immobilization utilizes a C-terminal γ chain fibrinogen interaction, and allows for 19-38% recovery of fibrinogen from plasma within two hours. Despite the brevity of the technique, each run required column regeneration by clfA removal with potential clfA contamination within purified fibrinogen samples[13]. Taking

advantage of the 'A:a' knob:hole interaction, one affinity method immobilized a non-optimized knob 'A'-mimic peptide (GPRPK) onto a Fractogel column with a 8-10 mg of plasma per mL of wet gel capacity[14]. However, sample purification required destructive buffers and produced fibrinogen with lowered clottability (78-92%). To overcome the disadvantages involved with fibrinogen purification from complex media mentioned above, this thesis will highlight the development of a novel purification method using an affinity-based approach with a stable, highly selective, and reusable GPRP-based peptide (Figure 4) coupled resin column which is demonstrated to purify native fibrinogen from plasma in a single rapid step with high recovery[1].

2.2 **Materials and Methods**

2.2.1 *Plasmid Descriptions*

2.2.1.1 Three Plasmid (3P) System

Fibrinogen Aα, Bβ, and γ chain expressing plasmids (in vector p584) were generously shared by Alisa Wolberg (University of North Carolina, Chapel Hill, NC, USA). Fibrinogen Aα, Bβ, and γ chains were cloned into the pcDNA 3.1 (+), pIRES/EGFP-puro, and pcDNA 3.1/Hygro (+) plasmids, respectively, using a Gibson assembly-based approach[15]. The fibrinogen-chain encoding cDNAs were excised from the p584 plasmids[3] using PCR primers containing overlapping sequences with the new plasmids. The fibrinogen coding cDNA and the new, linearized plasmid were assembled into a new plasmid following the NEBuilder HiFi DNA Assembly Master Mix protocol (New England Biolabs Inc., Ipswich, MA, USA). Correct insertion and sequence identity for new plasmid were confirmed with Sanger sequencing. These plasmids will be referred to in the text as Fgn Aα/pcDNA 3.1 (+), Fgn Bβ/pIRES-EGFP-puro, and Fgn γ/ pcDNA 3.1-Hygro (+) and taken together they comprise the three plasmid (3P) expression system.

2.2.1.2 Combined Single Plasmid (CSP) System

In order to establish an efficient recombinant expression system, a novel single DNA plasmid, referred to in this paper as Combined Single Plasmid (CSP), that encodes all three fibrinogen chains (Aα, Bβ, and γ) was designed, in collaboration with Genscript, inspired by the previously reported plasmid that was used by the aforementioned Chemo-Sero-Therapeutic Research Institute[4]. In addition, the plasmid contains two copies of the fibrinogen γ chain. Due to the repetitive elements present in the previously used single plasmid (including using the same promoter and five arylsulfatase (ARS) elements[4]) potentially leading to rearrangements between the repetitive sequence elements[16], the new CSP plasmid has no arylsulfatase (ARS) elements. The plasmid contains different promoters prior to sequences of all four chains, with one of the γ chains being codon optimized for expression in HEK and CHO cells, which enables site-directed mutagenesis into both strands of the γ chains for assurance of mutation upon sequencing validation. The map for the plasmid is shown in Figure 2.1.

2.2.2 *Mammalian Cell Transfections*

To facilitate mammalian transfections, the DNA fibrinogen plasmids were isolated at 100–500 ng/μL from transformed One Shot *E. coli* TOP10 or DH5α cells using a QIAGEN (Hilden, Germany) Mega Plasmid Kit Protocol. After purification, plasmid sequences were confirmed with Sanger sequencing.

2.2.2.1 Polyethylenimine (PEI) Transfections

For HEK Expi293™ (ThermoFisher) cell transfections, cells were grown for three passages post-thaw in Expi293™ expression media containing 1% Pen/Strep under 37°C, 8% CO_2 conditions on an orbital shaker platform, at a shaking rate of 116 rpm with cell viability >95%. Small scale transfections were performed in a suspension cell compatible 6-well plate with a cell

seeding density of roughly 3 million live cells. Plasmids were heat sterilized to eliminate potential bacterial contamination (80°C for 20 min), diluted with pre-warmed Expi293™ expression media and mixed at room temperature with PEI at desired ratios and incubated at room temperature for 30 min. The mixtures were then added to appropriate wells and incubated for the next five days under the same conditions. During the following days, small samples were collected to determine viability and daily protein expression levels and cells were imaged under a LEICA DMi8 microscope.

2.2.2.2 ExpiFectamine™ Transfections

For HEK Expi293™ (ThermoFisher) cell transfections, cells were grown for at least three passages post-thaw in Expi293™ expression media containing 1% Pen/Strep under 37°C, 8% CO_2 conditions on an orbital shaker platform, at a shaking rate of 116 rpm with cell viability >95%. Small scale transfections were performed in a suspension cell compatible 6-well plate (Cellstar, Greiner Bio One) with a cell seeding density of ~3 million live cells. Plasmids were heat sterilized to eliminate potential bacterial contamination (80°C for 20 min), diluted with pre-warmed Expi293™ expression media and mixed at room temperature with diluted ExpiFectamine™ at desired ratios and incubated at room temperature for 10–20 min. The mixtures were then added to appropriate wells and incubated for the next five days under the same conditions. One day post-transfection, specialized transfection enhancers were added at appropriate ratios to wells containing ExpiFectamine™. During the following days, small samples were collected to determine viability and daily protein expression levels and cells were imaged under a LEICA DMi8 microscope.

2.2.3 *Microscopy*

A small aliquot of cell solution was applied to a glass slide, a glass cover slip was placed on top of the sample, sealant was added to adhere the two surfaces, and samples were placed upside down on a Leica DMi8 epifluorescence microscope (Leica Microsystems Inc., Buffalo Grove, IL, USA) and imaged with a 10× air objective using a DSRed-T (553 nm) filter set. Images were taken with a Leica DFC9000GT SCMOS 4 Megapixel monochrome camera with each image measuring 2048 pixels.

2.2.3.1 Fluorescence Cell Image Processing

Representative brightfield and fluorescence images were first opened in ImageJ/FIJI[17]. Fluorescence images were processed by enhancing the window/level granularity and removing the bright outlier noise using a radius between 1–5 pixels. Different radii were tested to remove small specks of fluorescence, while maintaining the fluorescence of the cells. Finally, the fluorescence and brightfield images were merged to create a composite image.

2.2.4 *Assessing Mammalian Expression Systems*

2.2.4.1 ELISA Assays

Chicken IgY antifibrinogen antibody (Thermo PA1-9526) was diluted to 0.3 μg/mL in coating buffer (29 mM sodium carbonate, 71.4 mM sodium bicarbonate, pH 9.6), and added to each of the wells being used in a 96-well plate (Corning Costar®® black with clear flat bottom polystyrene assay plate). The 96-well plate was centrifuged at 500 rpm for 1 min and incubated at 37°C for 2 hours (or overnight at 4°C). The wells were then washed four times with 200 μL of PBS-T buffer (11.9 mM phosphates, 137 mM sodium chloride, 2.7 mM potassium chloride, 0.05% Tween-20 *v*/*v*), and the remaining protein-binding sites were blocked by adding 200 μL of 2% Milk in PBS-T to each well and incubating for 1 hour at 37°C followed by four PBS-T

washes. A total of 50 µL of samples, diluted 1/150 or 1/200 in Expi293™ expression media, were added to wells and incubated for 30 minutes at 37°C. In addition, fibrinogen standards ranging from 100 µg/L to 1.56 µg/L, along with negative controls containing only media were also included in separate wells (See Figure 2.2 for a representative standard curve). All samples, standards, and controls were done in triplicate. After incubation, wells were washed four times with PBS-T and 50 µL of antifibrinogen-rabbit antibody (Dako, A0080), was added to each well at a concentration of 5 µg/mL in 2% Milk in PBS-T and incubated for 30 minutes at 37°C. Wells were then washed using PBS-T buffer and 50 µL /well of goat anti-rabbit HRP antibody (Invitrogen, 31462), diluted to 10 µg/mL in 2% Milk in PBS-T, then added to each well and incubated for 30 minutes. Wells were then washed six times with 200 µL of PBS-T buffer. Finally, 200 µL of ABTS substrate was added to each well and incubated at room temperature while absorbance readings at 405 nm were taken every minute on a Synergy™ HT multi-mode microplate reader (BioTek Instruments).

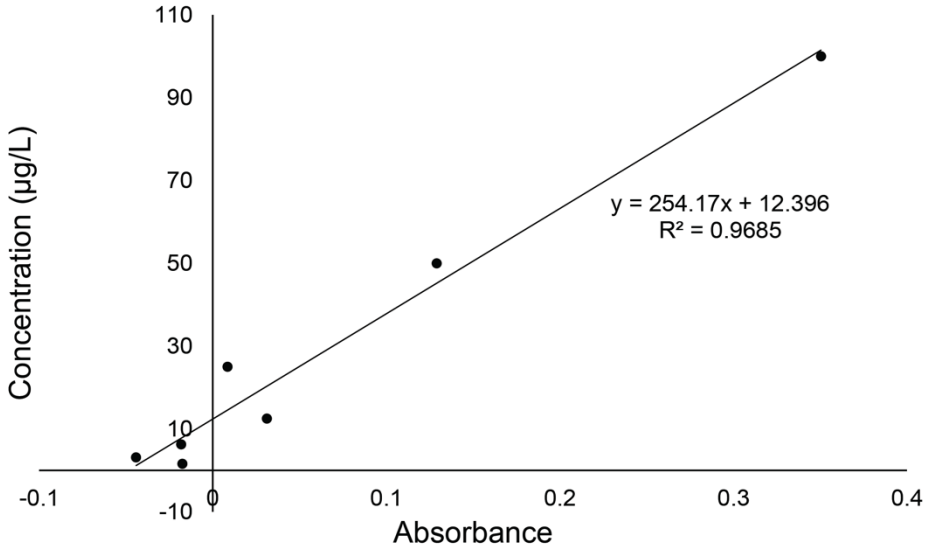

Figure 2.2: Representative ELISA assay standard curve. Absorbances of Peak 1 fibrinogen at the concentrations 100 µg/L, 50 µg/L, 25 µg/L, 12.5 µg/L, 6.25 µg/L, 3.125 µg/L, and 1.56 µg/L.

2.2.4.2 SDS-PAGE and Coomassie Gels

The presence of fibrinogen was routinely checked using SDS-PAGE with a 10% polyacrylamide gel employing standard techniques. Briefly, samples were mixed with reducing or non-reducing loading dye and heated at 98°C for 5 minutes before loading into individual wells. Electrophoresis was performed at 80 V for the initial 10 min stacking phase followed by the separation phase run at 120 V for another hour. The gel was then rinsed with water, stained with Gelcode Blue-Safe Protein Stain (AQ-2), then destained before imaging on an Azure Biosystems c300. For peptide coupling, the same procedure was followed except that the separation phase was run at 120 V for no longer than 50 min, and the gel was destained for two hours before imaging.

2.2.4.3 Western Blot

Western blotting initially followed the same procedure as described above for SDS-PAGE. Once electrophoresis was complete, however, the protein was transferred onto a PVDF membrane using a BIO-RAD Trans-Blot Turbo Transfer System. The transfer was run for 30 minutes at 25 V. The membrane was then removed and placed in 40 mL of 5% milk solution in TBS-T buffer, followed by shaking for 1 hour at room temperature or overnight at 4°C. A 40 mL solution of 1:2500 diluted primary rabbit antifibrinogen antibody (Dako) in TBST was added for an hour, after which the antibody solution was removed and washed with TBS-T three times for 5 minutes at room temperature. Then, a secondary mouse anti-rabbit antibody (Invitrogen) diluted 1:10,000 in 30 mL of TBS-T was added and shaken for one hour. The membrane was then washed again three times. Western blot detection reagents (Pierce ECL Western Blotting Substrate (ThermoFisher Scientific)) were then mixed at a 1:1 ratio and added on top of the

membrane. After incubating for one minute the reagents were poured off and the membrane was imaged using chemiluminescence on an Azure Biosystems c300.

2.2.5 *Optimization of the Peptide Coupling Process*

The synthetic peptide sequence for a novel fibrinogen affinity column was chosen based on fibrin knob 'A'-mimic peptide affinity tests performed previously[18]. The peptide GPRPFPAC had the lowest dissociation constant in those tests and was selected for this procedure based on those results. The synthetic peptide (Fmoc-GPRPFPAWK for the purification column or Fmoc-RPGPFAWPK for the scramble column; 0.5 mg/mL, 1276 Da) was first dissolved to make a 1 mM stock solution in dH_2O and dimethyl sulfoxide (DMSO). The peptide stock solution was mixed with 2 x coupling buffer (0.4 M $NaHCO_3$, and 1 M NaCl at pH 8.5), for a final peptide concentration of 0.4 mM. NHS-activated Sepharose 4 Fast Flow beads were washed (to ensure that the NHS group remained unhydrolyzed) with cold 1 mM HCl. Coupling of the synthetic peptide to the Sepharose beads was achieved by mixing solutions at a 0.5:1 ratio (coupling solution:resin) for 3 hours at room temperature. The remaining NHS binding sites of the resin were then blocked with blocking buffer (0.1 M Tris–HCl, pH 8.5) for 3 hours at 4°C. The Fmoc group protecting the N-terminal glycine of the peptide was then de-protected with 4-methylpiperidine (4MP), for 3 hours at room temperature. A glass column (Bio-Rad, Hercules, CA, USA) was then packed with resin by gravity flow and the column was washed with three column volumes (CVs) of blocking buffer followed by three CVs of low pH buffer (0.023 M sodium acetate, 0.077 M glacial acetic acid, 0.5 M NaCl, pH 4) followed by CVs of blocking buffer.

Although determined to remain reliable over many runs (discussed in section 2.3.2), once the column became unusable a new column was needed for future fibrinogen isolation from

pregnancy plasma (Chapter 4 section 4.2). Multiple attempts to make a new column using the process above resulted in ineffective columns for fibrinogen capture. In combatting issues of reproducing new GPRPFPAWK-based affinity columns, we adapted the above coupling process as follows. The synthetic peptide was first dissolved to make a 10 mM stock solution in dH_2O and DMSO. The peptide stock solution was mixed with 2 x coupling buffer (0.4 M $NaHCO_3$, and 1 M NaCl at pH 8.5), for a final peptide amount of 6 mg to enhance the number of peptides bound to the Sepharose beads. NHS-activated Sepharose 4 Fast Flow bead preparation, synthetic peptide coupling, and NHS binding site blocking steps remained the same. With help from Dr. Allen (East Carolina University, Greenville, NC, USA), we realized that our previous deprotection step was ineffective, and harmful to our peptide coupling process. We then designed a more reliable deprotecting step, adjusting to deprotection with a 20% 4MP in dimethylformamide (DMF) solution for 5 minutes at room temperature (repeat for two total washes), then 100% DMF for 2 minutes. The column packing process was not altered. An outline of the initial process and alterations of the deprotecting step are depicted in Figure 2.3.

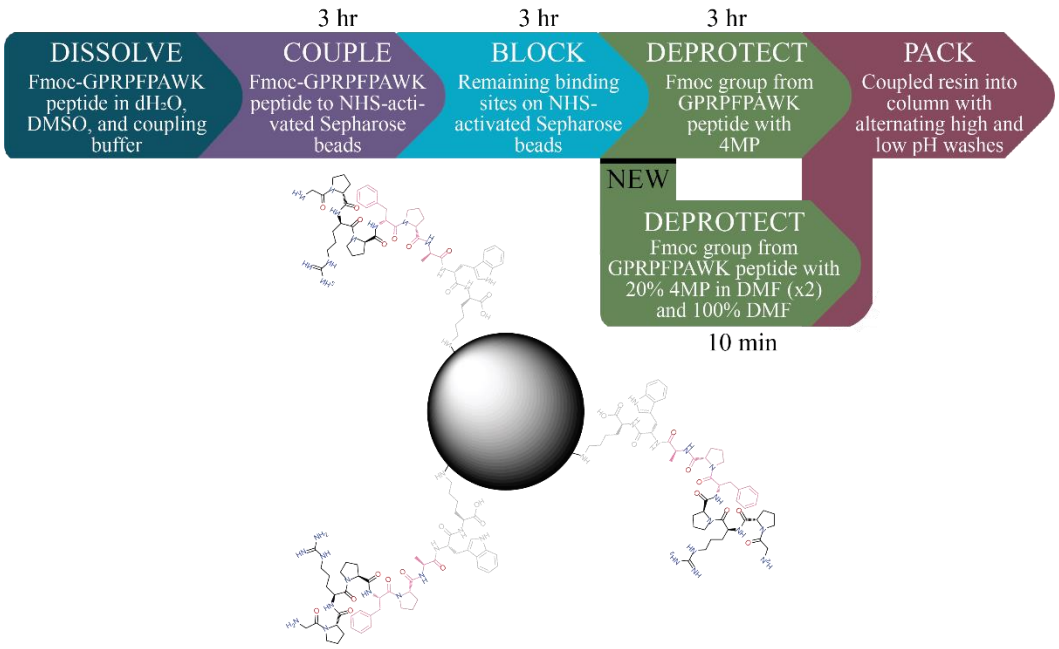

Figure 2.3: Fmoc-GPRPFPAWK peptide coupling to NHS-activated Sepharose. Flow diagram of peptide coupling protocol with indication of sample collection for use in Coomassie gel staining against standard peptide amounts. Alterations to the deprotecting step are indicated with the "NEW" section, that take the place of the above deprotecting step with only piperidine, as well as time variations for both steps. Final product is a Sepharose bead with activated GPRPFPAWK coupled peptide, shown below (not to scale).

Peptide coupling efficacy to the Sepharose beads was determined by SDS-PAGE and Coomassie gel staining of supernatant samples taken from different points in the coupling procedure against standard peptide concentrations of 100 ng, 300 ng, 600 ng, and 1000 ng (Figure 2.4). Plot profiles created for each standard were converted to corrected average gray values and a standard curve was plotted ($y = 0.7231x + 95.911$, $R^2 = 0.9883$). The corrected average gray values for unknown samples (pre-coupling, coupling supernatant/CS, and blocking supernatant/BS) were then inserted into the above equation, and their concentrations were found to be 654.6 ng, 139.8 ng, and 64.3 ng, respectively.

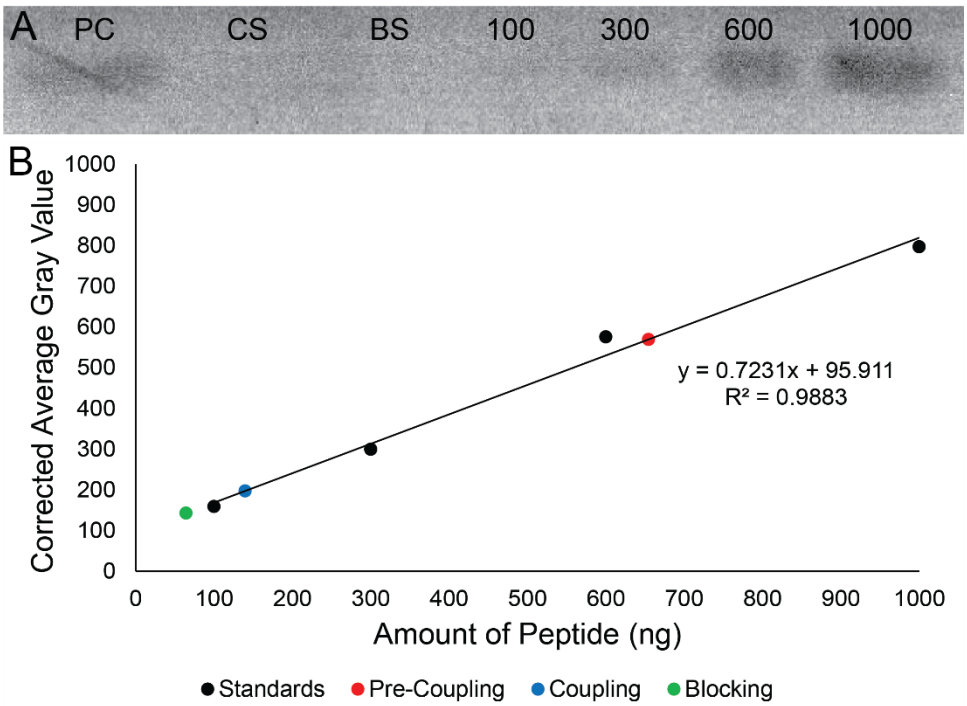

Figure 2.4: Representative peptide coupling efficacy for column development. (A) Coomassie gel staining of pre-coupling (PC), coupling supernatant (CS), blocking supernatant (BS), and peptide standards 100 ng, 300 ng, 600 ng, and 1000 ng. (B) Average pixel intensity correlation with peptide amount (ng) using Coomassie gel band's plot profiles taken from ImageJ/FIJI[17].

2.2.6 *Purification of Fibrinogen with the Peptide-Based Affinity Column*

2.2.6.1 Affinity Column Purification Tests

The binding abilities of both a 2 mL and 10 mL GPRPFPAWK peptide column were first assessed using Peak 1 fibrinogen (Enzyme Research Labs, South Bend, IN, USA). The column was equilibrated with 2–3 CVs of loading buffer (20 mM HEPES, 20 mM $CaCl_2$ and 150 mM NaCl, pH 7.4) at 0.5 mL/min. The desired amount of fibrinogen (typically ~1 mg) was diluted in loading buffer and flowed over a column at a concentration of 0.17–0.3 mg/mL at 0.3 mL/min. Three CVs of column flow through fractions were collected for further analysis. Next, the column was washed with 5 CVs of loading buffer at 0.5 mL/min and five CVs of fractions were

collected for further analysis. To elute the fibrinogen off the column, 2.5 CVs of elution buffer (1 M NaBr and 50 mM sodium acetate at pH 5.3) was run over the column at 0.3 mL/min and three CVs of fractions were collected and neutralized with 0.8 M sodium hydroxide. After all fractions were collected, the column was washed with 2 CVs of dH_2O and 2 CVs of 20% ethanol. The same procedure was used to test the scramble peptide (RPGPFAWPK) column as well.

Protein amounts (mg) were calculated by calculating the concentration spectrophotometrically using a Nanodrop 2000c (ThermoFisher Scientific), followed by a summation of all fractions for each individual chromatography step (flow through, wash, and elution). The percentage of protein detected in each step was then determined by calculating the percent yield using the pre-flow nanodrop concentration as the theoretical yield, and the summation nanodrop concentration of each step as the actual yield.

2.2.6.2 Optimization of Fibrinogen Purification from Blood Plasma

Human fresh frozen plasma (FFP) (Cone Bioproducts, Sequin, TX, USA) was run over the 2 mL and 10 mL GPRPFPAWK affinity columns to test their ability to separate fibrinogen from other plasma proteins. The FFP aliquot was thawed at 30°C and filtered with a 0.2 μm filter to remove large particulates. Benzamidine HCl (1 mM) was added to prevent fibrinogen to fibrin conversion by thrombin, and the solution was immediately added to a pre-equilibrated affinity column. The plasma flowed through the column under gravity. The column was washed, and the fibrinogen was eluted as described above. All elution fractions were adjusted to a pH of 7 and exchanged into HBS buffer (20 mM HEPES, 150 mM NaCl, pH 7.4) using a PD10 column.

In attempting to remove aggregates from fibrinogen purified from plasma by the GPRP-based affinity column using the updated deprotecting step protocol, as well as exchange samples into HBS buffer, a size exclusion chromatography (SEC) method was developed. A Superdex™

200 increase 10/300 GL column was first equilibrated into HBS buffer (150 mM NaCl, 20 mM HEPES at pH 7.4; filtered at 0.2 μm and degassed) overnight using an ÄKTA pure (General Electric Healthcare Systems, USA) fast protein liquid chromatogram. GPRP-based affinity chromatography elution fractions were then chosen based on protein amount and appropriate 260/280 values (~0.6), combined, and injected into a 5 mL loop. Sample was then applied to the column following an isocratic elution (100% HBS, filtered and degassed), and fractionated into 0.5 mL aliquots. Ultraviolet (UV) readouts were used to determine which fractions contained protein, and a subsequent Coomassie gel and western blot found that the predominant peak (fractions 8-14) contained purified fibrinogen (Figure 2.10).

2.2.6.3 Purification of Fibrinogen from Plasma with Ethanol Precipitation

Adapting an ethanol-precipitation-based purification method initially described by Doolittle, et al.[19], 100 mL of human fresh frozen plasma (FFP) (Cone Bioproducts, Sequin, TX, USA) was thawed at 37°C and then immediately placed on ice. Plasma was decalcified by adding 3 mM ethylenediaminetetraacetic acid (EDTA; final concentration), to inhibit coagulation, while sitting on ice for 5 minutes. Plasma was then centrifuged at 18,000*xg* for 20 minutes and the supernatant was collected. The 0.22 original volumes (OVs) of a 10 mM HEPES, 50% ethanol solution (pH 7.1, 3°C) was added to the supernatant, followed by centrifugation at 18,000*xg* for 20 minutes. A supernatant and pellet resulted from this centrifugation. The supernatant was poured off and the pellet retained. The pellet was washed with 0.5 OVs of a 10 mM HEPES, 7% ethanol solution (pH 6.5, 3°C) and centrifuged at 18,000*xg* for 20 minutes. The pellet was then resuspended in 0.25 volumes of a 55 mM citrate buffer (pH 6.5, 30°C) and cooled until reaching ~0°C. “Cold insoluble material” was removed by addition of a 10 mM HEPES, 20% ethanol solution (pH 7.1, 3°C) to a final concentration of 2% followed by centrifugation for 30 minutes at 18,000*xg*. The

supernatant was retained and the mucous-like pellet was discarded. The ethanol concentration in the supernatant was then increased to 8% by addition of 10 mM HEPES, 20% ethanol solution (pH 7.1, 3°C). The solution was then centrifuged at 18,000*xg* for 20 minutes resulting in a pellet of purified fibrinogen. The pellets were air dried and then suspended in 20 mM HEPES, 150 mM sodium chloride (pH 7.4).

2.2.6.4 Clottability and Turbidity Assays

The functionality of the fibrinogen isolated from human fresh frozen plasma (FFP) using both purification methods was assessed using a combination of clottability and turbidity assays. In both assays, Peak 1 fibrinogen (Enzyme Research Labs, South Bend, IN, USA) was used as a comparison for the FFP purified fibrinogen.

The clottability assay involved mixing a 1:1 volume ratio of 50 µL of 1 mg/mL fibrinogen (in 20 mM HEPES, 150 mM sodium chloride, pH 7.4), and 50 µL of 0.1 U/mL thrombin (in 20 mM HEPES, 150 mM sodium chloride, 10 mM calcium chloride, pH 7.4); when combined, the final concentration was 0.5 mg/mL and 0.05 U/mL, respectively. Before preparing the fibrinogen samples used for the reaction, the concentration of the fibrinogen was measured using a UV-visible spectrometer. After sample mixing, the reactions were incubated at 37°C for 2 hours. Once finished, the reactions were centrifuged for 1 hour at 13,000 rpm to pellet the polymerized material. The supernatant that resulted from the centrifugation was measured with a UV-visible spectrometer. The percent difference between initial and final amounts of soluble fibrinogen was calculated as the percentage of clottable material.

The turbidity assay was performed at 37°C in triplicate on a 96-well plate. All fibrinogen samples were prepared at a concentration of 0.8 mg/mL at 75 µL/well and the thrombin sample was prepared at a concentration of 0.1 U/mL at 75 µL/well; when combined, the final

concentration was 0.4 mg/mL and 0.05 U/mL, respectively. The fibrinogen and the thrombin samples were prepared in the same buffers as described in the clottability assay. The thrombin solution was added simultaneously to each well using a multichannel pipette and readings were taken at 350 nm every minute for 1 hour using a Synergy™ HT multi-mode microplate reader (BioTek Instruments).

2.3 **Results**

2.3.1 *Transient Expression Tests*

We initiated transient transfection of both 3P and CSP systems using the HEK Expi293™ mammalian cell system for the expression of recombinant fibrinogen. Initial experiments focused on the difference in fibrinogen expression levels between the transfection reagents polyethylenimine (PEI), and ExpiFectamine™ 293. Cells transfected with the 3P system and either PEI (3:1 PEI:DNA) or ExpiFectamine™ 293 (2 µL per 1 µg DNA) were monitored daily for cell viability (Figure 2.5A/B respectively). After five days, cell viability began to drop, at which point the protein was harvested. Biological replicates (3P1 and 3P2 in Figure 2.5A/B) displayed similar results for both transfection reagents, with an initial increase in live cells (per volume) in subsequent days post-transfection, and a similar increase in dead cells (per volume), while maintaining an overall cell viability of ≥93% and ≥81% for the first four days (PEI and ExpiFectamine™ 293, respectively). Control wells with only transfection reagents (PEI and ExpiFectamine™ 293) showed comparable cell viability values (≥91% and ≥85%, respectively) for the first four days, while wells containing only cells displayed higher cell viability values (≥95% and ≥94%, respectively) for the first four days. Despite their similarities in cell viabilities, cells transfected with the 3P system using PEI provided higher live cell densities over the five days post-transfection (max 1.1×10^7 live cells/mL) than cells transfected with the 3P system

using ExpiFectamine™ 293 (max 2.7×10^6 live cells/mL). Protein expression levels on days 3–5 post-transfection were then assessed using sandwich ELISA assays (Figure 2.5C). Expression levels were statistically the same (*p* value of 0.89) for both transfection reagents (PEI max of 12.1 mg/L and ExpiFectamine™ max of 12.7 mg/L). In conjunction with our findings of lowered live cells (per volume) using ExpiFectamine™, we chose to use PEI as the transfection agent moving forward.

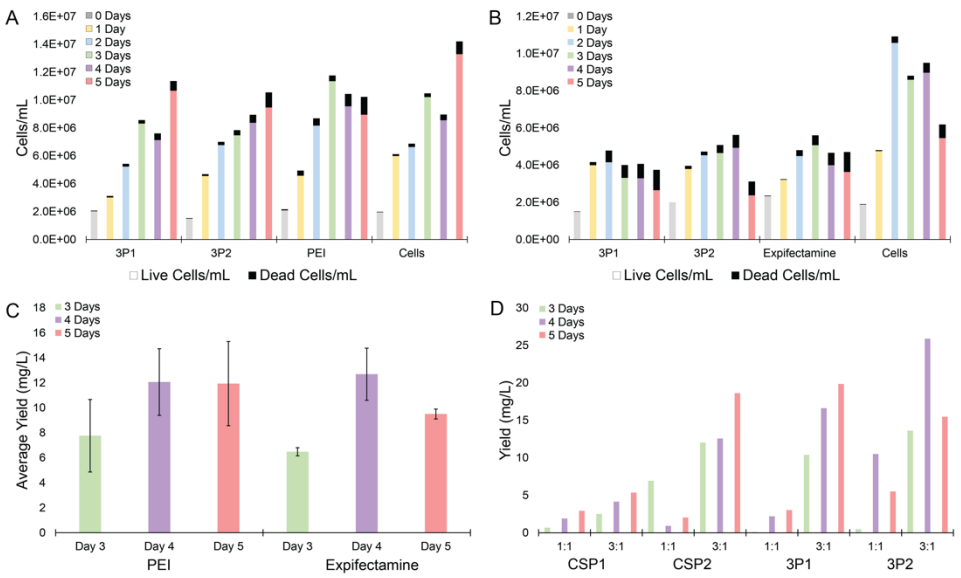

Figure 2.5: 6-well plate transfection cell viability and protein expression levels in HEK Expi293™ cells. Cell density values for the day of transfection and subsequent five days post-transfection of live (colored) and dead (black) cells transiently transfected with the 3P system using (A) PEI or (B) ExpiFectamine™. (C) ELISA assay results of average amount of protein harvested (mg/L) 3-5 days post-transfection from recombinant cells having used PEI or ExpiFectamine™. (D) ELISA assay results of protein harvested (mg/L) 3-5 days post-transfection from recombinant cells transfected with the CSP or 3P systems using a PEI:DNA ratio of 1:1 or 3:1.

The effectiveness of 3P and CSP expression plasmid systems was then compared using PEI:DNA ratios 1:1, and 3:1, with cell viability and protein expression levels monitored each day for five days (Figures 2.6A-C). Additionally, a 5:1 ratio was tested and found to produce comparable results to the 3:1 ratio for cell viability, and protein expression as determined from western blotting (Figure 2.6A&B). Biological replicates (3P1 and 3P2, CSP1 and CSP2) produced comparable results for all PEI:DNA ratios (Figure 2.6A). All wells exhibited similar growth patterns, with an initial increase and subsequent decrease or plateau in live cells (per

volume), while dead cells (per volume) values continually increased over five days post-transfection. For the 3P system, cell viability values were ≥97%, ≥94%, and ≥95% one day post-transfection for the 1:1, 3:1, and 5:1 ratios, respectively, and dropped to ≥56%, ≥71%, and ≥58% five days post-transfection (Figure 2.6A). For the CSP system, cell viability values were ≥95%, ≥92%, and ≥92% one day post-transfection for the 1:1, 3:1, and 5:1 ratios, respectively, and dropped to ≥88%, ≥65%, and ≥69% five days post-transfection (Figure 2.6A). The CSP wells at a 1:1 ratio showed the largest increase in cell density, while most other PEI:plasmid ratios showed comparable cell growth and viabilities.

Next, the protein expression was assessed at the different PEI:DNA ratios using sandwich ELISA assays. The 3:1 PEI:DNA ratio yielded elevated protein expression relative to the 1:1 ratio (Figure 2.5D), for both the 3P and CSP systems five days post-transfection. The protein yields were calculated as averages of 12 ± 9 mg/L, and approximately 18 ± 3 mg/L for the 3:1 ratio for CSP and 3P systems, respectively, while the 1:1 ratio for CSP and 3P systems gave fibrinogen yields of 2.5 ± 0.6 mg/L and 4 ± 2 mg/L, respectively. Next, using the 3:1 PEI:DNA ratio, we compared the expression levels of the 3P and CSP systems 3–5 days post-transfection (Figure 2.6C). The 3P system was found to give slightly higher protein expression levels relative to the CSP system (12 ± 3 mg/L and 8 ± 4 mg/L, respectively), although a drastic difference between systems was not observed. Since the CSP system was expected to produce higher protein levels, CSP-transfected cells were imaged using brightfield and fluorescence microscopy to assess if the expression efficiency was linked to transfection efficiency. The CSP encodes for a tdTomato fluorophore (Figure 2.1) that allows cells successfully transfected and expressing a fibrinogen Aα chain to fluoresce (Figure 2.6D). Cells incorporating the CSP system are shown in red. As shown in a representative microscopy image of cells transfected with CSP in Figure

2.6D, only 6 cells were fluorescent out of a total of 211, suggesting a low transfection efficiency for these transient cell lines.

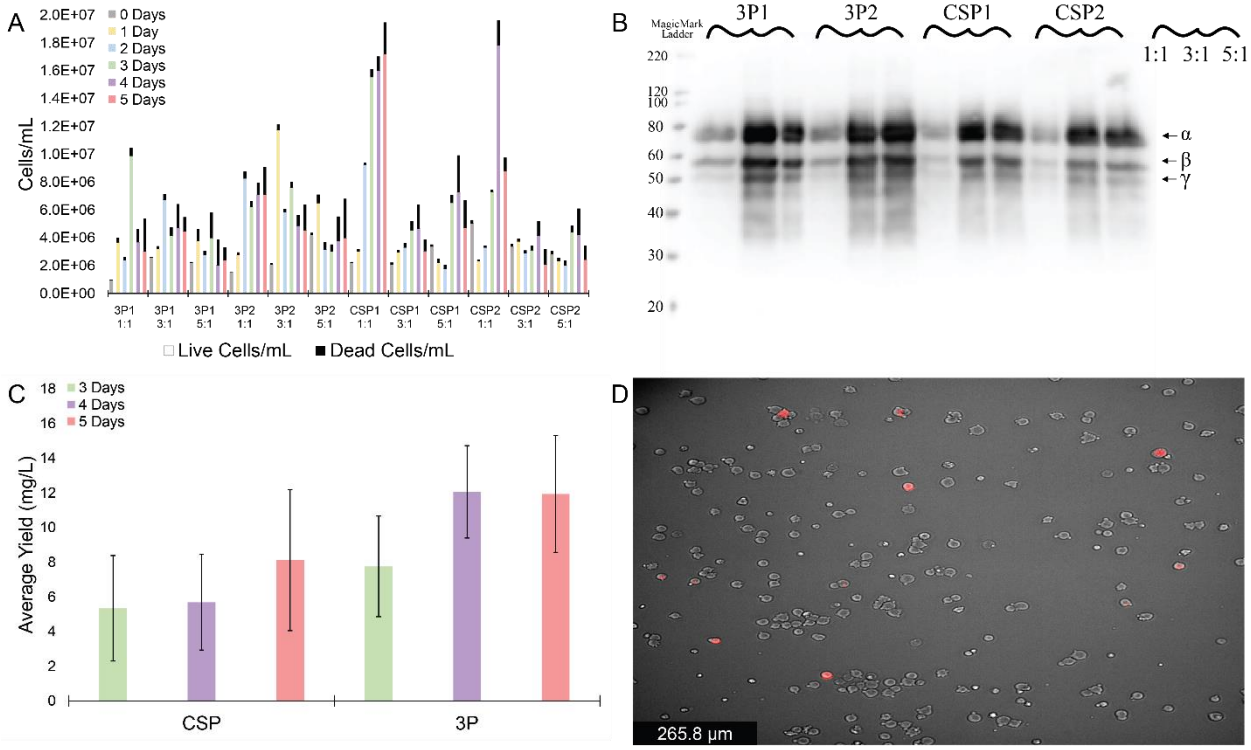

Figure 2.6: Cell viability and expression of the 3P and CSP systems using PEI. (A) Daily live (colored) and dead (black) cell counts for duplicate 3P and CSP expression systems at PEI:DNA ratios of 1:1, 3:1, and 5:1. (B) Western blot of protein expression for collected samples (3P1, 3P2, CSP1, and CSP2 at 1:1, 3:1, and 5:1 PEI:DNA ratios) 4 days post-transfection. (C) Sandwich ELISA assay average yields with standard error bars (mg/L; data taken from four experiments) for 3P and CSP expressions in HEK Expi293^{TM} cells transfected with 3:1 PEI:DNA ratio, 3–5 days post-transfection. (D) Representative fluorescence cell image of recombinant HEK Expi293^{TM} cells (red) among un-transfected cells (gray).

2.3.2 *Assessment of Peptide Affinity Purification*

An affinity chromatography column was developed through the coupling of a modified knob 'A'-mimic peptide, GPRPFPAWK, inspired by its enhanced affinity as compared to other common knob 'A'-mimics[18]. We initially tested the column's ability to capture fibrinogen using commercial purified fibrinogen (Peak 1 fibrinogen, Enzyme Research Labs). The results from the purification of Peak 1 fibrinogen (1 mg) with a 2 mL GPRPFPAWK peptide column are shown in a western blot in Figure 2.7A and depict a clear distribution of fibrinogen among different chromatography eluting steps. A negligible amount of protein was detected in the flow-through fractions during column loading (PF1–3 in Figure 2.7A). Although some fibrinogen was present in the wash phase fractions (W1–W5 in Figure 2.7A), protein was predominately found in the elution fractions collected (E1–E5 in Figure 2.7A). To validate the GPRPFPAWK column's specificity for fibrinogen, a 2 mL scramble peptide column (RPGPFAWPK) was constructed. Figure 2.7B shows the western blot for the protein distribution from the purification of Peak 1 fibrinogen (1.8 mg) with the scramble peptide column. The western blot shows that most of the protein was found in the flow-through (~66%) or wash (~23%) fractions, and little to no fibrinogen was detected in the elution fractions. These data validate the specificity of the GPRPFPAWK column towards fibrinogen capture. Next, we examined the reliability of the column after repeated purifications. A series of nine purification runs were conducted over nine separate days, each time with the same amount of fibrinogen (1 mg at 0.17 mg/mL) purified using a 2 mL GPRPFPAWK column, with the same number of fibrinogen collected for each of the steps. The amount of fibrinogen, determined spectrophotometrically, was nearly identical over the nine purifications for a defined purification step (Figure 2.7C)**.** These data demonstrate the reproducibility of the capture and elution of fibrinogen, with an average elution yield of 54 ± 4%.

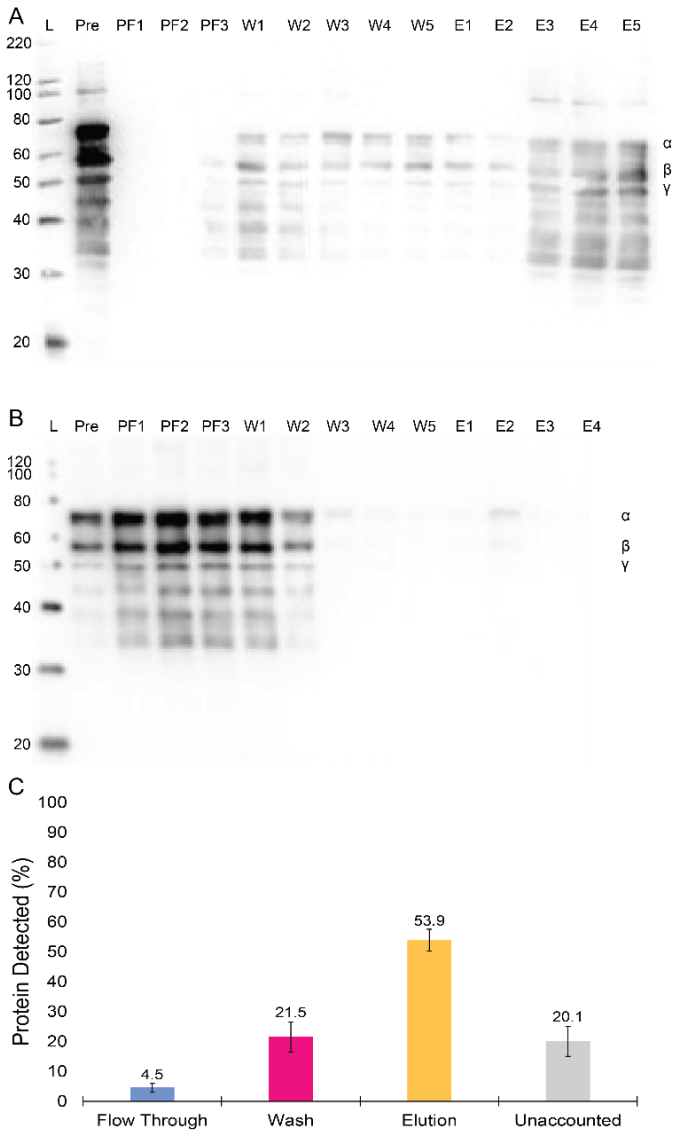

Figure 2.7: Assessment of selectivity and robustness of the GPRPFPAWK affinity column purification for Peak 1 fibrinogen. (A) Western blot showing fibrinogen before and after running over the GPRPFPAWK affinity column. Lane labels are as following: Ladder (L; kDa), the pre-column loading (Pre), and fractions from the column flow through (PF1–3), washes (W1–5), and elutions (E1–5). (B) Western blot showing fibrinogen before and after running over the RPGPFAWPK, scramble peptide column. Lane labels are the same as in (A). (C) Bar chart showing the average fibrinogen yields off the column over 9 separate runs with standard error bars shown.

2.3.3 *Fibrinogen Purification from Blood Plasma*

Having demonstrated fibrinogen capture and repeatability for the GPRPFPAWK affinity column, we examined its ability to purify fibrinogen selectively from a complex medium, fresh frozen human plasma (FFP), using the same 2 mL affinity column. Fractions collected from each major step in the chromatography process were assessed with Coomassie stained SDS-PAGE and western blot analysis (Figure 2.8A/B). From the western blot, fibrinogen was predominantly found in the elution steps. These data show that the column selectively purifies fibrinogen from plasma. From 2 mL of FFP added over the column, a combined 2.3 ± 0.4 mg was collected in the elution fractions, based on the ELISA assay. For comparison, an ELISA assay for fibrinogen content in the plasma estimated 3 mg, well within the estimated range of 1.5–4.2 g/L[20, 21]. Using these values, we estimate a ~75% recovery yield during the purification of fibrinogen from FFP with this GPRPFPAWK column.

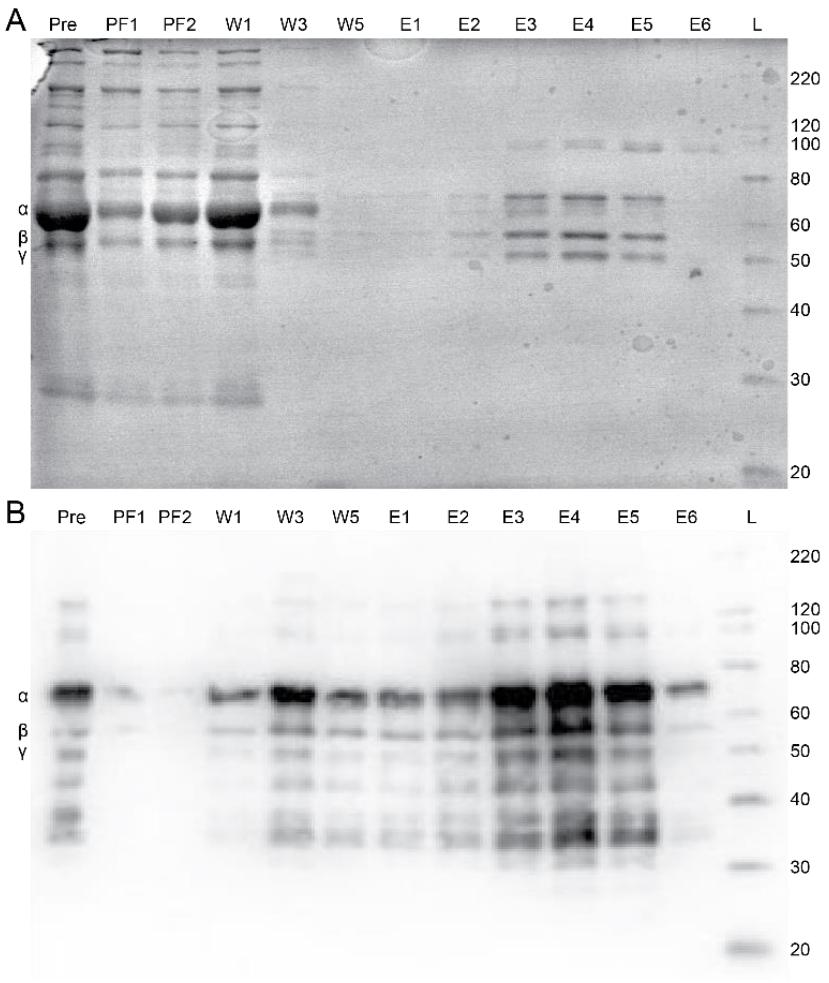

Figure 2.8: Selective purification of human fibrinogen from fresh frozen plasma with the GPRPFPAWK affinity column. (A) Coomassie and (B) Western blot images showing plasma proteins before and after running over the GPRPFPAWK affinity column, with similar eluting steps discussed in Figure 2.7. The Coomassie gel shows high selectivity for fibrinogen in the elution fractions.

2.3.4 *Assessing Plasma Purified Fibrinogen Functionality*

To further demonstrate the purity and functional integrity of the peptide-column isolated fibrinogen from human FFP, we initiated clotting by combining 0.05 U/mL thrombin and 0.5 mg/mL purified fibrinogen (final concentrations) to measure the clottability percentage. Clottability is the gold-standard for measuring functional integrity of fibrinogen and is

determined by the loss of soluble protein upon thrombin conversion of fibrinogen to insoluble fibrin. From this analysis, the fibrinogen isolated from plasma using the GPRPFPAWK column was found to be 86 ± 5% clottable, which is comparable to the commercial, highly-purified Peak 1 fraction from Enzyme Research Labs (Table 2.1). For reference, we also tested the clottability of the fibrinogen purified from FFP using the standard ethanol-based purification method that yielded a clottability of 80 ± 6%.

Table 2.1: Clottability values of fibrinogen purified by the GPRPFPAWK affinity column.

Fibrinogen Source	Clottability (%)
Peak 1 commercial[1]	84 ± 3
Plasma, Purified by GPRPFPAWK column	86 ± 5
Plasma, Purified by ethanol precipitation	80 ± 6

[1] Note that Enzyme Research Labs estimates ≥ 95% clottable for this Peak 1 fibrinogen. The difference between our value and the estimated value may be due to the uncertainty in determining the amount of protein at the endpoint.

To further evaluate the fidelity of the fibrinogen sample isolated from the GPRPFPAWK column, we monitored turbidity changes in the sample upon polymerization induced by thrombin. Turbidimetry is a complementary approach to clottability and monitors gel polymerization in real time through the change in scattering at 350 nm. The turbidity trace for the human fibrinogen sample isolated from FFP using the GPRPFPAWK column had a nearly identical lag phase and polymerization rate to that of the commercial Peak 1 fibrinogen (Figure 2.9). Taken together with clottability and the SDS-PAGE and western blot analysis (Table 2.1 and Figure 2.8), human fibrinogen isolated from plasma using our rapid GPRPFPAWK affinity column yielded a highly pure and functional form of fibrinogen that is comparable to commercial standards and is of better quality to that of standard isolation techniques.

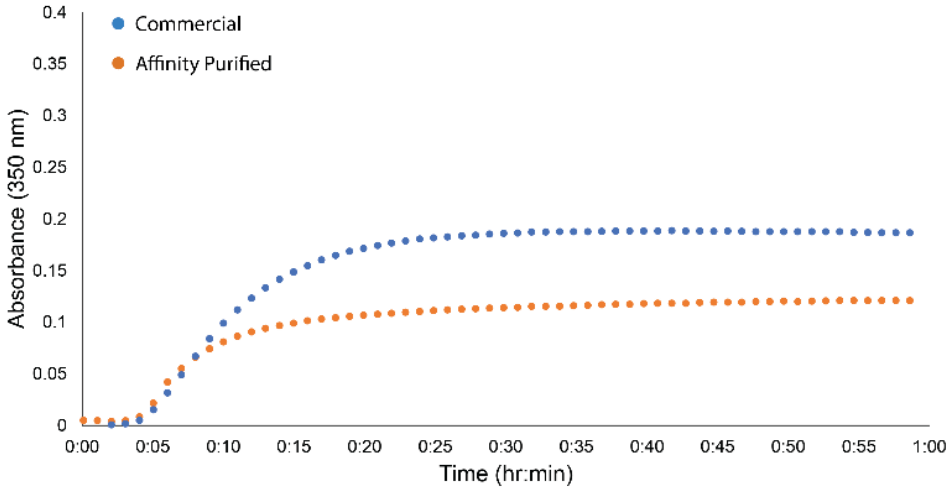

Figure 2.9: Turbidity of fibrinogen isolated from FFP using GPRPFPAWK affinity column. Representative turbidity traces from commercial samples (blue) and affinity purified samples (orange).

2.3.5 *Assessing New Deprotection and Purification from Blood Plasma Protocols*

The updated column utilizing the new deprotection step was then assessed on its ability to adequately purify functional fibrinogen from FFP. A 2 mL sample of FFP was run over the new 2 mL GPRP-based column and the amount of fibrinogen captured, determined spectrophotometrically, was found to be ~3.9 mg over four 1 mL elution fractions. These four elution fractions were then run through a size exclusion column for secondary purification from potential contaminants, and buffer exchange into a more suitable buffer for polymerization. The produced chromatogram displayed three single peaks, with one peak displaying a much larger UV signal thought to contain the purified fibrinogen (Figure 2.10A). Coomassie gel and western blot imaging of each of the single peaks showed highly pure fibrinogen in comparison to the reference peak 1 commercial fibrinogen bands for SEC fraction 8-14, whereas SEC fractions 19-20 and 46-47 were determined to have negligible amounts of fibrinogen (Figure 2.10). An ELISA for fibrinogen content in SEC fractions 9-13 estimated 3.2 mg captured, showing a ~50%

isolation from the ELISA values for a pre-flow sample (~6.7 mg). Finally, clottability of the purified fibrinogen was assessed and found to be 98.6 ± 0.4% clottable, which is comparable to the commercial, highly-purified Peak 1 fraction from Enzyme Research Labs value of 98.9 ± 0.2% clottable.

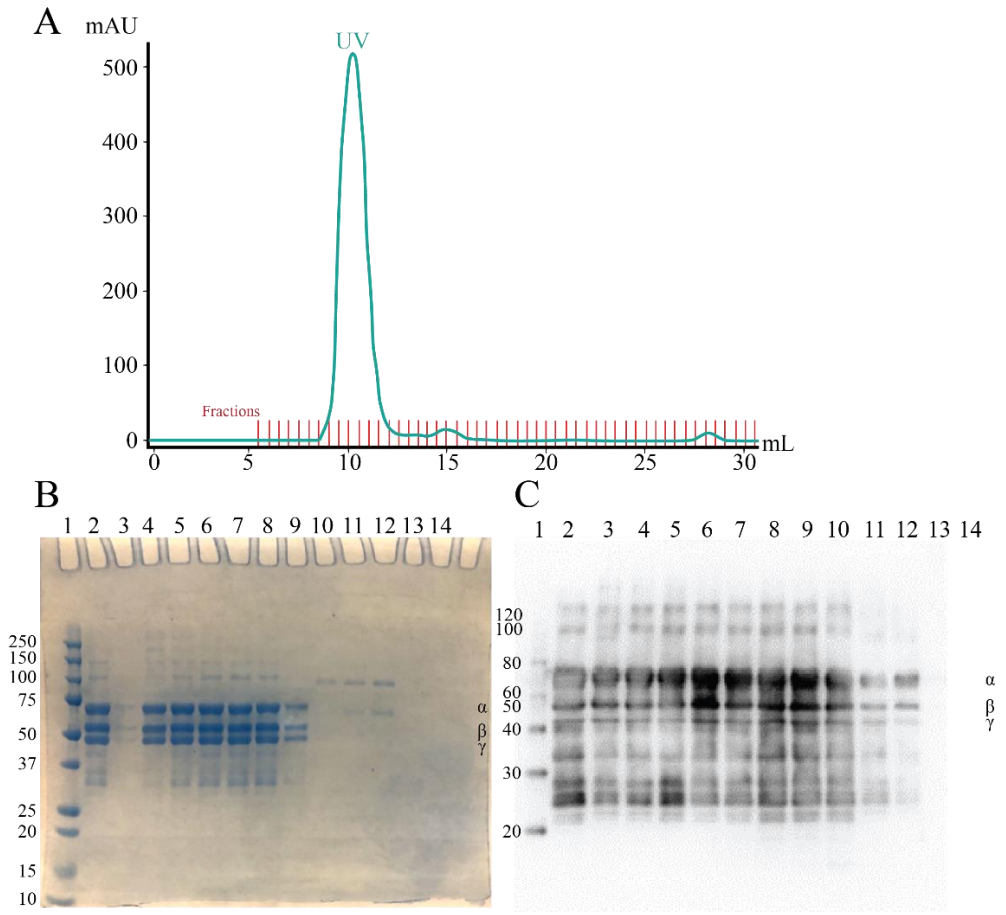

Figure 2.10: Assessing SEC fibrinogen plasma purification. (A) Fast protein liquid chromatogram of combined elution fractions from GPRP-based affinity chromatography, showing one dominant UV peak from fractions 8-14, and smaller peaks near fraction 22, and 46 (negligent peaks as determined by (B) Coomassie gel and (C) western blot). Labels for Coomassie gel and western blot are the same: 2 = Peak 1 commercial fibrinogen, 3-10 = SEC fractions 8-15, 11-12 = SEC fractions 19-20, and 13-14 = SEC fractions 46-47; except for label 1 in (B) is Precision Plus^{TM} All Blue protein standard and in (C) is MagicMark^{TM} protein standard.

2.4 **Discussion**

The first successful demonstration for expressing and isolating recombinant fibrinogen using stable cell lines was undertaken at Susan T. Lord's laboratory where they established the use of adherent CHO cells in a roller bottle system using a two-step procedure with a two-plasmid system[3]. More recently, several companies have established stable fibrinogen expression systems. The Chemo-Sero-Therapeutic Research Institute used stably transfected CHO cells with a novel single plasmid encoding a single copy of genes for the Aα and Bβ chains and two copies of the γ chain in their fibrinogen system. Using suspension CHO DG44 cells, they reported high yields of expressed fibrinogen (up to 1.4 g/L)[4]. The company Fibriant developed a recombinant protein expression system that involved separate plasmids for each of the Aα, Bβ, and γ chains. Plasmids were co-transfected into a PER.C6 cell line and fibrinogen was then purified using ion exchange chromatography[22]. However, both of these companies exclusively create wild-type fibrinogen for therapeutic purposes, and the expense of CHO DG44 and PER.C6 cells makes them inaccessible to most academic labs. Thus, there is an important need for creating high-yield recombinant fibrinogen systems that will enable structure–function studies of fibrinogen variants.

Here we report initial results in establishing a transient recombinant fibrinogen system for human fibrinogen using HEK Expi293™ cells. While transient fibrinogen expression was used in initial studies of the creation of recombinant protein to assess pathways of fibrinogen assembly[23] there have been no studies assessing and optimizing transient fibrinogen expression as a tool for functional studies of this globular protein. We tested two different plasmid systems, 3P and CSP, and two separate methods of transfection, PEI and ExpiFectamine™. In comparing PEI- and ExpiFectamine™-based expression levels, we were surprised to find little difference

between these two methods for the 3P system, with PEI producing a maximum expression of 12 mg/L and ExpiFectamine™ producing a maximum expression of approximately 13 mg/L. This is in apparent contrast to some protein systems[24], however, another study comparing the expression of antibodies using PEI Max and ExpiFectamine™ also found comparable yields between the two approaches (7 vs. 13 mg/L)[25]. The large difference in cost between the two approaches, PEI Max for approximately USD 20/L and ExpiFectamine™ for approximately USD 1000/L, strongly favors the use of PEI Max for future studies. Though we did not test the CSP system using ExpiFectamine™, this plasmid may produce higher yields and may warrant future study. Testing fibrinogen yields at different PEI:DNA ratios showed that a 3:1 ratio provided the highest protein yields for both the 3P and CSP systems, even though cell densities were sometimes higher at a 1:1 ratio. This suggests that transfection efficiencies were likely lower at the 1:1 ratio. Next, comparing the CSP and 3P systems using a 3:1 PEI:DNA ratio, we found that the 3P system produced higher protein yields. Moreover, as the CSP plasmid encoded a tdTomato fluorophore, we assessed transfection efficiency for this plasmid using fluorescence microscopy. We found that only 3–5% of cells were fluorescent, suggesting a low transfection efficiency. This is likely due to the size of the plasmid (17,190 bp). Encoding a tdTomato tag in the plasmid also enables the possibility for fluorescence-based cell sorting. Future tests will attempt to isolate fluorescence-positive cells using the CSP system to increase protein yields.

Taken together, our results indicate that HEK Expi293™ cells can transiently produce modest levels of fibrinogen, comparable to expression levels originally reported by the Lord laboratory for a stable CHO-cell based expression system[3, 26, 27]. Our transient fibrinogen yields were below more recent stable-cell based expression system yields[4, 22], suggesting that if large

amounts of fibrinogen are desired, a stable cell system may be required. Additional optimization methods and testing other suspension cell lines may increase transient protein yields.

Further assessing the cost-effectiveness of our transient expression system, we created an approximate expense report based on our experimental setup comparing transfection reagents and plasmid systems (Table 2.2). Multiple ELISA concentration values for samples taken five days post-transfection were averaged together to obtain a yield in mg/L for our transient system (Table 2.2A). The most pertinent expenses were then determined and included the cost of transfection reagents, media, and labor. Transfection reagent cost was calculated using 20 USD/L for PEI and 1000 USD/L for ExpiFectamine™, and the estimated price to obtain 10 mg based on the average yield for each condition. Media cost (Expi293™ expression media at $328/L) for the transient system included media usage for starting a cell line, sub-culturing for three passages, initial (200 mL) and final (1 L) scaling up of the system for transfection, daily sample collection, and one ELISA (1.334 L total media usage). Labor cost was evaluated by summing the approximate active time spent on the total process (31 hours) divided by four weeks to obtain hours worked per week, and multiplying by the average hourly salary for a graduate student ($16.66/hour). Total expense summed all transfection reagent, media, and labor costs and was used to gauge the price/mg of protein expressed for each condition. It is clear from this that PEI at a 3:1 ratio was the most cost-effective solution, with both plasmid systems producing similar results.

These findings were then compared to a theorized similar cost breakdown for stable expression systems using the same transfection reagents and plasmids (Table 2.2B). Yields for each condition were estimated to be 2.5 times great than transient yields. Transfection reagent cost was similarly calculated using 20 USD/L for PEI and 1000 USD/L for ExpiFectamine™,

however, the price was based on their usage for an initial 6 well-plate transfection rather than a 1 L culture batch. Media cost included the usage of either Expi293™ expression media (136 mL at $328/L) or Dulbecco's modified eagle medium + fetal bovine serum (448 mL at $408/L), antibiotics (20% of neomycin at $170, puromycin $332, and hygromycin at $243 for 3P, and only neomycin for CSP), and cell sorting sessions (2 sessions with $40 for setup and $145 for sorting). Labor cost was evaluated by summing the approximate active time spent on the total process (105 hours) divided by eighteen weeks to obtain hours worked per week, and multiplying by the average hourly salary for a graduate student ($16.66/hour). Total expense again summed all transfection reagent, media/antibiotic/sorting, and labor costs and was used to gauge the price/mg of protein expressed for each condition. Similar trends were produced with PEI at a 3:1 ratio as the most cost-effective solution for both plasmid systems. Comparing transient vs. stable cost breakdowns, we are given very similar price/mg expenses for all conditions, other than ExpiFectamine^{TM} which gave noticeably better results for the theorized stable system. Analyzing the expense report as a whole, the main difference between transient and stable systems was found to be the total expense, which favors transient expression with lower costs for all conditions. Additionally, the transient system is similarly cost-effective for producing fibrinogen, with a much shorter timescale for expression (4 vs. 18 weeks). In total, this breakdown reassures our efforts towards using the tdTomato fluorophore of our CSP for fluorescent cell sorting to establish our own stable expression system with a similar cost-effectiveness compared to our above established transient expression system for human fibrinogen.

Table 2.2: Cost breakdown of each experimental condition for both our transient and a theorized stable expression system. (A) Transient transfection expenses reporting price per mg of expressed fibrinogen for the 3P system using either ExpiFectamine™ or PEI at ratios of 1:1 and 3:1, and for the CSP system using PEI at ratios of 1:1 and 3:1. (B) Theorized stable transfection expenses reporting price per mg of expressed fibrinogen for the 3P system using either ExpiFectamine™ or PEI at ratios of 1:1 and 3:1, and for the CSP system using PEI at ratios of 1:1 and 3:1.

A Transient Transfection Cost Breakdown

Plasmid	Transfection Reagent	Ratio (Reagent:Plasmid)	Days Post-Transfection	Average Yield (mg/L)	Transfection Reagent Expense ($/L)	Media Expense ($/L)	Labor Expense ($/week)	Number of Weeks	Total Expense ($/L)	Yield Expense ($/mg)
3P	PEI	1:1	5	4.26	46.93	437.55	129.12	4	1000.95	234.89
		3:1		15.72	12.72				966.73	63.66
CSP		1:1	5	2.47	80.99				1035.00	405.34
		3:1		13.67	14.63				968.64	73.22
3P	Expifectamine	2 µL/1 µg DNA	5	11.73	852.32	437.55	129.12	4	1806.33	153.96

B Stable Transfection Cost Breakdown

Plasmid	Transfection Reagent	Ratio (Reagent:Plasmid)	Days Post-Transfection	Theorized Yield (mg/L)	Transfection Reagent Expense ($/L)	Media + Antibiotics + Sorting Expenses ($/L)	Labor Expense ($/week)	Number of Weeks	Total Expense ($/L)	Yield Expense ($/mg)
3P	PEI	1:1	5	10.65	0.00025	746.39	97.18	18	2495.69	234.27
		3:1		39.31	0.00075				2495.69	63.49
CSP		1:1	5	6.17	0.00025	631.39			2380.69	385.63
		3:1		34.18	0.00075				2380.69	69.66
3P	Expifectamine	2 µL/1 µg DNA	5	29.33	7.41	746.39	97.18	18	2503.10	85.34

To complement the development of a rapid expression system for recombinant fibrinogen, we have also presented herein a novel affinity purification method for rapid protein isolation from complex media. The two most common methods of isolating fibrinogen either involve precipitation or affinity purification. Precipitation approaches involve either using ethanol, ammonium sulfate, polyethylene glycol (PEG) or cryoprecipitation, to remove fibrinogen from solution. These approaches, however, require large amounts of plasma[12]. Prior affinity-based approaches for purifying fibrinogen used either immobilized proteins, such as clumping factor A (clfA)[13] or peptides, such as GPRPK[14], that specifically bind fibrinogen. In this chapter, a novel peptide column using a fibrin knob 'A'-mimic peptide, GPRPFPAWK, coupled to NHS-activated Sepharose beads, was introduced as a faster and more efficient way of purifying fibrinogen from

solution and human fresh frozen plasma. The peptide was designed and optimized for binding fibrinogen[18], making it ideal for affinity purification.

Isolating fibrinogen from plasma using one of the precipitation methods typically follows a similar procedure, often involving several time-consuming rounds of precipitation and centrifugation resulting in the fractionation of plasma proteins. For example, in the case of cryoprecipitation[12], fresh frozen plasma must be left in a −80°C freezer for 12 hours, and then thawed for several hours before a 15 min centrifugation at 1000*xg* creates a fibrinogen pellet. The process recovers roughly 40% of the original fibrinogen. Precipitation methods typically require large quantities of FFP, have a maximum recovery of about 60%, result in relatively low purity fibrinogen, and can often be quite slow[14], although multi-step procedures involving sequential precipitation with different precipitants have been reported that can result in high-purity fibrinogen[28].

Previous attempts have been made to purify fibrinogen using affinity chromatography by immobilizing proteins or peptides to Sepharose beads. One of these methods used clfA immobilized to glutathione-conjugated Sepharose beads, which targeted the C-terminus of the fibrinogen γ chain[13]. ClfA-based purification of fibrinogen from plasma resulted in yields of 6 mg of fibrinogen per 8 mL of plasma, which is roughly 19–38% recovery in a total time of about two hours. While this method produced rapid purification, it required the clfA protein, tedious regeneration of the column each run by removing the clfA using 10 mM glutathione, and resulted in small amounts of clfA contamination in the isolated fibrinogen sample.

An affinity method using a non-affinity optimized knob ‘A’-mimic peptide (GPRPK) has also been previously reported[14]. The peptide was immobilized on Fractogel TSK AF-CDI 650 contained in a glass column. The capacity of the column was 8–10 mg of plasma per mL of the

wet gel, at a loading flow rate of 6 mL/hour. However, the authors reported that up to 4 mg of plasma per mL bound to a Fractogel column without peptide. The method required fairly harsh elution buffers, such as triethanolamine (TEA) buffer at neutral pH containing 2–6 M urea, or acetate buffer, pH 4.5 with 2 M urea, and thus required "extensive dialysis" after elution. After dialysis, the clottability of the fibrinogen ranged from 78–92%.

In our methods, we used an enhanced GPRPFPAWK peptide, selected from a library of GPRP knob mimics, for high affinity to fibrinogen[18]. Comparing purification runs using the GPRPFPAWK peptide vs. a scramble peptide RPGPFAWPK (Figure 2.7) showed that the high affinity peptide column was specific to fibrinogen and that the binding was likely associated with the GPRP motif. This is in contrast to previously utilized Fractogel GPRP column in which nearly half of the fibrinogen bound to the Fractogel alone, albeit more weakly[14].

We next assessed the repeatability of the column and found little to no degradation in performance for nine independent purifications using the same column. The average fibrinogen elution yield in these tests, which used fibrinogen at fairly low concentrations (1 mg at 0.17 mg/mL) was 54 ± 4%, which is comparable to, if not better than other precipitation and affinity-based approaches.

We then assessed the ability of the column to isolate fibrinogen from FFP. Figure 2.8 shows purity of the elution fractions as compared to all the proteins in the initial plasma sample, demonstrating that the GPRPFPAWK peptide column can isolate fibrinogen from a complex media. Using an ELISA assay to quantify the fibrinogen in the plasma and the elution fractions, we determined that the column captured and eluted approximately 75% of the fibrinogen loaded onto the column. This was surprisingly higher than the column's capture efficiency for commercial fibrinogen (Figure 2.7C). The differences in results could have arisen from the

higher concentration of fibrinogen in plasma (~1.5 g/L) than in our purified fibrinogen tests (0.17 g/L). Lifetimes of the GPRPFPAWK-fibrinogen interaction are roughly 10–500 seconds (based on the reported off-rates for GPRPFPAC[18]), thus having a shorter time of fibrinogen on the column, which occurs when the protein is loaded at higher concentrations, could be linked to the increased protein yields.

To confirm protein functionality from the GPRP-based affinity column, we subjected plasma-purified fibrinogen to turbidity and clottability tests. The clottability was comparable to fibrinogen purchased from Enzyme Research Labs. Our clottability estimates are likely lower bounds as the method required taking solution spectra before clotting and after clotting when the sample has been centrifuged for an hour. Spectra before clotting had 260/280 ratios of approximately 0.6, while spectra after clotting and centrifugation typically had ratios higher than 0.6, perhaps due to scattering from low quantities of remaining polymerized material. Turbidity curves of affinity purified fibrinogen also had similar lag phases and slopes to the commercial grade fibrinogen, suggesting similar polymerization kinetics. Small differences in max absorbance likely come from a slight mismatch in concentrations between the samples or slight differences in the posttranslational modifications of the FFP sample. Early reports have shown that fibrinogen samples linked to specific disease types (e.g., congenital dysfibrinogenemia) exhibit altered turbidity traces due to alterations in the structure of the protein and/or glycosylation[29, 30]. Future studies will be aimed at resolving the link between the glycosylation architecture and fibrinogen structure–function as well as studying the molecular origins of hypo- and dysfibrinogenemias[31-34].

Thus, the results show that a GPRPFPAWK peptide-based affinity column enables the rapid and effective purification of fibrinogen from complex media. This affinity-based method,

including a buffer exchange using a PD-10 column (or size exclusion chromatography in place of PD-10 column usage), is significantly faster than other reported methods (the purification in its entirety can be completed in under 4.5 hours). The method purifies 50–75% of available fibrinogen from a solution, which is better than many other purification methods. The fibrinogen obtained from this method, without any further polishing steps, has a clottability of ≥85% (≥98% for SEC adaptation), and turbidity curves appear similar to commercial preparations. Finally, the column can be used to purify as little as 2 mL of plasma, which is a significant advancement over other purification methods for fibrinogen structure–function studies of samples acquired to examine fibrinogen-linked diseases in human patient studies.

2.5 **Conclusion**

In total, this chapter shows that fibrinogen can be expressed transiently with yields comparable to those reported earlier from stable cell lines, and purified from complex media using a GPRPFPAWK-based peptide affinity column. Fibrinogen purified from this fibrinogen-specific, and robust column is shown to be highly clottable without any polishing. These results enable future studies of both recombinant and plasma-purified fibrinogen looking at structure–function relationships in fibrinogen molecules containing different glycoforms and from patients suffering from various dysfibrinogenemias.

References

1. Popovic, G.; Kirby, N. C.; Dement, T. C.; Peterson, K. M.; Daub, C. E.; Belcher, H. A.; Guthold, M.; Offenbacher, A. R.; Hudson, N. E., Development of Transient Recombinant Expression and Affinity Chromatography Systems for Human Fibrinogen. *International Journal of Molecular Sciences* **2022,** *23* (3), 1054.

2. Assenberg, R.; Wan, P. T.; Geisse, S.; Mayr, L. M., Advances in recombinant protein expression for use in pharmaceutical research. *Current opinion in structural biology* **2013,** *23* (3), 393-402.

3. Binnie, C. G.; Hettasch, J. M.; Strickland, E.; Lord, S. T., Characterization of purified recombinant fibrinogen: partial phosphorylation of fibrinopeptide A. *Biochemistry* **1993,** *32* (1), 107-113.

4. Hirashima, M.; Imamura, T.; Yano, K.; Kawamura, R.; Meta, A.; Tokieda, Y.; Nakashima, T., High-level expression and preparation of recombinant human fibrinogen as biopharmaceuticals. *The Journal of Biochemistry* **2016,** *159* (2), 261-270.

5. Boshart, M.; Weber, F.; Jahn, G.; Dorsch-H, K.; Fleckenstein, B.; Schaffner, W., A very strong enhancer is located upstream of an immediate early gene of human cytomegalovirus. *cell* **1985,** *41* (2), 521-530.

6. Watanabe, S.; Watanabe, S.; Sakamoto, N.; Sato, M.; Akasaka, K., Functional analysis of the sea urchin-derived arylsulfatase (Ars)-element in mammalian cells. *Genes to Cells* **2006,** *11* (9), 1009-1021.

7. Jun-ichi, M.; Satoshi, T.; Kimi, A.; Fumi, T.; Akira, T.; Kiyoshi, T.; Ken-ichi, Y., Expression vector system based on the chicken β-actin promoter directs efficient production of interleukin-5. *Gene* **1989,** *79* (2), 269-277.

8. Deer, J. R.; Allison, D. S., High-level expression of proteins in mammalian cells using transcription regulatory sequences from the Chinese hamster EF-1α gene. *Biotechnology progress* **2004,** *20* (3), 880-889.

9. Carswell, S.; Alwine, J. C., Efficiency of utilization of the simian virus 40 late polyadenylation site: effects of upstream sequences. *Molecular and Cellular Biology* **1989,** *9* (10), 4248-4258.

10. Kozak, M., An analysis of 5'-noncoding sequences from 699 vertebrate messenger RNAs. *Nucleic acids research* **1987,** *15* (20), 8125-8148.

11. Kozak, M., Point mutations define a sequence flanking the AUG initiator codon that modulates translation by eukaryotic ribosomes. *Cell* **1986,** *44* (2), 283-292.

12. Brennan, M., Fibrin glue. *Blood reviews* **1991,** *5* (4), 240-244.

13. Liu, C.-Z.; Cheng, H.-J.; Chang, L.-Y., A new feasible method for fibrinogen purification based on the affinity of Staphylococcus aureus clumping factor A to fibrinogen. *Protein expression and purification* **2008,** *61* (1), 31-35.

14. Kuyas, C.; Haeberli, A.; Walder, P.; Straub, P., Isolation of human fibrinogen and its derivatives by affinity chromatography on Gly-Pro-Arg-Pro-Lys-Fractogel. *Thrombosis and haemostasis* **1990,** *63* (03), 439-444.

15. Gibson, D. G.; Young, L.; Chuang, R.-Y.; Venter, J. C.; Hutchison III, C. A.; Smith, H. O., Enzymatic assembly of DNA molecules up to several hundred kilobases. *Nature methods* **2009,** *6* (5), 343-345.

16. Bzymek, M.; Lovett, S. T., Instability of repetitive DNA sequences: the role of replication in multiple mechanisms. *Proceedings of the National Academy of Sciences* **2001,** *98* (15), 8319-8325.

17. Schindelin, J.; Arganda-Carreras, I.; Frise, E.; Kaynig, V.; Longair, M.; Pietzsch, T.; Preibisch, S.; Rueden, C.; Saalfeld, S.; Schmid, B., Fiji: an open-source platform for biological-image analysis. *Nature methods* **2012,** *9* (7), 676-682.

18. Stabenfeldt, S. E.; Gossett, J. J.; Barker, T. H., Building better fibrin knob mimics: an investigation of synthetic fibrin knob peptide structures in solution and their dynamic binding with fibrinogen/fibrin holes. *Blood, The Journal of the American Society of Hematology* **2010,** *116* (8), 1352-1359.

19. Doolittle, R.; Schubert, D.; Schwartz, S., Amino acid sequence studies on artiodactyl fibrinopeptides: I. Dromedary camel, mule deer, and cape buffalo. *Archives of Biochemistry and Biophysics* **1967,** *118* (2), 456-467.

20. Simurda, T.; Asselta, R.; Zolkova, J.; Brunclikova, M.; Dobrotova, M.; Kolkova, Z.; Loderer, D.; Skornova, I.; Hudecek, J.; Lasabova, Z., Congenital afibrinogenemia and hypofibrinogenemia: Laboratory and genetic testing in rare bleeding disorders with life-threatening clinical manifestations and challenging management. *Diagnostics* **2021,** *11* (11), 2140.

21. Neerman-Arbez, M.; Casini, A., Clinical consequences and molecular bases of low fibrinogen levels. *International journal of molecular sciences* **2018,** *19* (1), 192.

22. Piechocka, I.; Kurniawan, N.; Grimbergen, J.; Koopman, J.; Koenderink, G., Recombinant fibrinogen reveals the differential roles of α-and γ-chain cross-linking and molecular heterogeneity in fibrin clot strain-stiffening. *Journal of Thrombosis and Haemostasis* **2017,** *15* (5), 938-949.

23. Hartwig, R.; Danishefsky, K., Studies on the assembly and secretion of fibrinogen. *Journal of Biological Chemistry* **1991,** *266* (10), 6578-6585.

24. da Silva Junior, H. C., Transient Gene Expression in Human Expi293 Cells. In *Insoluble Proteins: Methods and Protocols*, Springer: 2022; pp 319-325.

25. Fang, X. T.; Sehlin, D.; Lannfelt, L.; Syvänen, S.; Hultqvist, G., Efficient and inexpensive transient expression of multispecific multivalent antibodies in Expi293 cells. *Biological procedures online* **2017,** *19* (1), 1-9.

26. Gorkun, O. V.; Veklich, Y. I.; Weisel, J. W.; Lord, S. T., The conversion of fibrinogen to fibrin: recombinant fibrinogen typifies plasma fibrinogen. *Blood, The Journal of the American Society of Hematology* **1997,** *89* (12), 4407-4414.

27. Gorkun, O. V.; Henschen-Edman, A. H.; Ping, L. F.; Lord, S. T., Analysis of Aα251 fibrinogen: the αC domain has a role in polymerization, albeit more subtle than anticipated from the analogous proteolytic fragment X. *Biochemistry* **1998,** *37* (44), 15434-15441.

28. Blomback, B.; Blomback, M. In *Purification of bovine and human fibrinogen*, ACTA CHEMICA SCANDINAVICA, MUNKSGAARD INT PUBL LTD 35 NORRE SOGADE, PO BOX 2148, DK-1016 COPENHAGEN …: 1956; pp 147-147.

29. OKUDE, M.; YAMANAKA, A.; MORIMOTO, Y.; AKIHAMA, S., Sialic acid in fibrinogen: effects of sialic acid on fibrinogen-fibrin conversion by thrombin and properties of asialofibrin clot. *Biological and Pharmaceutical Bulletin* **1993,** *16* (5), 448-452.

30. Riedelová-Reicheltová, Z.; Kotlín, R.; Suttnar, J.; Geierová, V.; Riedel, T.; Májek, P.; Dyr, J. E., A novel natural mutation AαPhe98Ile in the fibrinogen coiled-coil affects fibrinogen function. *Thrombosis and haemostasis* **2014,** *111* (01), 79-87.

31. Bowley, S. R.; Okumura, N.; Lord, S. T., Impaired protofibril formation in fibrinogen γN308K is due to altered D: D and "A: a" interactions. *Biochemistry* **2009,** *48* (36), 8656-8663.

32. Simurda, T.; Vilar, R.; Zolkova, J.; Ceznerova, E.; Kolkova, Z.; Loderer, D.; Neerman-Arbez, M.; Casini, A.; Brunclikova, M.; Skornova, I., A novel nonsense mutation in FGB (c. 1421G> A; p. Trp474Ter) in the beta chain of fibrinogen causing hypofibrinogenemia with bleeding phenotype. *Biomedicines* **2020,** *8* (12), 605.

33. Castaman, G.; Giacomelli, S. H.; Biasoli, C.; Contino, L.; Radossi, P., Risk of bleeding and thrombosis in inherited qualitative fibrinogen disorders. *European journal of haematology* **2019,** *103* (4), 379-384.

34. Simurda, T.; Zolkova, J.; Kolkova, Z.; Loderer, D.; Dobrotova, M.; Skornova, I.; Brunclíkova, M.; Grendar, M.; Lasabova, Z.; Stasko, J., Comparison of clinical phenotype with genetic and laboratory results in 31 patients with congenital dysfibrinogenemia in northern Slovakia. *International Journal of Hematology* **2020,** *111*, 795-802.

Chapter 3

Improvement of Fibrinogen Cryo-EM Model Resolution

3.1 **Introduction**

3.1.1 *Static Model of a Dynamic Protein: Fibrinogen Structural Determination*

Utilizing the traditional methods of x-ray crystallography and electron microscopy, researchers have gathered a great deal of information on the structure of fibrinogen[1, 2]. The trinodular structure of fibrinogen first confirmed by electron microscopy (EM)[2] describes nodous fibrinogen filaments (like strings on a bead), which are now known as the globular β- and γ-nodules of the D region, as well as the E region containing the N-termini of all six polypeptide chains. X-ray crystallography of fibrinogen has led to further analysis of these regions with a 3.3 Å resolution overall structure of human fibrinogen[1], and higher resolution structures of the more rigid globular domains (D fragment, γ-γ dimer, and E fragment)[3-7].The requirement of crystallization has presented a more static model of fibrinogen (planar-sigmoidal shape), despite most studies noting an intrinsic flexibility about fibrinogen's central E and coiled-coil regions that lead to a lack of electron density in those areas. Additional areas of flexion/disorder predominantly include the highly dynamic αC-connector, portions of the N-termini of all three chains and the C-termini of Bβ and γ chains as first discussed in Chapter 1, and residues along the coiled-coil region. Methods able to discern the flexible features of fibrinogen are needed in order to better understand this conformationally dynamic protein, and the roles these modifications may have on the overarching properties of fibrinogen in immunity or hemostasis. Cryogenic electron microscopy (cryo-EM) is one such method for more natural state structural determination with the ability to depict heterogeneous structures or inherent flexibility of conformationally dynamic molecules like fibrinogen.

3.1.2 *Understanding Cryogenic Electron Microscopy*

3.1.2.1 Electron Microscopy

Optical microscopy uses visible light, which limits the resolution of images to >175 nm. Electron microscopy was thus developed to enhance the resolution of imaging, as electrons have wavelengths 100,000 times shorter than light. With an inverse dependence on wavelength, resolution for electron microscope images can reach near-atomic values (<4 Å). Transmission electron microscopy (TEM) utilizes a condensed beam of electrons focused onto a specimen to obtain an electron density from the diffraction pattern of the electrons scattered by the sample[8]. Specifically, TEM gathers information about a sample's structure from a lack of electrons reaching direct electron detectors (DED), which is understood as elastic scattering due to a sample's composition. A sub-technique of TEM, negative-stain EM, provides high contrast images at modest resolution by heavy metal salt layer application to the sample, leading to a high signal-to-noise ratio[9]. This common technique serves as an adequate initial step towards structural determination, as it is rather inexpensive and easy to conduct due to a lack of specific imaging conditions. Capitalizing on the ability of EM to provide adequate structural information, while also allowing for native state imaging, cryo-EM was selected for the structural determination of fibrinogen. Whereas negative stain EM requires sample dehydration, cryo-EM utilizes vitrification (flash-freezing in non-crystalline water) of the sample in an aqueous environment[9]. This process preserves the natural state of specimens, diminishes the effect of radiation damage, is relatively instant compared to the days required to crystalize samples for x-ray crystallography[1], and enhances viewing distributions by freezing specimens in random orientations. Lowered conformational specificity brought on by sample vitrification can highlight other natural state conformations of specimens that exhibit flexibility, opening/closing of

subunits, or binding/unbinding of ligands. Although, high degrees of flexibility can cause lowered resolution capabilities as multiple conformations are averaged together and diminish congruency.

3.1.2.2 Cryo-EM Sample Preparation

The level of resolution required to afford highly-defined structural information for biological samples like fibrinogen, necessitates sample properties, preparation, and imaging to be appropriately established[9]. Sample preparation depends on the molecule of interest, but always focuses on homogenizing the sample as much as possible by biochemical means. Heterogeneity can come from compositional (subunit presence or absence) or conformational (different flexible states of a molecule) variation, which can be addressed with optimal buffer conditions and/or limiting the available molecular conformations, respectively[9]. Homogenized samples were added onto TEM mesh grids made of copper, containing roughly 200-400 squares per inch. Excess solution was removed by blotting the applied sample with filter paper, and the grid was then rapidly plunged into a liquid ethane bath, which maintained its liquid state due to an outer liquid nitrogen bath. The rapid cooling process forms the thin layer of vitreous ice around the sample, which will remain at cryogenic temperatures until imaging. The ice layer thickness is critical, as it can affect the quality of the image obtained. Optimal ice thickness is around 100 nm, as this provides enough support for the sample while still allowing the electron beam to penetrate and image the sample[10]. Thicker ice layers will result in reduced contrast and resolution of the sample, while thinner ice layers provide low signal-to-noise ratio and increased radiation damage to the sample. Frozen samples were loaded into a microscope and data acquisition began by collecting multiple microscope images (micrographs) at different orientations and defocus values to capture the three-dimensional structure of the particle. Thousands of images can be collected

from a single grid, which can be imaged multiple times barring degradation, and can be stored at appropriate temperatures indefinitely. Ideal sample preparation and imaging can thus provide a sufficient number of particles at random orientations to be used for structural analysis via image processing software.

3.1.2.3 CryoSPARC – A Cryo-EM Image Processing Software

One of the major challenges in cryo-EM is the image processing and structural determination of macromolecular complexes. Cryo-EM images contain low signal-to-noise ratios and molecular structures can be obscured by buffer or neighboring molecules. Specialized software programs are required to extract the information from the images and generate 3D models of the molecules. One such software program is CryoSPARC, a user-friendly, web-based platform for cryo-EM image processing and structural determination. CryoSPARC uses a hierarchical workflow that allows for the automated processing of raw data and the generation of un-biased high-resolution 3D models[11]. The program includes modules for data preprocessing, particle picking, 2D and 3D classification, global and local refinement, and validation. A more in-depth understanding of each step of image analysis from data preprocessing to validation is described below.

3.1.2.4 CryoSPARC Data Preprocessing

Micrographs were processed adequately in order to obtain high-quality reconstructions of molecules. This included correcting for astigmatism, contrast transfer function (CTF), and defocus[12]. Significant contrast in imaging is not attained by simply passing an electron beam through a sample, but rather contrast occurs from a molecular structure's interference with the electron beam source leading to the select transmission of electrons around the molecules in a sample[13]. This interference causes the elastic scattering of electrons in different directions that

arrive at a detector with various path lengths due to scattering along separate areas of a molecule's electron density. Variation in the angle of scattering will cause the scattered components of electron wavefunctions to interfere with one another constructively or destructively, and is mathematically described by a microscope's CTF. Estimation of this CTF is imperative to correct for defocus and blur of images prior to analyzing micrographs. CryoSPARC models CTF through equation 1 below:

$$CTF = -\cos\left(\pi \Delta z \lambda_e f^2 - \frac{\pi}{2} C_s \lambda_e^3 f^4 + \phi\right) \quad \textbf{(1)}$$

where the sinusoidal function is defined by defocus (Δz), wavelength of incident electrons (λ_e), spatial frequency or periodicity of a molecule's structure across space (f), spherical aberration (loss of definition from lens surface geometry; C_s), and phase shift (applicable for multi-angled images taken using a phase plate; ϕ). Applying the desired terms into the estimated function above, CryoSPARC's patch-based CTF estimation job corrects for defocus globally in individual micrographs and locally for specific particles by creating a "defocus landscape" that even accounts for the lack of "flatness" in samples due to molecules freezing at different levels within vitrified ice[11].

3.1.2.5 CryoSPARC Particle Picking

Once preprocessing occurred, micrographs entered into the image analysis pipeline, beginning with distinguishing the particles of interest from background noise and contaminants (i.e. ice crystals, carbon grid edges, undesired molecular orientations)[13]. CryoSPARC offers multiple options for this stage of analysis, and particle picking often revolves around selecting manually or automatically, and accuracy of particle selections. Manual selection of particles is the most time-consuming method, and is only recommended for picking small-subsets of particles to use as templates for automated particle picking. As such, blob picking was conducted

for initial automated particle selection, however, a large selection of particles were characterized by contaminants that were separated from the desired particle picks by 2D classification. This method utilizes Laplacian-of-Gaussian based filtering, whereby points or regions of an image are detected by their intensity differences from background noise[14]. Utilizing 2D classes of interest, template picking was another method used to detect particles of interest more accurately, however, this also introduces biased selection of particles that can lead to inaccurate structural determination. Using a similar approach to template picking, a neural network can be trained for the optimization of particle picking based off selected 2D templates. While CryoSPARC has jobs for this purpose (Topaz Train), this thesis focuses predominately on blob picking for unbiased initial particle selection to potentially obtain multiple native fibrinogen conformations.

3.1.2.6 CryoSPARC 2D Classification

With a collection of selected particles, grouping and alignment of the data into homogeneous classes was conducted. Initial classification of particle picks was warranted to isolate particles of interest from empty field or contaminant picks, to assess the representation of orientations for the molecule present in the micrographs, and to provide high quality average classes with great signal-to-noise ratios for 3D reconstruction[15]. This process is rooted in the *K*-means clustering algorithm, which seeks to divide *n* observations into *k* clusters based on each observation's mean similarity to a cluster. Application of this algorithm for cryo-EM is known as 2D multi-reference alignment (MRA), and involves iterative classification of images into *K* seed templates based on which template they most resemble while averaging images (reinforcing consistent features among particles and averaging out background noise) between iterations until an appropriate solution of templates is achieved[13]. High amounts of *K* templates lead to poor results due to a low amount of image classes, while too few templates can lead to the assignment of many class

averages for enhanced signal-to-noise ratios with the drawback of "group collapse" (less common viewpoints are averaged out)[15].

3.1.2.7 CryoSPARC 3D Reconstruction

3D structural reconstruction is the combination of 2D image projections into an estimated electron density map of a molecule[13]. The tomographic information provided from micrographs are noisy molecular projections at random orientations and heights within a sample that also face distortion from a microscope's CTF. As such, algorithms such as stochastic gradient descent (SGD) and branch-and-bound maximum likelihood are used for the iterative optimization of initial macromolecular models for 3D reconstruction. Computational calculations for structural mapping of cryo-EM data signifies a non-convex optimization problem, where multiple feasible, locally optimal structures are present. SGD iteratively adjusts initial model parameters to minimize the gradient of difference between the observed and simulated data, combating the selection of local optima solutions through inclusion of a random selection of images for reconstruction between modular calculations to explore all 3D map space[11]. CryoSPARC's Homogeneous Refinement Job utilizes this algorithm and was used to produce high-resolution reconstructions with relatively small amounts of data. The branch-and-bound maximum likelihood algorithm on the other hand focuses on searching for the global maximum likelihood of the observed data[11]. By first calculating a lower bound over the entire space of positions by which the optimal model could exist, this process can then exclude regions of search space exceeding these bounds from future searches. Iterative subtraction of regions not defining the optimal reconstruction of 2D projections accelerates the computational calculations necessary for 3D reconstruction. CryoSPARC's Non-Uniform Refinement Job utilizes this algorithm, and,

although more computationally expensive than the Homogeneous Refinement Job, was able to procure higher resolution reconstructions than SGD.

3.1.2.8 CryoSPARC 3D Refinement and Validation

Upon 3D reconstruction of an initial molecular map, refinement of the structure's resolution and quality is required to then be able to accurately describe the molecule in a biological sense. Refinement followed similar steps to 2D classification by using an iterative 3D projection matching process that modifies orientation parameters for the computation of reprojections that decrease the difference between observed and simulated data[15]. Global resolution of refined structures was assessed predominately by the production of a Fourier shell correlation (FSC) curve. By splitting the adjusted dataset in half, programs independently compute volumes from each subset and resolution is determined by the correlation of those individual volumes. Specifically, the resolution is often defined as the spatial frequency at which the FSC curve drops below a predefined threshold (often 0.143)[16]. Refined structure maps were rendered in a 3D protein visualization program, ChimeraX[17], to be used for structural analysis. ChimeraX is also capable of mask production for volume maps that isolate a particular area of interest within a molecule to be used for local refinement to more accurately depict protein electron density[18].

Although FSC curves provide a resolution from the individual refinement of two halves of an adjusted dataset, a structure's validity is not fully confirmed by this metric alone. In particular, more flexible molecules (like fibrinogen) may undergo averaging of different molecular conformations, which will undermine a structure's biological significance. Validation of the cryo-EM determined structure was established by computing local resolutions of the map (depicting specific resolutions present throughout regions of a volume) and corroborating visible features with known structures (i.e. those determined crystallographically).

3.1.3 *Developing a Dynamic Model of Fibrinogen with Cryogenic Electron Microscopy*

A proper workflow for the structural determination by single-particle cryo-EM reconstruction includes sample assessment, purification, and imaging, microscope CTF estimation and correction, suitable particle selection (differentiating the target molecule from noise/contaminants), 2D classification, 3D reconstruction and refinement, and validation (Figure 3.1). Steps may be repeated or skipped depending on the quality of the images taken, desired final resolution, if templates are available, etc. With its streamlined single-particle analysis software designed for non-specialists, CryoSPARC supplies researchers with a combination of algorithms in an accessible workspace to refine 3D structures of desired molecules at high resolutions[11], with certain software packages even directed towards molecular motion visualization for flexible proteins[19]. As such, this image processing software was used as a valuable tool in the enhanced structural refinement of fibrinogen's D region.

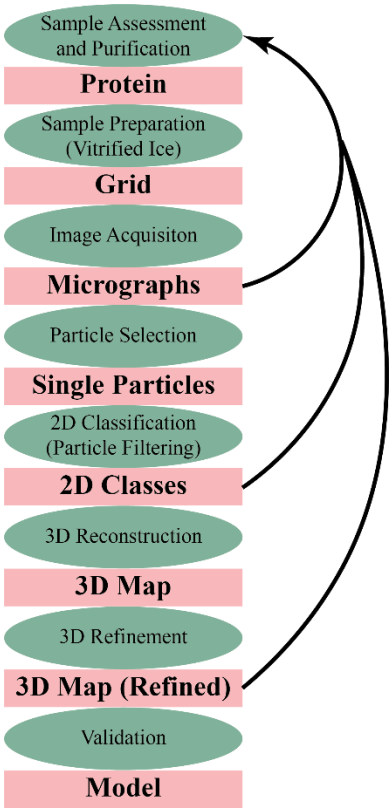

Figure 3.1: Steps for single-particle cryo-EM structural determination. (Green) Individual techniques for the pipeline of image analysis towards model reconstruction, with (pink) waypoints along the way used as places to assess whether improved sample preparation methods, better micrographs, more selective particle picking, enhanced 2D classes, or greater 3D refinement is needed.

3.1.4 *Initial Steps Towards Structural Determination: Hudson Lab Previous Work*

The work proposed below is in continuation with previous Hudson lab member's results: Elizabeth Viverette[20], Jose de la Garza, and Wyatt Peele. That includes initial negative stained and vitrified cryo-EM whole fibrinogen structural analysis, and low-resolution refinement of fibrinogen's D region. The main issue impeding whole fibrinogen structural refinement was too few intact molecules at consistent angular orientations, causing less common native structures to be averaged out. However, the D region was continually present as a more rigid two-nodular

structure, and an initial volume was created around 17 Å. Continued refinement of the particle picking process provided a global resolution of 4.2 Å.

3.2 **Materials and Methods**

3.2.1 *Data Set 1: Sample and Grid Preparation (without Fmoc-GPRPFPAWK)*

Peak 1 fibrinogen (Enzyme Research Labs, South Bend, IN, USA) confirmed by western blotting to contain all polypeptide chains (2.2.4.3 protocol followed) was further purified of potential aggregates by SEC (2.2.6.2 protocol followed) and sent to the National Institute of Environmental Health Sciences (NIEHS, Raleigh, NC, USA) for freezing and cryo-EM imaging. Samples were frozen at a concentration of 0.2 mg/ml with a back blot time of 2.3 seconds on a size 200 gold mesh grid using a Leica GP1 freezing device. The grids were then screened using a ThermoFischer Talos Artica cryo-TEM microscope and analyzed to ensure proper protein density, ice layer thickness, and lack of orientational preference before imaging a collection of 7,292 micrographs.

3.2.2 *Data Set 2: Sample and Grid Preparation (with Fmoc-GPRPFPAWK)*

Peak 1 fibrinogen (Enzyme Research Labs, South Bend, IN, USA) purified of potential aggregates by SEC (2.2.6.2 protocol followed; Figure 3.2) at the National Institute of Environmental Health Sciences (NIEHS, Raleigh, NC, USA) for freezing and cryo-EM imaging. Fibrinogen sample was mixed with Fmoc-GPRPFPAWK knob ‘A’-mimic peptide (1 mM stock solution in dH_2O and 50 µL DMSO per 1 mg peptide) and diluted with HBS buffer (150 mM NaCl, 20 mM HEPES, 10 mM $CaCl_2$, pH 7.4) to give a final fibrinogen concentration of 0.05 mg/mL with either Fmoc-GPRPFPAWK final concentrations of 100 µm or 500 µm. All samples used back blotting (2.5 seconds) onto sized 300 UF gold mesh grids using a Leica GP1 freezing device. The grids were then screened using a ThermoFischer Talos Artica cryo-TEM microscope

and analyzed to ensure proper protein density, ice layer thickness, and lack of orientational preference before imaging a collection of 3,163 micrographs.

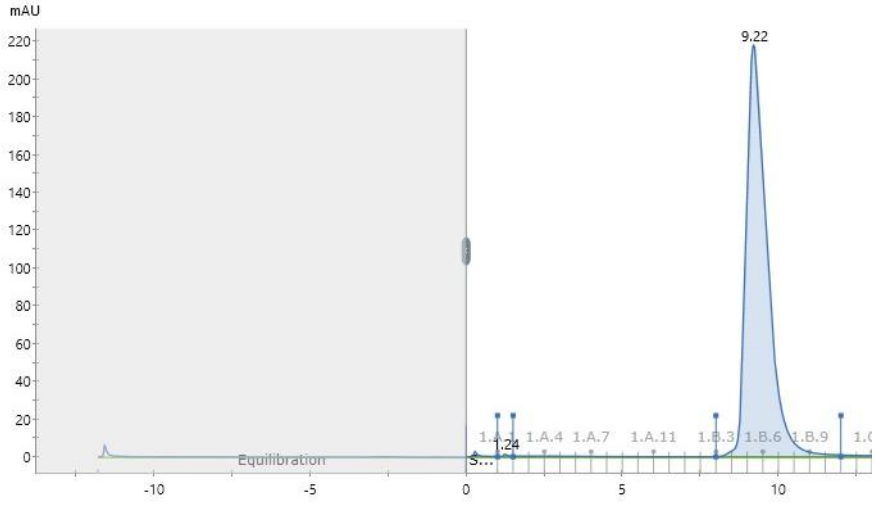

Figure 3.2: SEC purification readout. Fast protein liquid chromatogram of Peak 1 fibrinogen purification, showing one dominant UV peak from fractions 1.B.5-1.B.8.

3.3 **Results**

3.3.1 *Data Set 1: D Region Without Fmoc-GPRPFPAWK*

Micrographs (7,292) were imported into CryoSPARC and underwent data preprocessing by way of patch CTF estimation and micrograph curation (selection of adequate micrographs from CTF fits, and ice thickness) jobs. The previously described 4.2 Å resolved structure was similarly imported into CryoSPARC and used to create a set of 1,000 templates for the selective, automatic template particle picking of fibrinogen's D region using a circular box size of 150 Å (>2x the D region's diameter). Initial inspection of the selection resulted in approximately 2.9 million particle picks, which were subsequently classified into 550 2D classes. These classes then underwent multiple rounds of manual selection for the removal of "junk" classes (classes containing multiple D regions in sight, contaminants, or poorly imaged D regions) and further 2D classification to facilitate stack cleaning of classes. This process was repeated until a high-

quality set of particles was selected (~2.3 million particles), of which a representative sampling can be seen in Figure 3.3. It is important to note the quality of the 2D classes seen here, specifically that the β- and γ-nodules are easily discernible and present signs of secondary structure. Despite this, there is also an absence of coiled-coil-D domain remnants expected to conjoin to the D region nodule structures. Angular reconstruction using these 2D classes via SGD ab-initio structure determination provided an initial 3D volume (Figure 3.3), which further underwent homogeneous refinement to reveal a structure with a global FSC curve resolution of 4.27 Å.

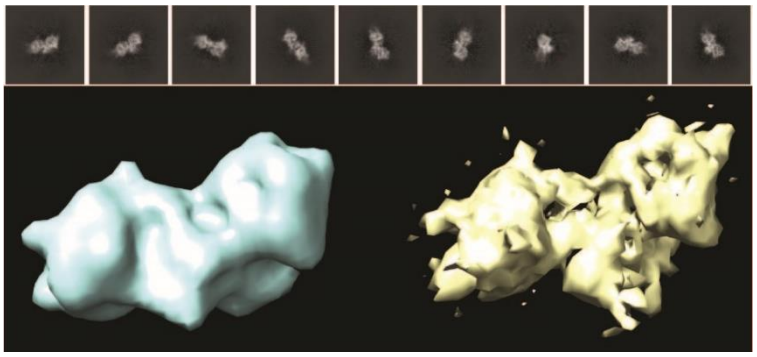

Figure 3.3: 2D and 3D structures of fibrinogen's D region. (Top) Selection of 2D class averages used for (left) angular ab-initio reconstruction with subsequent (right) homogenous refinement (4.27 Å).

Although close to the defined threshold for a high-resolution structure (<4 Å)[15], the homogeneously refined 3D volume has no easily discernible secondary structure. Suspecting that the 2D classification stage may have been inadequate in fully separating desirable particle picks, 3D classification was conducted using a batch expectation maximization algorithm to separate particle picks into 9 volume classes (Figure 3.4). The presence of 3 major particle class distributions signifies the potential presence of discrete heterogeneous states.

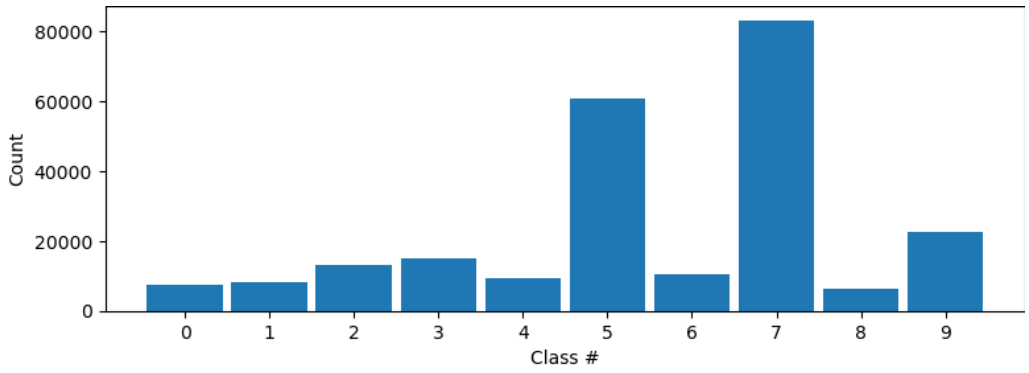

Figure 3.4: Batch class distribution of particles. 3D classification of the adjusted dataset led to the assortment of particles into 9 classes – Class 0 (7,492), Class 1 (8,089), Class 2 (13,048), Class 3 (15,183), Class 4 (9,339), Class 5 (60,901), Class 6 (10,393), Class 7 (83,214), Class 8 (6,220), and Class 9 (22,485).

The particles of class 7 (most prominent classification of particles from Figure 3.4) were then homogeneously refined to a global FSC resolution of 5.04 Å, which, although displayed higher resolution, also visually fit the D region segment of 3GHG more clearly (Figure 3.5C). This volume enhancement can also be understood through the FSC curves of particle extraction with (Figure 3.5A) and without (Figure 3.5B) "binning" (pixel averaging to save computation efforts in early processing). The noticeable increase in the slope of the curve after unbinning is indicative of more accurate comparison between half map structures used in creating the fitting FSC curves.

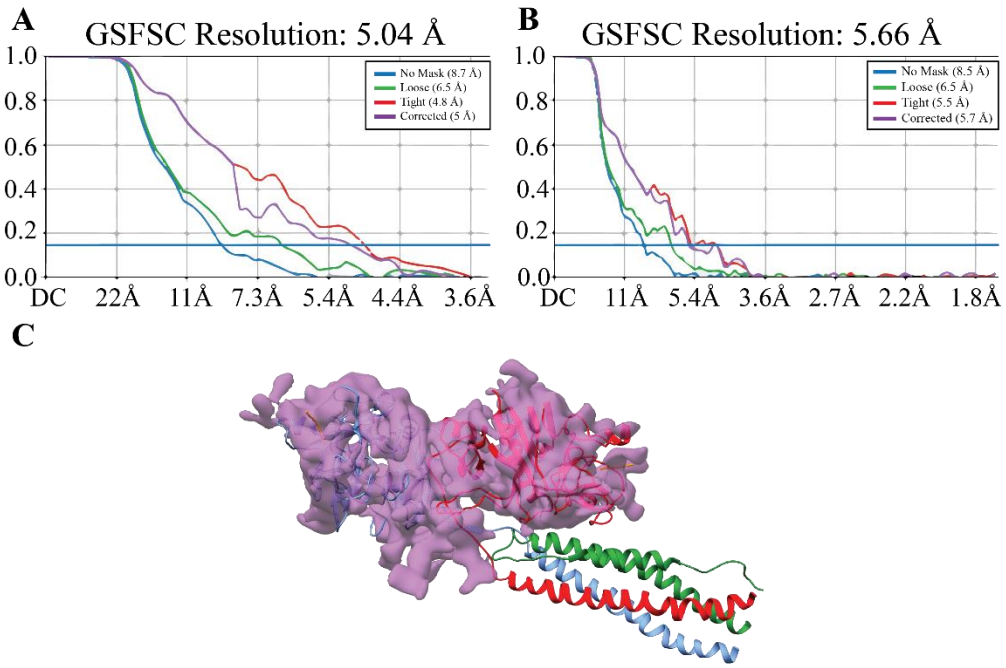

Figure 3.5: Further refinement of 3D reconstruction and validation of the model. Gold-standard FSC (GSFSC) curves of binned (A) and unbinned (B) particle data. (C) 3D refined structure of unbinned particle data with D region portion of 3GHG fitting to the model: Aα chain (green), Bβ chain (red), and γ chain (blue), GPRV and GHRP peptides bound to holes 'a' and 'b,' respectively (orange).

3.3.2 *Data Set 2: D Region With Fmoc-GPRPFPAWK*

Unlike the grids frozen without the addition of Fmoc-GPRPFPAWK peptide, the presence of a knob 'A'-mimic peptide seemingly aided in "fibrinogen-specific protofibril-like formation." That is to say that adding peptide to fibrinogen samples prior to freezing led to the development of long fibers (Figure 3.6), despite the absence of fibrin monomers needed for typical fiber formation. Samples frozen with 500 μM peptide provided the best grids for imaging and were used for the procurement of 3,163 micrographs. These were then imported into CryoSPARC and underwent data preprocessing by way of patch CTF estimation and micrograph curation (selection of adequate micrographs from CTF fits, and ice thickness) jobs.

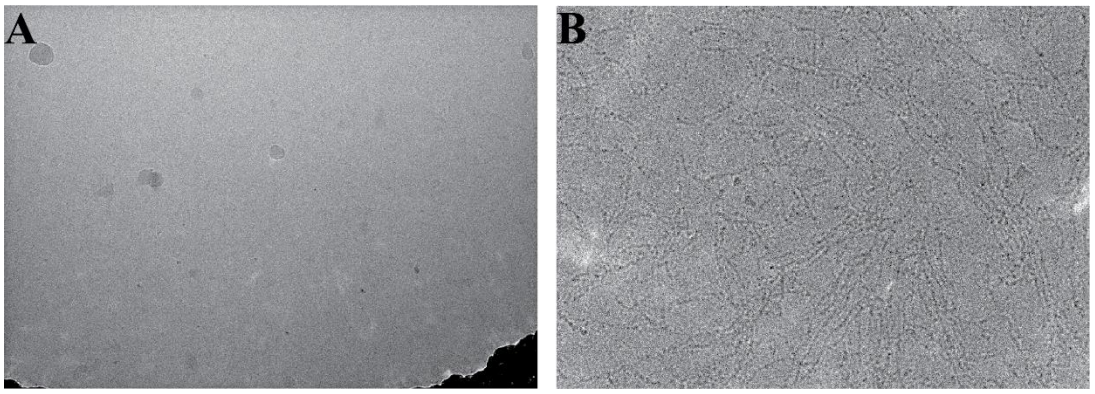

Figure 3.6: Micrographs of frozen fibrinogen samples. Representative micrograph images of flash frozen fibrinogen samples without (A) and with (B) Fmoc-GPRPFPAWK peptide.

With enhanced visual clarity of fibrinogen molecules, blob picking was chosen for non-biased, automated particle selection of the D region using a circular box size of 200 Å. Initial inspection of the selection resulted in approximately 7.5 million particle picks, which were subsequently extracted and classified into 550 2D classes. This initial classification produced clearly defined D regions with visible coiled-coil-D domains, along with other interesting classes that will be touched on in the Future Directions section of this thesis resembling γ-γ dimers, the coiled-coil region itself, the DDE complex, and even paired γ-γ dimers. Focused rounds of 2D classification and selection of solely isolated D region structure (no γ-γ dimer picks) led to the grouping of ~100,000 particle picks into 56 classes. These classes were then used as templates for automated, selective particle picking in order to obtain more D region-specific particle picks for 3D reconstruction. The use of template particle picking and multiple rounds of 2D classification and selection produced approximately 30,000 more picks for a total of ~130,000 particle picks into 64 classes (Figure 3.7). Clearly visible secondary structure within these 2D classes is optimal to produce high-resolution 3D structures. The clarity of the D region's β- and γ-nodules along with the presence of coiled-coil-D domains displays greater quality than those classes obtained from Data Set 1.

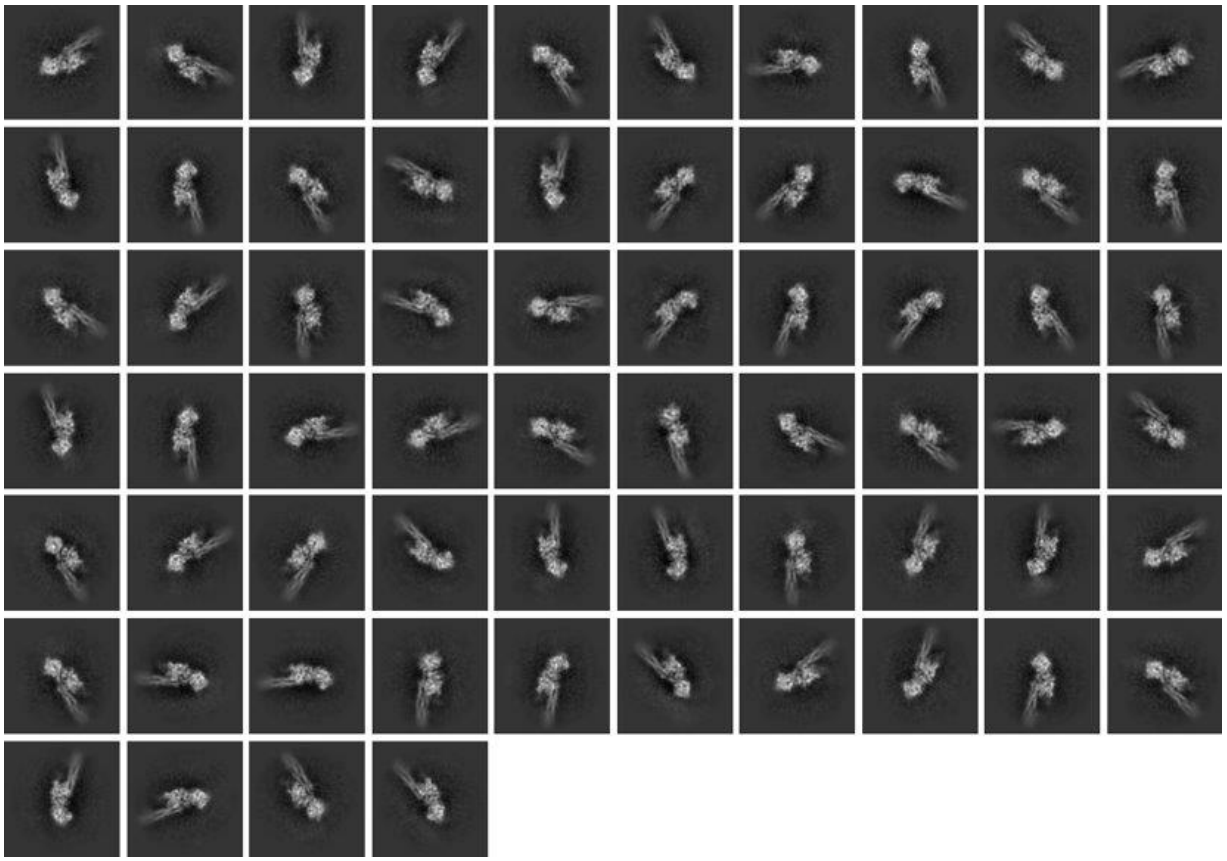

Figure 3.7: Selected 64 templates of fibrinogen's isolated D region classifying 131,929 particle picks.

Angular reconstruction using these 2D classes via multiple rounds of SGD homogeneous refinement produced a 3D volume with a GSFSC global resolution value of 3.70 Å. This was further refined via branch-and-bound maximum likelihood non-uniform refinement to a GSFSC global resolution value of 3.66 Å (Figure 3.8A). The produced volume contained cylindrical projections of the coiled-coil-D domain characteristic of alpha helices for cryo-EM data, as well as rod-like projections throughout the β- and γ-nodules signifying highly resolved internal structure (Figure 3.8B). Fitting a D fragment portion of a known PDB structure (3GHG[1]) to the refined volume showed high similarity for both nodule and coiled-coil portions. Fitting was further assessed by producing a molecular map from 3GHG at a resolution of 3.66 Å, and

adjusting the produced volume to the same threshold level as the non-uniform refined volume to give a correlation value of 0.5429.

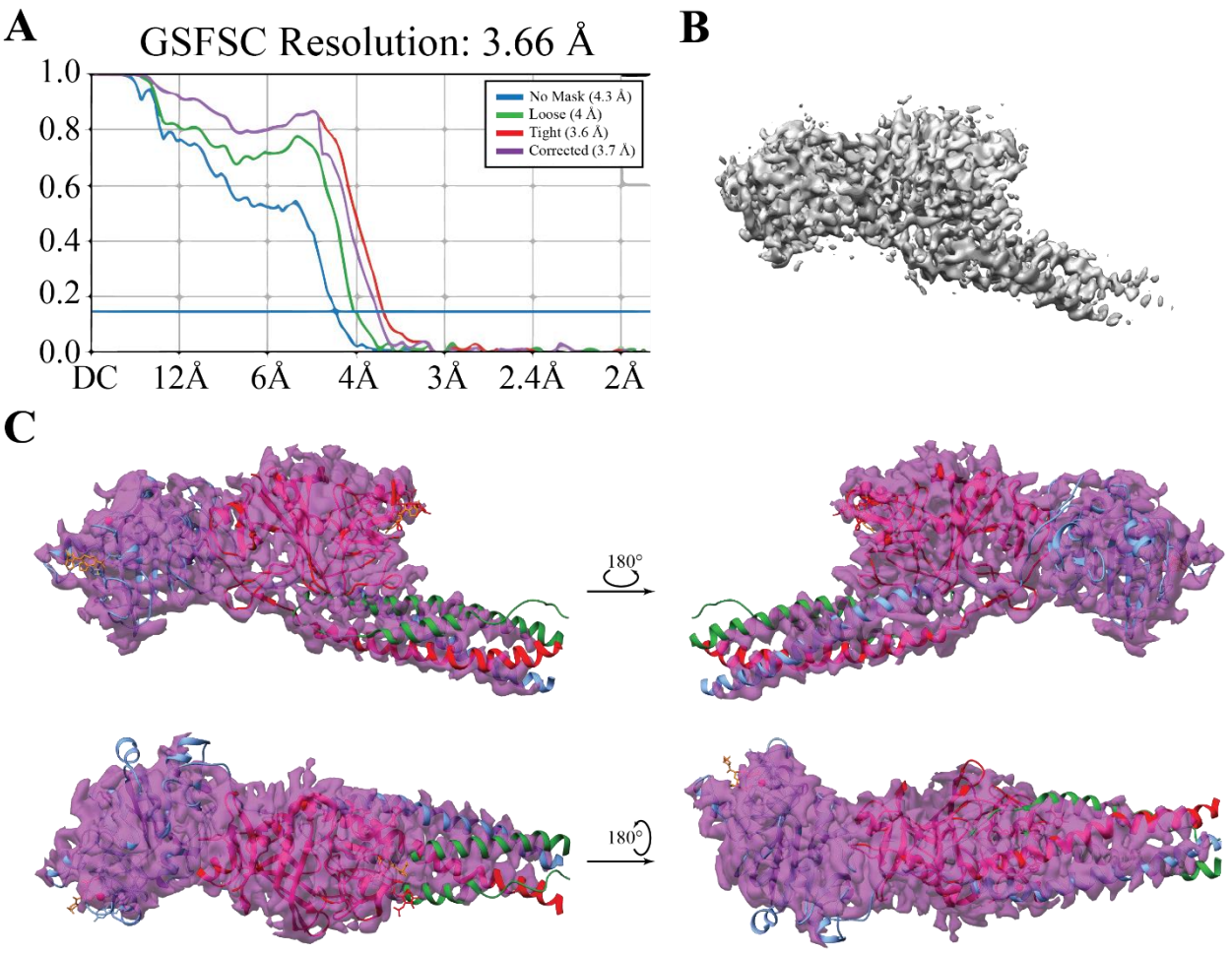

Figure 3.8: Non-uniform refined 3D volume of fibrinogen's D region. (A) GSFSC global resolution curves for a (B) non-uniform refined angular reconstruction map. (C) Various rotational views of a D region fragment of 3GHG with the 3.66 Å volume overlaying the structure.

Despite the high-resolution value produced from the GSFSC curves in Figure 3.8, there remained areas of the volume that did not precisely match the 3GHG structure. Seeking to better understand this, CryoSPARC's Local Resolution Estimation Job was utilized to produce a map

containing resolution for each voxel similar to that produced by the *blocres* program[21]. The local resolution map created was then used to color the refined map with USCF Chimera's Surface Color tool (Figure 3.9). Resolutions for the internal portions of the nodules ranged from 3.4-4 Å, while most outer sections of the refined volume displayed resolutions from 4.5-5.5 Å. There also existed certain areas of the nodules with resolutions ranging from 7-10+ Å.

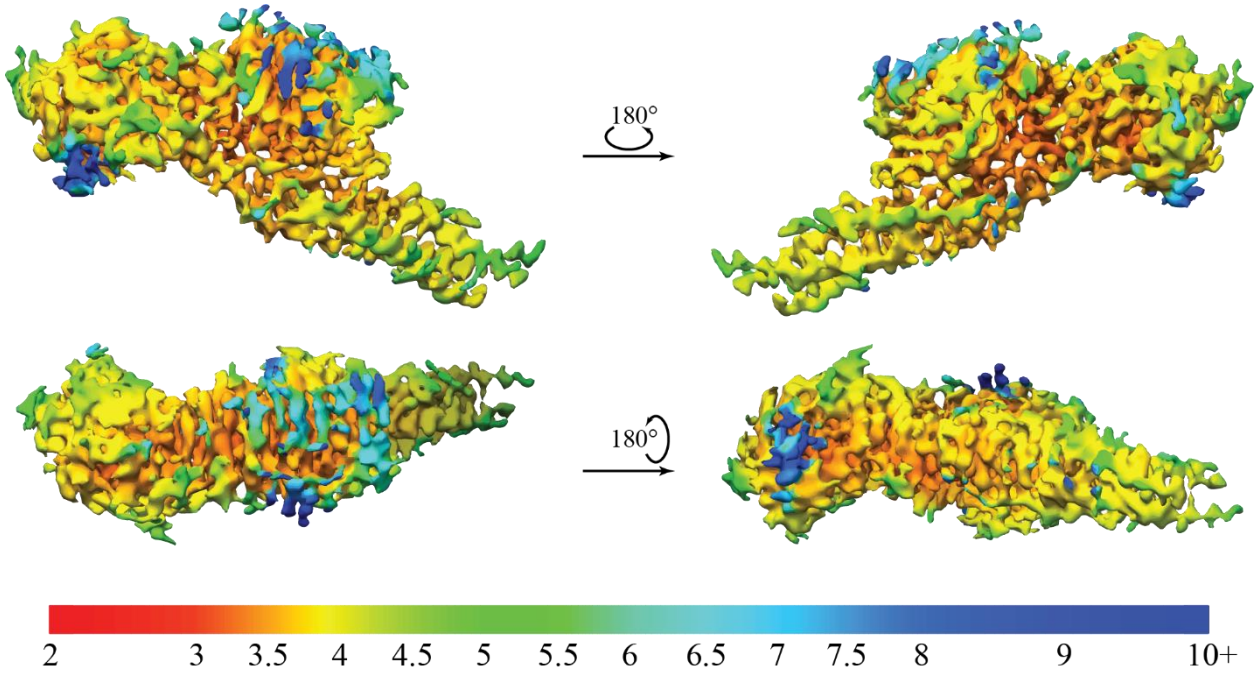

Figure 3.9: Local resolution various rotational views for non-uniform refined 3D volume of fibrinogen's D region.

Non-uniform resolutions for the refined volume with select areas of intermediate-to-low resolutions indicated the potential for a more heterogeneous structure/different conformational states of the D region. Exploration of the volumes flexibility was conducted via 3D Variability Analysis (3DVA[19]) in CryoSPARC, where a combination of an Expectation-Maximization algorithm and Probabilistic Principal Component Analysis (PCA) allowed for the continuous reconstruction of a family of 3D structures. Three principal modes of variability were input, of which one resultant component was chosen for analysis. A volume series of 20 frames was

opened into USCF Chimera and a movie created showcasing flexion of the coiled-coil-D domain, as well as closing of hole ‘a’ (only 5 frames are shown below).

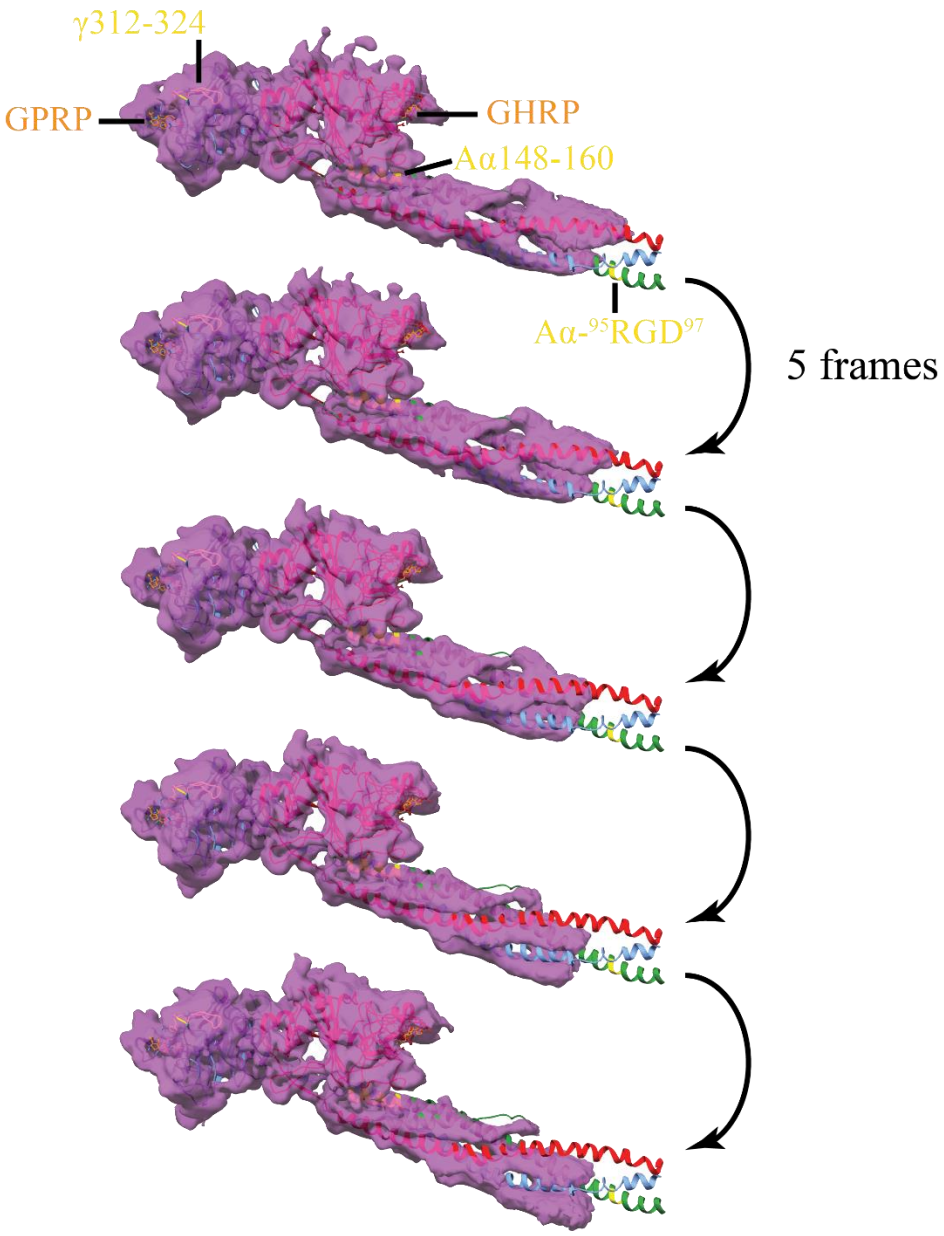

Figure 3.10: Volume series of 3D Variability Analysis. Five representative frames separated by 5 frames each of a single component of variability highlighting flexibility of the non-uniform refined D region structure of fibrinogen. D region portion of 3GHG was fit to the first frame and remained stationary throughout the entire video and is characterized by an alpha (green), beta (red), and gamma (blue) chain with areas of interest highlighted in yellow and known peptide knob mimics in orange.

3.4 **Discussion**

The development of a consensus structure for human fibrinogen has predominately fallen under x-ray crystallographic studies and has depicted a more static structure with a slight bend/twist about the central E region for a planar sigmoidal shape[1]. Recently, however, evidence of a more conformationally dynamic fibrinogen structure has begun to surface by way of molecular dynamic (MD) simulations[22], AFM[23, 24], EM[25], and other low-resolution structural techniques[26]. The data provided in this chapter further corroborates the evidence for "fibrinogen's dynamism" in solution by the high-resolution technique of cryo-EM and intuitive image processing and structural determination software (CryoSPARC).

Multiple "flexible hinge sites" hypothesized to aid in fibrin gel mechanical properties[1] have been previously identified and include portions of the coiled-coil region, fibrinogen-specific cryptic plasminogen/tPA binding sites (Aα148-160) between the coiled-coil-D domain and β-nodules, and the interface between β- and γ-nodules for uncovering of tPA-specific binding sites (γ312-324)[27]. This intrinsic flexibility has been highlighted by MD simulations focused on the D region, whereby large molecular bending centered around a hinge site located in the coiled-coil region was identified[22]. This was explored further by solution-phase small angle x-ray scattering (SAXS) and TD-HDXMS which experimentally determined that a rotation between β- and γ-nodules was caused by hinging of fibrinogen at the coiled-coil region, and suggested to impact protofibril formation by assisting knob:hole alignment[26]. The work presented in this chapter presents additional evidence for this flexion about a hinge location in the coiled-coil region near a known cryptic binding epitope for platelet integrin αIIbβ3 (Aα-^{95}RGD^{97}) through 3DVA in CryoSPARC[28]. One direct observation of the continuous family of 3D reconstructions (Figure 3.10) is the "conformational breathing" present for hole 'a' (Figure 3.11). Here a marked

decrease in the size of hole 'a' is noted, which highlights the potential for fibrinogen's flexion to affect knob:hole interactions in congruence with the suggested regulation of receptor binding epitope accessibility by the internal conformational flexibility of fibrinogen[26]. Another less obvious finding of the 3DVA structures shows the slight movement of the β-nodule away from the coiled-coil-D domain. The β-nodule is thought to be anchored to this position in fibrinogen to cover the cryptic plasminogen/tPA binding sites (Aα148-160), and is released during polymerization to allow for plasminogen's interaction with fibrin for the activation of fibrinolysis[27]. This intrinsic flexibility about the coiled-coil region may highlight the importance of fibrinogen's dynamic nature for the initiation of fibrin fiber breakdown.

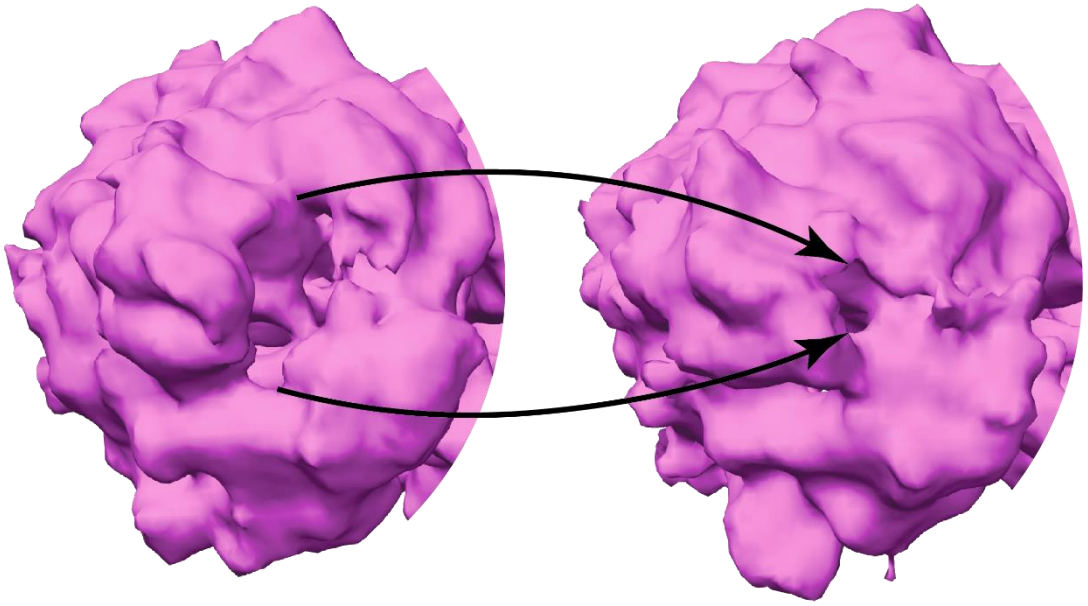

Figure 3.11: Frames 0 and 19 of 3DVA derived volumes highlighting the conformational breathing of hole 'a.'

The addition of ligands in structural determination methodology has long been conducted in order to orchestrate rigidification of proteins upon binding for more clearly defined structures. The work above discusses two data sets, one in which fibrinogen alone was frozen for imaging,

and the other in which a high-affinity knob ‘A’-mimic (Fmoc-GPRPFPAWK) like that used in Chapter 2 was added prior to sample freezing. Data set 2 showed the most promising micrographs and produced a 3.66 Å global resolution structure. Although the addition of Fmoc-GPRPFPAWK seemingly produced the clearer representation of fibrinogen’s in-solution structure, the reason for this enhanced quality is not fully understood. In particular, knob ‘A’-mimic peptide addition led to the formation of protofibril-like fibrinogen-specific fibers, different from those normally understood as formed by fibrin monomers upon thrombin’s cleavage of FpA and FpB. The binding mechanism of these high affinity peptides may have in a sense elucidated fibrinogen-specific packing interactions not previously discussed in the literature. However, data set 2 involved optimized sample purification and preparation techniques and future work should attempt to decrease the ice thickness of fibrinogen samples frozen without peptide for a more accurate statement of the influence of knob ‘A’-mimics on fibrinogen’s in-solution structure.

3.5 **Conclusion**

This chapter showcases the use of cryo-EM and the imaging software, CryoSPARC for the reconstruction of the highest global resolution 3D volume of fibrinogen’s D region to date (3.66 Å). The proposed 3D reconstruction displays important secondary structure detail including portions of the coiled-coil-D domain, unable to be reproduced in previous cryo-EM volumes. Local resolution of this volume displayed non-uniform resolution, which suggested structural heterogeneity confirmed by three-dimensional variability analysis. Fibrinogen’s intrinsic flexibility along the coiled-coil region was visualized, and its potential role in knob:hole interactions for polymerization and elucidation of a cryptic binding site for fibrinolysis was indicated.

References

1. Kollman, J. M.; Pandi, L.; Sawaya, M. R.; Riley, M.; Doolittle, R. F., Crystal structure of human fibrinogen. *Biochemistry* **2009,** *48* (18), 3877-3886.

2. Hall, C., Electron microscopy of fibrinogen and fibrin. *Journal of Biological Chemistry* **1949,** *179* (2), 857-864.

3. Yee, V. C.; Pratt, K. P.; Côté, H. C.; Le Trong, I.; Chung, D. W.; Davie, E. W.; Stenkamp, R. E.; Teller, D. C., Crystal structure of a 30 kDa C-terminal fragment from the γ chain of human fibrinogen. *Structure* **1997,** *5* (1), 125-138.

4. Kostelansky, M. S.; Betts, L.; Gorkun, O. V.; Lord, S. T., 2.8 Å crystal structures of recombinant fibrinogen fragment D with and without two peptide ligands: GHRP binding to the "b" site disrupts its nearby calcium-binding site. *Biochemistry* **2002,** *41* (40), 12124-12132.

5. Pechik, I.; Madrazo, J.; Mosesson, M. W.; Hernandez, I.; Gilliland, G. L.; Medved, L., Crystal structure of the complex between thrombin and the central "E" region of fibrin. *Proceedings of the National Academy of Sciences* **2004,** *101* (9), 2718-2723.

6. Spraggon, G.; Everse, S. J.; Doolittle, R. F., Crystal structures of fragment D from human fibrinogen and its crosslinked counterpart from fibrin. *Nature* **1997,** *389* (6650), 455-462.

7. Everse, S. J.; Spraggon, G.; Veerapandian, L.; Riley, M.; Doolittle, R. F., Crystal structure of fragment double-D from human fibrin with two different bound ligands. *Biochemistry* **1998,** *37* (24), 8637-8642.

8. Williams, D. B.; Carter, C. B.; Williams, D. B.; Carter, C. B., *The transmission electron microscope*. Springer: 1996.

9. Thompson, R. F.; Walker, M.; Siebert, C. A.; Muench, S. P.; Ranson, N. A., An introduction to sample preparation and imaging by cryo-electron microscopy for structural biology. *Methods* **2016,** *100*, 3-15.

10. Passmore, L. A.; Russo, C. J., Specimen preparation for high-resolution cryo-EM. *Methods in enzymology* **2016,** *579*, 51-86.

11. Punjani, A.; Rubinstein, J. L.; Fleet, D. J.; Brubaker, M. A., cryoSPARC: algorithms for rapid unsupervised cryo-EM structure determination. *Nature methods* **2017,** *14* (3), 290-296.

12. Zhang, K., Gctf: Real-time CTF determination and correction. *Journal of structural biology* **2016,** *193* (1), 1-12.

13. Singer, A.; Sigworth, F. J., Computational methods for single-particle electron cryomicroscopy. *Annual review of biomedical data science* **2020,** *3*, 163-190.

14. Kong, H.; Akakin, H. C.; Sarma, S. E., A generalized Laplacian of Gaussian filter for blob detection and its applications. *IEEE transactions on cybernetics* **2013,** *43* (6), 1719-1733.

15. Cheng, Y.; Grigorieff, N.; Penczek, P. A.; Walz, T., A primer to single-particle cryo-electron microscopy. *Cell* **2015,** *161* (3), 438-449.

16. Rosenthal, P. B.; Henderson, R., Optimal determination of particle orientation, absolute hand, and contrast loss in single-particle electron cryomicroscopy. *Journal of molecular biology* **2003,** *333* (4), 721-745.

17. Pettersen, E. F.; Goddard, T. D.; Huang, C. C.; Meng, E. C.; Couch, G. S.; Croll, T. I.; Morris, J. H.; Ferrin, T. E., UCSF ChimeraX: Structure visualization for researchers, educators, and developers. *Protein Science* **2021,** *30* (1), 70-82.

18. Aiyer, S.; Zhang, C.; Baldwin, P. R.; Lyumkis, D., Evaluating local and directional resolution of cryo-EM density maps. *cryoEM: Methods and Protocols* **2021**, 161-187.

19. Punjani, A.; Fleet, D. J., 3D variability analysis: Resolving continuous flexibility and discrete heterogeneity from single particle cryo-EM. *Journal of structural biology* **2021,** *213* (2), 107702.

20. Viverette, E. G., Using Cryo-Electron Microscopy to Determine the 3-Dimensional Structure of Fibrinogen. **2021**.

21. Cardone, G.; Heymann, J. B.; Steven, A. C., One number does not fit all: mapping local variations in resolution in cryo-EM reconstructions. *Journal of structural biology* **2013,** *184* (2), 226-236.

22. Köhler, S.; Schmid, F.; Settanni, G., The internal dynamics of fibrinogen and its implications for coagulation and adsorption. *PLoS computational biology* **2015,** *11* (9), e1004346.

23. Sit, P. S.; Marchant, R. E., Surface-dependent conformations of human fibrinogen observed by atomic force microscopy under aqueous conditions. *Thrombosis and haemostasis* **1999,** *82* (09), 1053-1060.

24. Zuev, Y. F.; Litvinov, R. I.; Sitnitsky, A. E.; Idiyatullin, B. Z.; Bakirova, D. R.; Galanakis, D. K.; Zhmurov, A.; Barsegov, V.; Weisel, J. W., Conformational flexibility and self-association of fibrinogen in concentrated solutions. *The Journal of Physical Chemistry B* **2017,** *121* (33), 7833-7843.

25. Beijbom, L.; Larsson, U.; Kavéus, U.; Hebert, H., Structure analysis of fibrinogen by electron microscopy and image processing. *Journal of ultrastructure and molecular structure research* **1988,** *98* (3), 312-319.

26. Pinelo, J. E.; Manandhar, P.; Popovic, G.; Ray, K.; Tasdelen, M. F.; Nguyen, Q.; Iavarone, A. T.; Offenbacher, A. R.; Hudson, N. E.; Sen, M., Systematic mapping of the

conformational landscape and dynamism of soluble fibrinogen. *Journal of Thrombosis and Haemostasis* **2023**.

27. Mican, J.; Toul, M.; Bednar, D.; Damborsky, J., Structural biology and protein engineering of thrombolytics. *Computational and structural biotechnology journal* **2019,** *17*, 917-938.

28. Litvinov, R. I.; Farrell, D. H.; Weisel, J. W.; Bennett, J. S., The Platelet Integrin alphaIIbbeta3 Differentially Interacts with Fibrin and Fibrinogen. *Blood* **2015,** *126* (23), 3444.

Conclusions

4.1 Human Fibrinogen Synthesis, Purification, and Structural Determination

Fibrinogen is a remarkably dynamic protein both for its physiological roles in a multitude of bodily processes (hemostasis, wound healing, inflammation, disease provocation and defense)[1], and for its display of a broad conformational landscape[2]. While recent experiments have expanded the knowledge for this protein's heterogeneous structural behavior[2-4], there remains little information about how fibrinogen mutations linked to select human pathologies impact the structure and function of fibrinogen. Techniques for the enhanced production of mutationally modified fibrinogen, rapid purification of fibrinogen from complex media, and improved native state structural assessment of fibrinogen are therefore necessary to establish proper structure-function relationships encompassing this complex protein.

A system for the transient recombinant expression of fibrinogen utilizing HEK Expi293™ mammalian cells was reported in this thesis. Transfection efficacy was compared between a three-plasmid (3P) system for each of fibrinogen's chains and a combined single plasmid (CSP) containing all chains, with slight favorability seen for the 3P system. Additionally, transfection reagents PEI and ExpiFectamine™ were determined to produce similar protein yields, despite ExpiFectamine™'s large cost difference relative to PEI. Continued optimization of transfection efficiency for our transient system yielded a 3:1 PEI:DNA ratio for the highest protein production. Future work focusing on the creation of stable cells successfully incorporating the CSP for increased cell sorting ability may elevate protein yields to commercial levels without the need for more costly cell systems currently used[5].

A complementary method for fibrinogen isolation from complex media using affinity chromatography was developed. The method for coupling a synthetic GPRPFPAWK knob "A"-

mimic peptide to NHS-activated Sepharose beads was optimized, and found to remain effective over multiple uses of the column for protein isolation without significant alterations to purification results. Specificity for fibrinogen was tested through creation of a scramble peptide column and found to likely involve the GPRP motif. For use in isolation from complex medias, approximately 75% of fibrinogen was rapidly purified from blood plasma without effecting protein functionality after buffer exchanging from elution solution. In comparing this to current fibrinogen purification methods, our GPRP-based affinity chromatography is much faster, less harmful, more easily reproducible, and produces more functional fibrinogen when partnered with a buffer exchanging method like PD-10 or SEC. This has significantly opened the door to study *ex vivo* samples from human patients and animal samples.

Lastly, this thesis introduces the highest global resolution cryo-EM structure of fibrinogen to date (3.66 Å). Additionally, local resolution and 3D variant analysis of the produced structure indicates high-resolution evidence for flexing of the D region, which further corroborates fibrinogen's conformational dynamism, as previously suggested by lower resolution methods in our laboratory[2].

Future Directions

4.2 *Ex vivo* Studies on Purified Human Fibrinogen from Pregnant Women

4.2.1 *Variations in Fibrinogen Structure During Pregnancy*

Although fibrinogen circulates in the blood stream predominately in its high molecular weight form (HMW-fgn, 340 kDa, ~ 70% of total fibrinogen), two low molecular weight forms exist from partial hydrolysis of either one αC region (LMW-fgn, 305 kDa, ~ 26% of total fibrinogen) or both (LMW'-fgn, 270 kDa, ~ 4% of total fibrinogen)[6]. Serving as an acute-phase reactant, spikes in fibrinogen concentration are evident with increases in inflammation. This

most likely occurs from increased biosynthesis of HMW-fgn, leading to a higher HMW:LMW-fgn ratio[7]. This total fibrinogen concentration increase is also present for the physiologically hypercoagulable state of pregnancy, with rising levels expected from the first to third trimester and a subsequent drop to normal values at the end of puerperium (6 weeks post-delivery), along with expected alterations to fibrinogen's glycan content[7-16]. This change in the coagulation system is likely the result of hormonal changes (increased oestrogen levels), with enzymatic relative equilibration of the HMW:LMW-fgn ratio during pregnancy, followed by insufficient regulation of the ratio shortly following delivery (amplified HMW-fgn)[6, 7, 11]. Higher HMW-fgn levels are associated with faster polymerization and thicker, more porous fiber networks from the presence of the αC regions[17, 18]. One factor that has been minimally tested, however, is the differences in the sugar content and/or structure of fibrinogen during pregnancy[9, 10]. For example, decreases in the sialic acid content of fibrinogen, such as with asialofibrinogen (lacking any sialic acid), displays a marked decrease in polymerization rates with thicker fiber formation[2]. During pregnancy, one study has indicated that the sialic acid content for women decreases during the third trimester (5.0±0.07 mol sialic acid per mol fibrinogen vs. 5.3±0.06 mol/mol control), helping to explain the hypercoagulable state of gestation[10]. With the previous changes in the sialic acid content of pregnant women only focusing on one time-period during gestation, we hypothesize that the sialic acid content of pregnant adult fibrinogen will decrease from the second to third trimester. Future efforts of our lab will focus on the isolation of fibrinogen from plasma samples collected from pregnant women during both their second and third trimesters. Purification of fibrinogen from the blood plasma of pregnancy samples will utilize the high-affinity GPRPFPAWK knob 'A'-mimic peptide column developed in the Hudson lab described in Chapter 2[19]. Fibrinogen concentration will be assessed by an ELISA before performing structural

and functional comparison tests to fibrinogen purified from healthy non-pregnant patients in the same manner. Structural comparison should include western blot protein detection using polyclonal fibrinogen-specific antibodies. Assessment of the sialic acid content can be determined via a sialic acid (NANA) colorimetric assay kit (BioVision Incorporated), and mass-spectrometry. Functional comparison will include turbidity/turbidimetry assays (described in Chapter 2 section 2.2.6.4). Scanning electron microscopy images of formed clots from purified samples can also provide a close-up look at the fibrin network morphological differences during pregnancy.

4.2.2 *Pregnancy Sample Information*

As proof-of-concept, we have begun isolating a few pregnancy patient samples, by Prof. Linda May at BSoM, with samples obtained from a previous pregnancy study supported by the NIH. These samples were obtained from 16 non-fasted, pregnant women (18-40 years old) during the second (16 weeks) and third (36 weeks) trimesters. Women were recruited when at <16 weeks gestation, and were otherwise free from any history of thromboembolic events.

4.2.3 *Preliminary Results*

Following a similar process described in Chapter 2 (section 2.2.6.2), human fibrinogen was isolated from two plasma samples collected during the 2nd ("pre"; ~700 µL) and 3rd ("post"; ~600 µL) trimesters, respectively using the GPRP-based affinity column, with subsequent aggregation removal and purification by SEC. Concentrations for collected samples were then determined by an ELISA following the procedure described in Chapter 2 (section 2.2.4.1), with results shown in Figure 4.1. Isolation of small amounts of fibrinogen from both the 2nd (0.65 mg) and 3rd (0.51 mg) trimester samples are inadequate for the suggested next steps, indicating a separate pregnancy study collecting larger volumes of blood may be necessary to enhance yields.

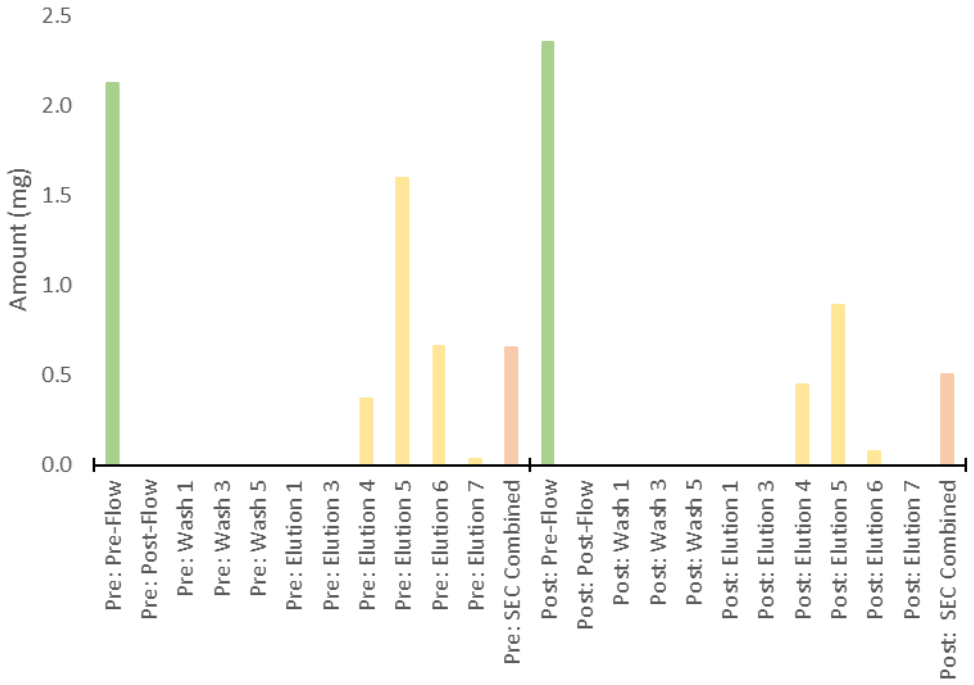

Figure 4.1: Pregnancy plasma fibrinogen purification sample concentrations. 2nd trimester (pre) amounts (mg): pre-flow = 2.13, elution 4 = 0.37, elution 5 = 1.60, elution 6 = 0.67, elution 7 = 0.03, SEC combined = 0.65. 3rd trimester (post) amounts (mg): pre-flow = 2.36, elution 4 = 0.45, elution 5 = 0.89, elution 6 = 0.08, SEC combined = 0.51. All steps without visible bars above returned negative values determined to be negligent fibrinogen amounts: Pre: and post: post-flows, washes 1, 3, and 5, and elutions 1, and 3, as well as post: elution 7.

4.3 **Fibrinogen-Specific Protofibril-Like Modelling**

4.3.1 *Evidence for Fibrinogen Self-Assembly*

The process of fibrin polymerization has long been studied due to its impact on hemostasis and other pathological conditions[20]. However, some evidence reveals fibrinogen alone to "polymerize" without thrombin's cleavage of FpA/B to elicit knobs "A/B," through noncovalent intermolecular association between D interfaces of adjacent fibrinogen molecules[21]. This phenomenon has also been showcased in a congenital dysfibrinogenemia resulting in inefficient

fibrin clot assembly highlighting a variant of fibrinogen (Tokyo II), whereby normal D:E region interactions as well as D:D region interactions persisted and short fibrillar segments were visualized[22]. A more recent study focusing on the hydrodynamic behavior of in-solution fibrinogen explains the self-assembly of fibrinogen molecules by way of extensive non-covalent, intermolecular interactions mediated by the entanglement of adjacent highly dynamic αC regions intramolecularly bound to their respective E regions[4, 23]. By then theoretically modeling the experimental data, it was indicated that fibrinogen's available conformations converted between flexed and rod-like shapes. Resolving the intricacies of fibrinogen self-association may describe the mechanism of crosslinking in more depth and shed light on the fundamentals of intermolecular fibrin assembly. Our lab's future efforts will focus on this phenomenon through the creation of intermediate-resolution molecular structures highlighting fibrinogen-specific protofibril-like interactions (such as γ-γ dimers and DDE complexes) formed under cryogenic conditions, like those shown in Chapter 3 (Figure 3.6B), utilizing CryoSPARC's 3DVA function to segment the flexing of fibrinogen-based structures into their principal components.

4.3.2 *Preliminary Results*

As discussed in Chapter 3, the addition of an fmoc-protected version of the high affinity knob "A"-mimic peptide to the fibrinogen samples prior to the freezing process resulted in "fibrinogen-specific protofibril-like formation." Upon initial particle picking and 2D classification described for the fiber containing micrographs, more interesting classes presented themselves resembling whole fibrinogen molecular views, γ-γ dimers, DDE complexes, multi-stranded fibrils (beyond two strands), and paired γ-γ dimerized fibrinogen molecules (Figure 4.2). The representative classes shown below are made up of approximately 270,000 particle picks. Exploration of each class type (based on color variations) will undergo further 2D

classification and selection before 3D reconstruction and analysis of the produced volumes. Efforts to procure high-resolution reconstructions of all class types will likely involve the collection of more micrograph images from which to increase the amount of clear particle pick orientations for enhanced 2D class averages.

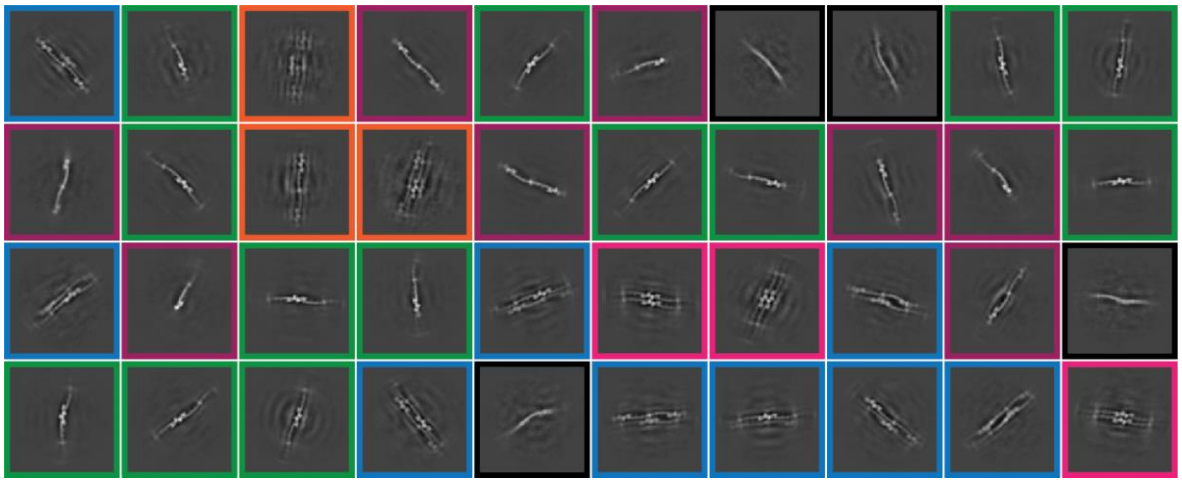

Figure 4.2: Representative 2D class averages from fibrinogen-specific protofibril-like particle picks. Classes include whole fibrinogen molecules (purple), γ-γ dimers (green), DDE complexes (blue), multi-stranded fibrils (orange), paired γ-γ dimerized fibrinogen molecules, and non-specific structures most likely representative of blurred whole fibrinogen molecules due to conformational variability (black).

Initial efforts were focused on achieving a high-resolution structure of the whole molecule of in-solution fibrinogen. Multiple rounds of 2D classification and selection of class averages similar to those in Figure 4.2 (purple classes) led to ~48,000 particle picks separated into 7 classes. These particles were used in the reconstruction of an initial volume that was then refined to obtain a global resolution of 7.34 Å (Figure 4.3A&B). Despite this intermediate resolution value, visualization of the refined volume indicated that the overall structure was likely a much lower resolution. Additionally, the reconstructed volume does not showcase an isolated whole fibrinogen molecule as the ends of the molecule show some extra D region volume likely due to

γ-γ dimer formation and the absence of the αC-domain. Performing 3DVA on the refined structure led to the development of a volume series of 20 frames that was used to create a movie demonstrating the conformational breathing of fibrinogen from a rod-like to a flexing shape (Figure 4.3C), with a "bottom" view (Figure 4.3C right) structure exhibiting a slight central bent conformation like that shown in negative stain TEM class averages (Figure 1.5)[2]. Production of multiple high-resolution native state conformations of fibrinogen from a rod-like to flexing structure will fundamentally alter the current static understanding of this conformationally dynamic intrinsically flexible protein, and may uncover the role of flexion on the processes of polymerization and fibrinolysis.

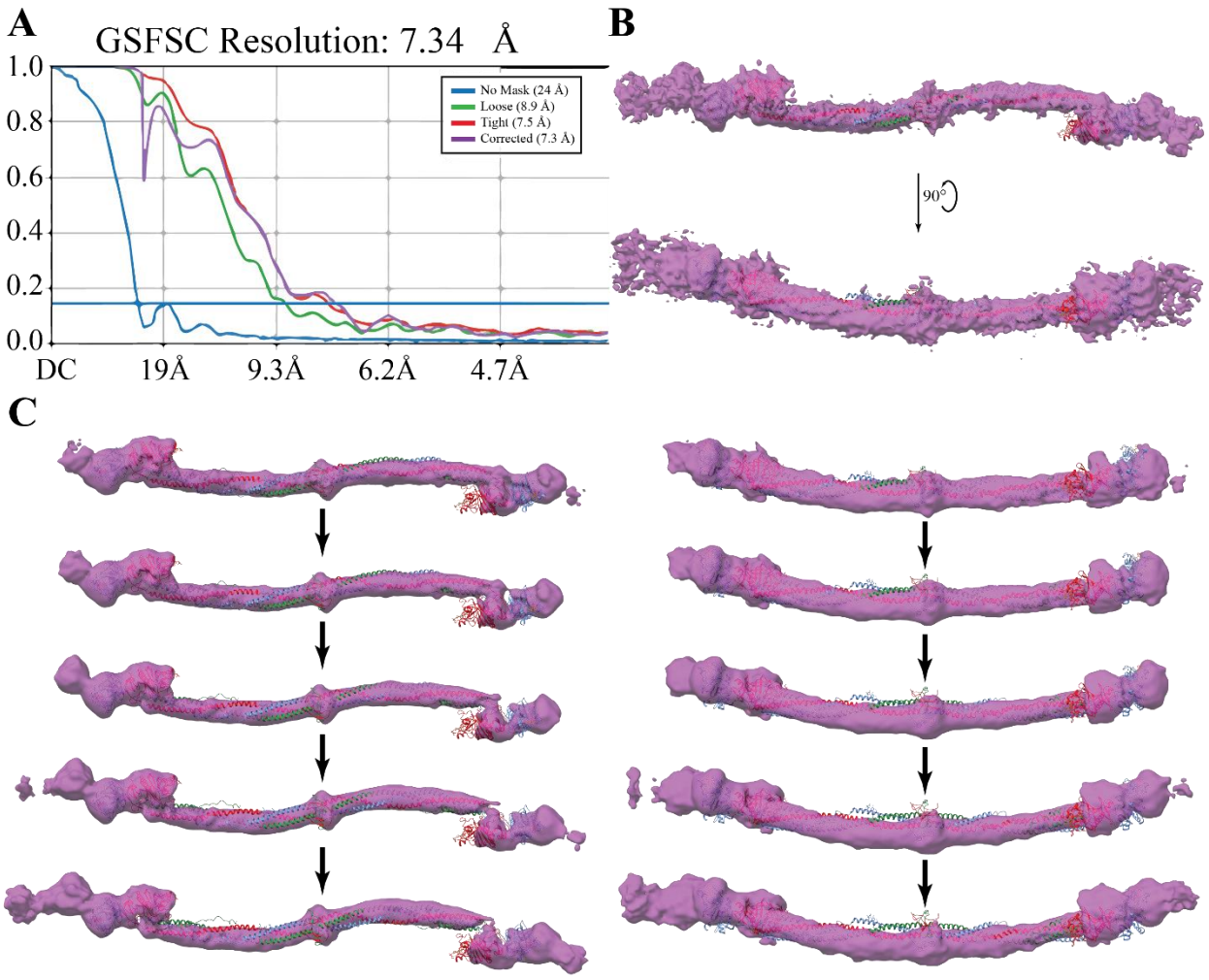

Figure 4.3: Initial modelling of a whole fibrinogen molecule. (A) GSFSC global resolution curves for a (B) homogeneously refined angular reconstruction map fit with a known PDB crystal structure of a whole fibrinogen molecule (3GHG). (C) Five representative frames separated by 5 frames each of a single component of variability highlighting flexibility of the homogeneously refined structure of fibrinogen from "side" (left) and "bottom" (right) views. 3GHG was fit to the first frame and remained stationary throughout the entire video and is characterized by alpha (green), beta (red), and gamma (blue) chains.

In conclusion, the insights of this thesis are three-fold. Firstly, our transient recombinant human fibrinogen expression system provides a less costly and time-intensive avenue for protein production compared to current stable systems for fibrinogen. Secondly, our affinity-based approach for fibrinogen isolation from complex media displays more rapid and selective purification of functional fibrinogen than gold-standard methods. Thirdly, high-resolution analysis of the in-solution 3D reconstruction of fibrinogen's D region suggests a more conformationally dynamic structure for fibrinogen than standard model representations. These critical findings seek to expand the field of fibrinogen research by enhancing synthesis, purification, and structural determination methods of human fibrinogen for the future efforts of better understanding fibrinogen's structural relationship to downstream biological functions.

References

1. Vilar, R.; Fish, R. J.; Casini, A.; Neerman-Arbez, M., Fibrin (ogen) in human disease: both friend and foe. *Haematologica* **2020,** *105* (2), 284.

2. Pinelo, J. E.; Manandhar, P.; Popovic, G.; Ray, K.; Tasdelen, M. F.; Nguyen, Q.; Iavarone, A. T.; Offenbacher, A. R.; Hudson, N. E.; Sen, M., Systematic mapping of the conformational landscape and dynamism of soluble fibrinogen. *Journal of Thrombosis and Haemostasis* **2023**.

3. Köhler, S.; Schmid, F.; Settanni, G., The internal dynamics of fibrinogen and its implications for coagulation and adsorption. *PLoS computational biology* **2015,** *11* (9), e1004346.

4. Zuev, Y. F.; Litvinov, R. I.; Sitnitsky, A. E.; Idiyatullin, B. Z.; Bakirova, D. R.; Galanakis, D. K.; Zhmurov, A.; Barsegov, V.; Weisel, J. W., Conformational flexibility and self-association of fibrinogen in concentrated solutions. *The Journal of Physical Chemistry B* **2017,** *121* (33), 7833-7843.

5. Hirashima, M.; Imamura, T.; Yano, K.; Kawamura, R.; Meta, A.; Tokieda, Y.; Nakashima, T., High-level expression and preparation of recombinant human fibrinogen as biopharmaceuticals. *The Journal of Biochemistry* **2016,** *159* (2), 261-270.

6. Kaijzel, E.; Koolwijk, P.; Van Erck, M.; Van Hinsbergh, V.; De Maat, M., Molecular weight fibrinogen variants determine angiogenesis rate in a fibrin matrix in vitro and in vivo. *Journal of Thrombosis and Haemostasis* **2006,** *4* (9), 1975-1981.

7. Manten, G. T.; Franx, A.; Sikkema, J.; Hameeteman, T. M.; Visser, G. H.; de Groot, P. G.; Voorbij, H. A., Fibrinogen and high molecular weight fibrinogen during and after normal pregnancy. *Thrombosis research* **2004,** *114* (1), 19-23.

8. Uchikova, E. H.; Ledjev, I. I., Changes in haemostasis during normal pregnancy. *European Journal of Obstetrics & Gynecology and Reproductive Biology* **2005,** *119* (2), 185-188.

9. Nellenbach, K.; Kyu, A.; Guzzetta, N.; Brown, A. C., Differential sialic acid content in adult and neonatal fibrinogen mediates differences in clot polymerization dynamics. *Blood Advances* **2021,** *5* (23), 5202-5214.

10. Maghzal, G. J.; Brennan, S. O.; George, P. M., The sialic acid content of fibrinogen decreases during pregnancy and increases in response to fibrate therapy. *Thrombosis research* **2005,** *115* (4), 293-299.

11. Adler, G.; Duchinski, T.; Jasinska, A.; Piotrowska, U., Fibrinogen fractions in the third trimester of pregnancy and in puerperium. *Thrombosis research* **2000,** *97* (6), 405-410.

12. Cortet, M.; Deneux-Tharaux, C.; Dupont, C.; Colin, C.; Rudigoz, R.-C.; Bouvier-Colle, M.-H.; Huissoud, C., Association between fibrinogen level and severity of postpartum haemorrhage: secondary analysis of a prospective trial. *British journal of anaesthesia* **2012,** *108* (6), 984-989.

13. Hansen, A. T.; Andreasen, B. H.; Salvig, J. D.; Hvas, A.-M., Changes in fibrin D-dimer, fibrinogen, and protein S during pregnancy. *Scandinavian journal of clinical and laboratory investigation* **2011,** *71* (2), 173-176.

14. Liu, X.-h.; Jiang, Y.-m.; Shi, H.; Yue, X.-a.; Wang, Y.-f.; Yang, H., Prospective, sequential, longitudinal study of coagulation changes during pregnancy in Chinese women. *International Journal of Gynecology & Obstetrics* **2009,** *105* (3), 240-243.

15. Réger, B.; Péterfalvi, Á.; Litter, I.; Pótó, L.; Mózes, R.; Tóth, O.; Kovács, G. L.; Losonczy, H., Challenges in the evaluation of D-dimer and fibrinogen levels in pregnant women. *Thrombosis research* **2013,** *131* (4), e183-e187.

16. Karlsson, O.; Jeppsson, A.; Hellgren, M., A longitudinal study of factor XIII activity, fibrinogen concentration, platelet count and clot strength during normal pregnancy. *Thrombosis Research* **2014,** *134* (3), 750-752.

17. McPherson, H. R.; Duval, C.; Baker, S. R.; Hindle, M. S.; Cheah, L. T.; Asquith, N. L.; Domingues, M. M.; Ridger, V. C.; Connell, S. D.; Naseem, K. M., Fibrinogen αC-subregions critically contribute blood clot fibre growth, mechanical stability, and resistance to fibrinolysis. *Elife* **2021,** *10*, e68761.

18. Holm, B.; Brosstad, F.; Kierulf, P.; Godal, H., Polymerization properties of two normally circulating fibrinogens, HMW and LMW. Evidence that the COOH-terminal end of the a-chain is of importance for fibrin polymerization. *Thrombosis research* **1985,** *39* (5), 595-606.

19. Popovic, G.; Kirby, N. C.; Dement, T. C.; Peterson, K. M.; Daub, C. E.; Belcher, H. A.; Guthold, M.; Offenbacher, A. R.; Hudson, N. E., Development of Transient Recombinant Expression and Affinity Chromatography Systems for Human Fibrinogen. *International Journal of Molecular Sciences* **2022,** *23* (3), 1054.

20. Weisel, J. W.; Litvinov, R. I., Fibrin formation, structure and properties. *Fibrous proteins: structures and mechanisms* **2017**, 405-456.

21. Mosesson, M. W.; Siebenlist, K. R.; Hainfeld, J. F.; Wall, J., The covalent structure of factor XIIIa crosslinked fibrinogen fibrils. *Journal of structural biology* **1995,** *115* (1), 88-101.

22. Mosesson, M. W.; Siebenlist, K. R.; DiOrio, J. P.; Matsuda, M.; Hainfeld, J. F.; Wall, J., The role of fibrinogen D domain intermolecular association sites in the polymerization of

fibrin and fibrinogen Tokyo II (gamma 275 Arg--> Cys). *The Journal of clinical investigation* **1995,** *96* (2), 1053-1058.

23. Litvinov, R. I.; Yakovlev, S.; Tsurupa, G.; Gorkun, O. V.; Medved, L.; Weisel, J. W., Direct evidence for specific interactions of the fibrinogen αC-domains with the central E region and with each other. *Biochemistry* **2007,** *46* (31), 9133-9142.

APPENDIX – Fibrinolysis: An Illustrated Review

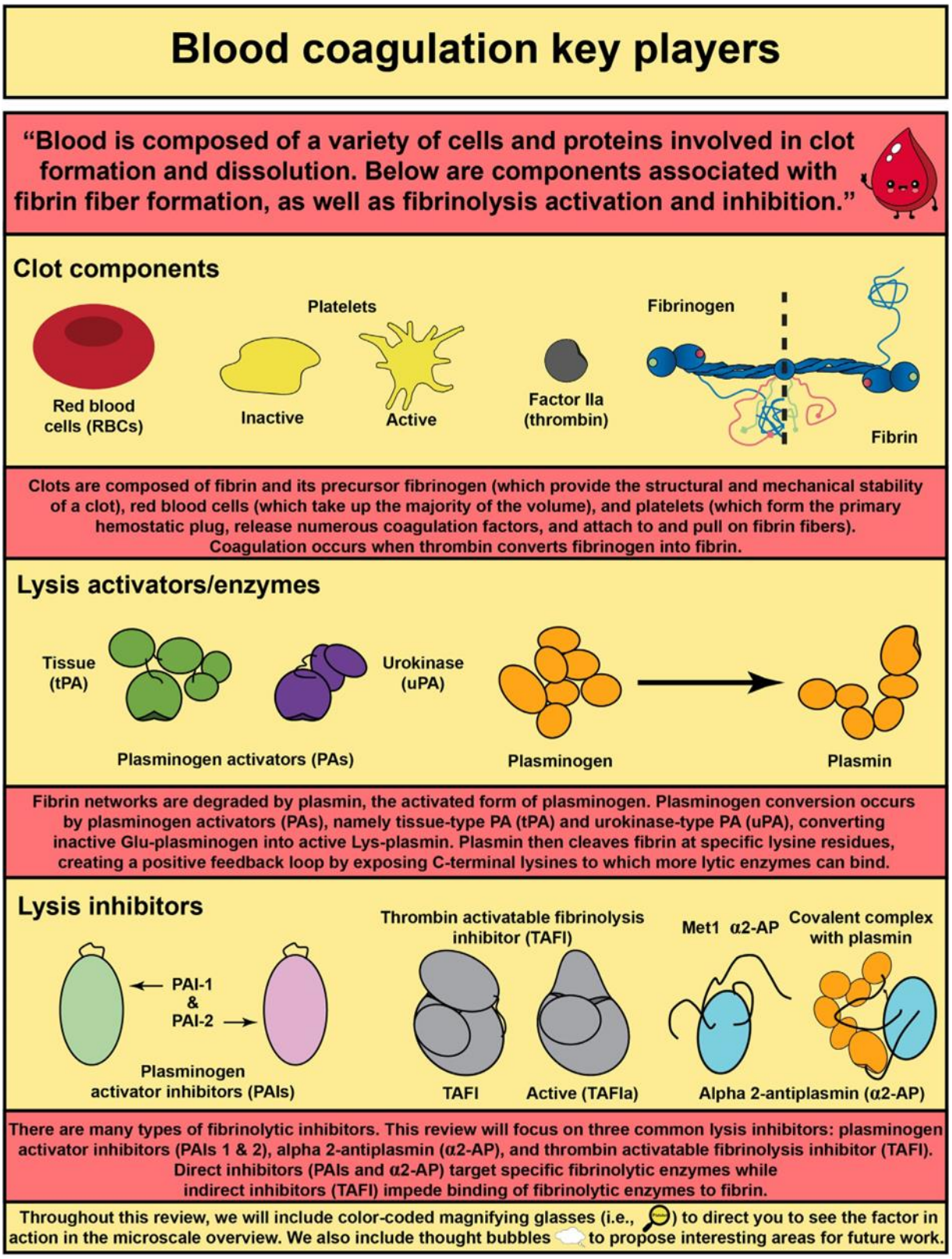

Fibrinolysis[1-3]
The enzymatic degradation of blood clots

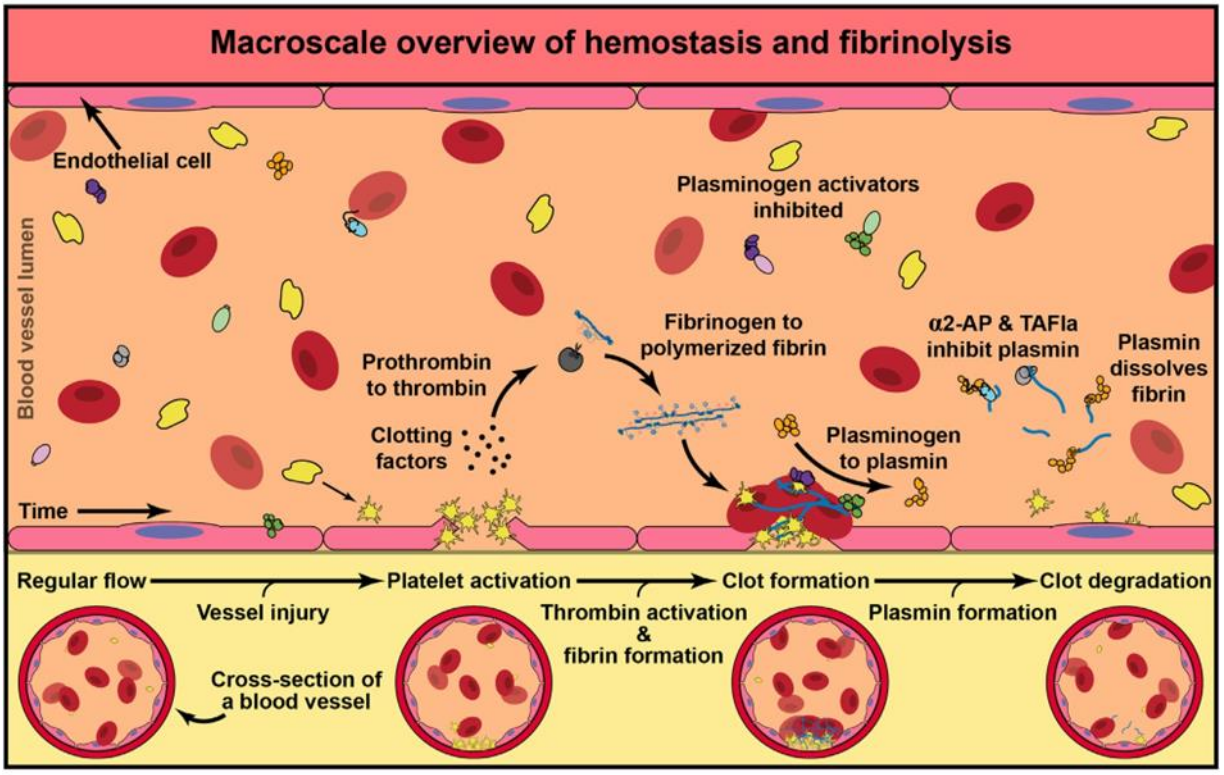

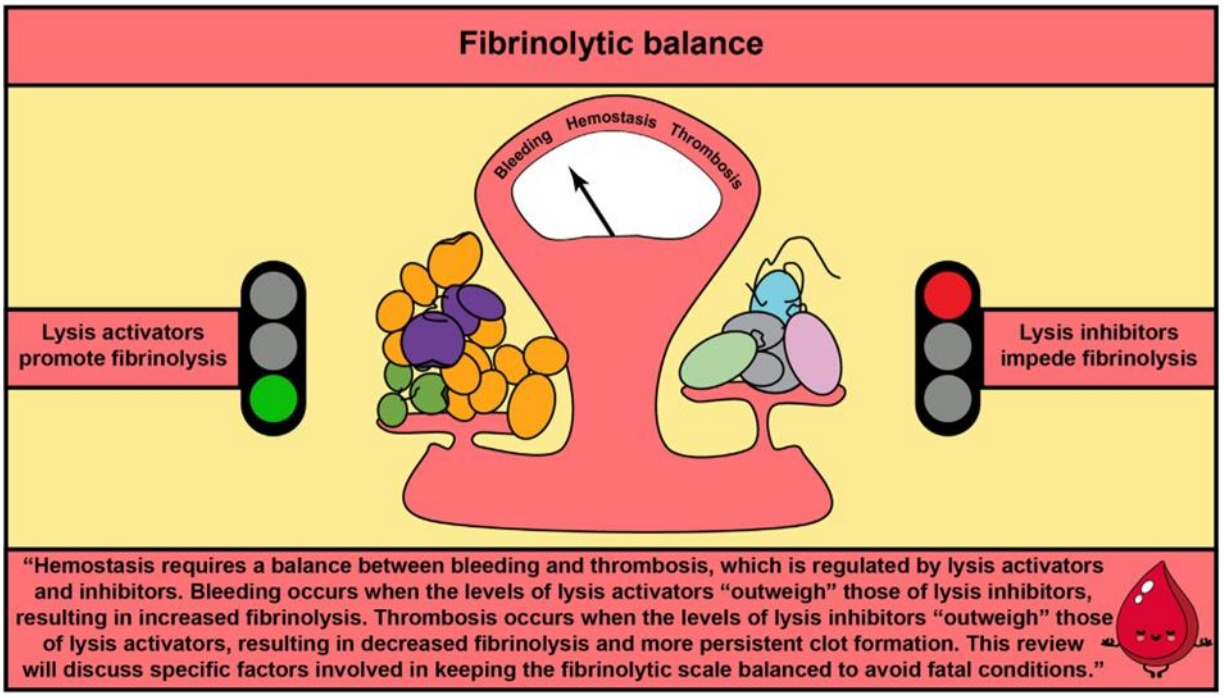

Fiber polymerization and digestion[4-11]

Formation fundamentals[4-10]

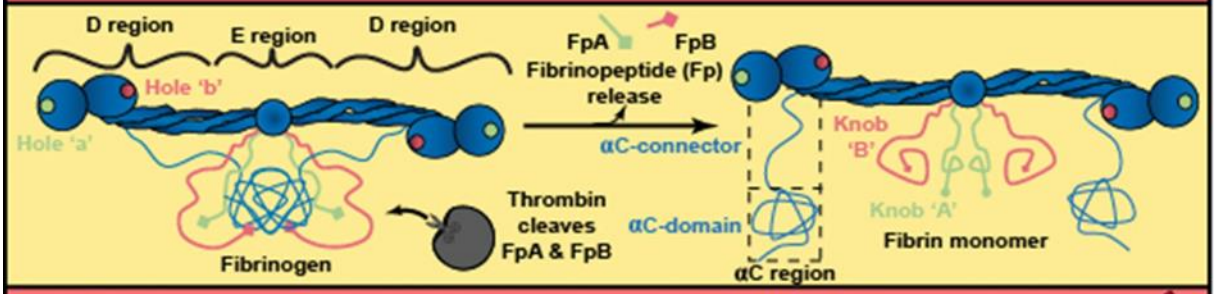

"Thrombin cleavage of fibrinopeptides A and B (FpA/B) converts fibrinogen into fibrin, exposing knobs 'A' and 'B' for binding to holes 'a' and 'b', respectively (1). Fibrin monomers interact in a half-staggered manner to form protofibrils that laterally aggregate into a fibrin network stabilized by FXIIIa cross-linking. Network digestion into smaller fibrin-based molecules (see FDP's below) occurs at specific molecular locations (2)."

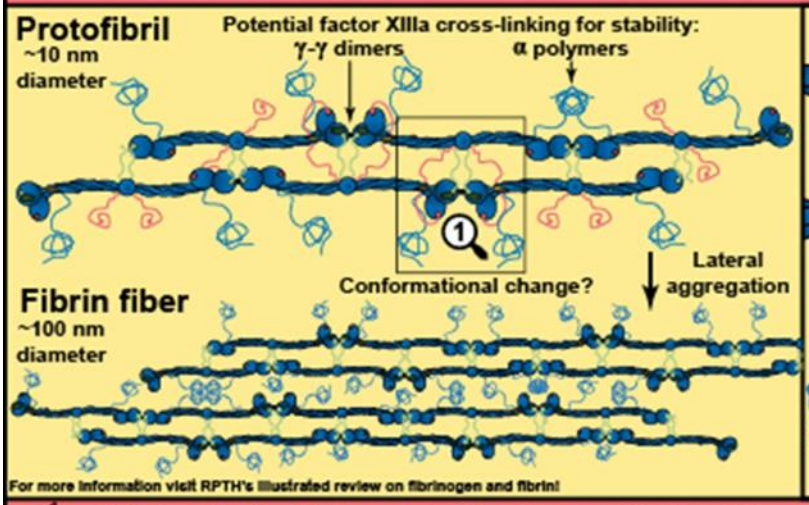

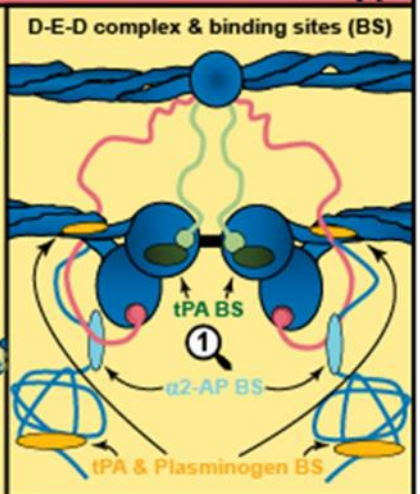

"It is hypothesized that a conformational change of the β nodules reveals cryptic plasminogen/tPA binding sites (Aα 148-160) after fibrinogen to fibrin conversion. Similarly, a change between β and γ nodules may uncover tPA-specific binding sites (γ 312-324). Although the above binding sites are involved in fibrinolysis activation, α2-AP binding sites on the αC region exhibit inhibition of fibrinolysis by plasmin deactivation."

Fibrin degradation products (FDPs)[11]

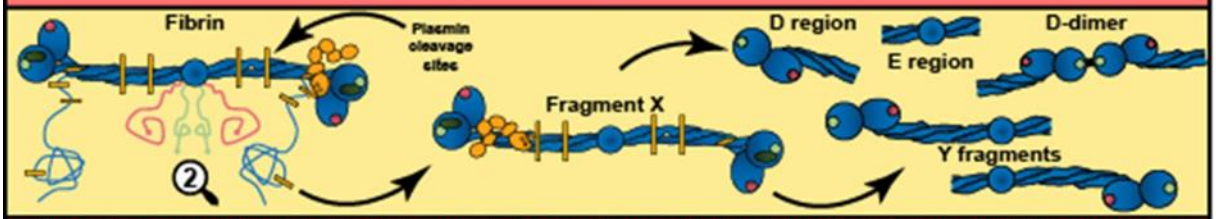

Plasmin-mediated fibrinolysis results in fibrin degradation products (FDPs). The αC region is fully removed by cleavage at residues α 230 and α 206 to give fragment X. This is further degraded at points along the coiled-coil region, where degradation of FXIIIa ligated fibrin may result in the release of D-dimer fragments.

Plasmin-mediated fibrinolysis[12-29]

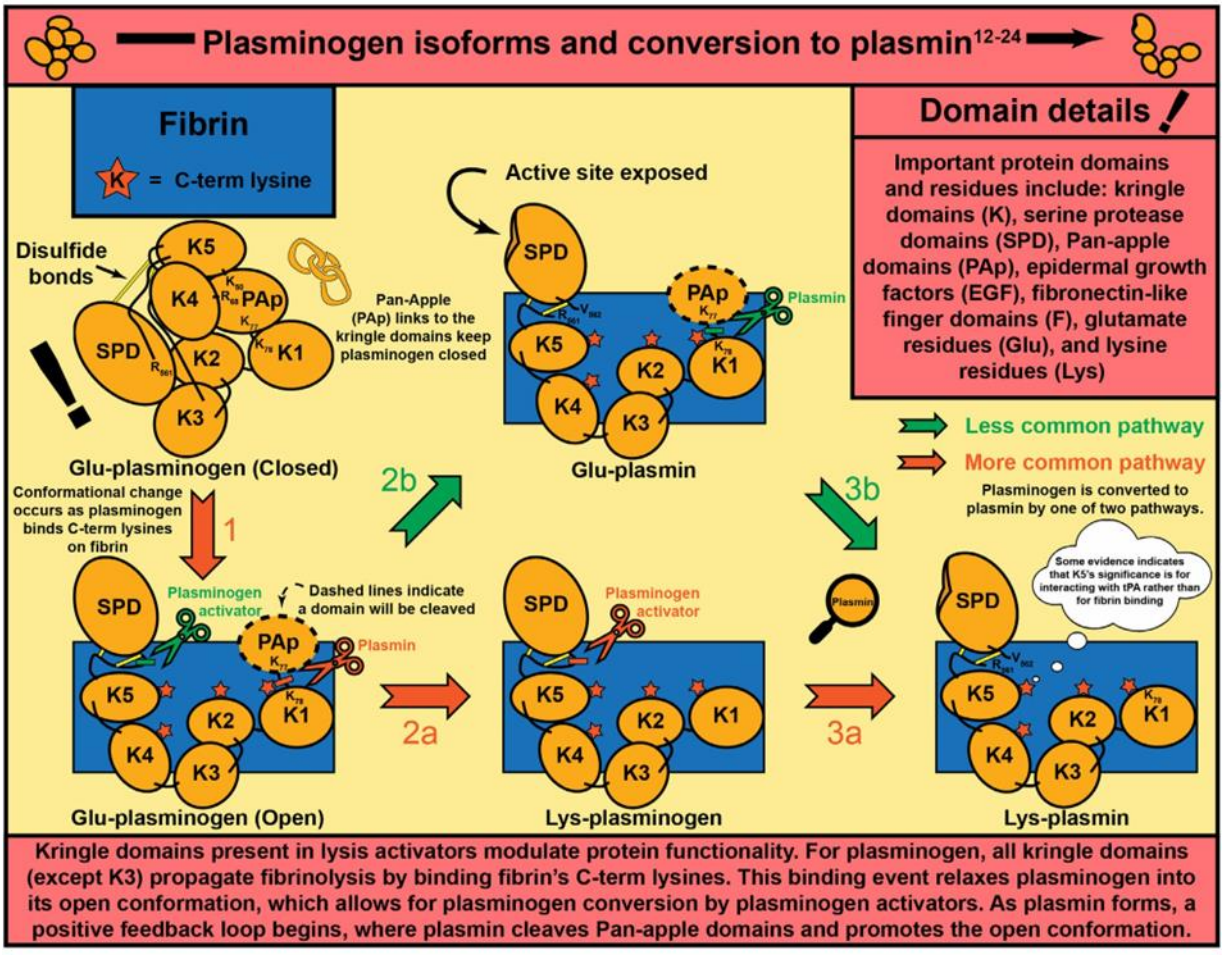

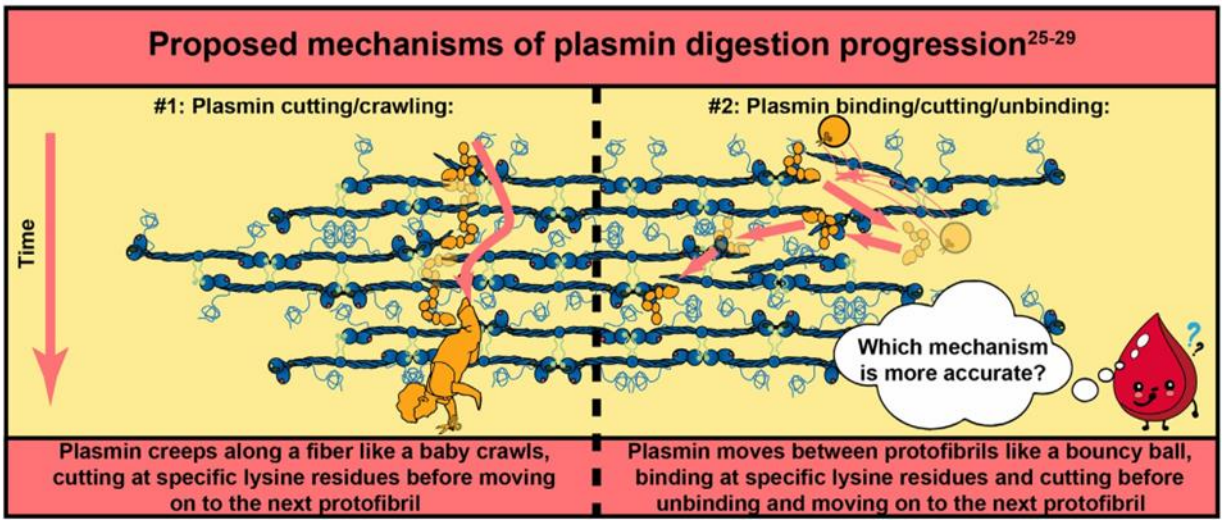

Plasminogen activators' role in fibrinolysis

Plasminogen activators (PAs)[30-40]

Tissue-type PA (tPA)

Single chain (sc-tPA)

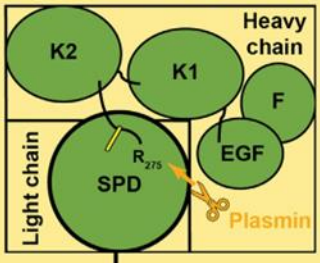

Two chain (tc-tPA)

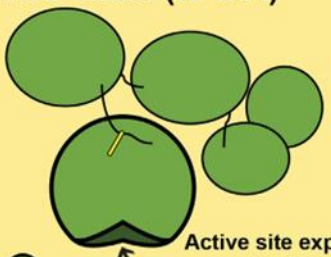

Active site exposure of catalytic triad: His 322, Asp 371, Ser 478

tPA is released from endothelial cells

tPA's finger domain (F) helps bind fibrin. Thus, tPA forms a trimeric complex with fibrin and plasminogen, whereas uPA only forms a dimeric complex with plasminogen.

The inactive single chain forms of tPA and uPA are converted to their active two chain forms by plasmin cleavage of distinct residues (tPA=Arg, uPA=Lys)

Plasminogen activators (PAs) initiate fibrinolysis by converting plasminogen into plasmin by cleaving a distinct arginine residue (R 561).

Urokinase-type PA (uPA)

Elevated levels of uPA are associated with cancer

Single chain (sc-uPA)

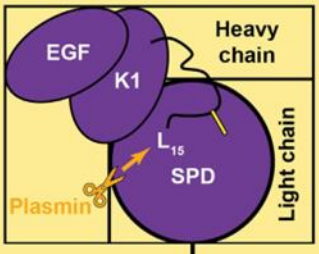

Two chain (tc-uPA)

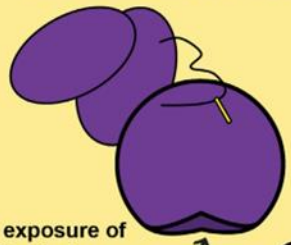

Active site exposure of catalytic triad: His 204, Asp 255, and Ser 356

"tPA and uPA differ in their plasminogen conversion by targeting fibrin-bound or circulating plasminogen, respectively. tPA's fibrin specificity comes from the presence of a fibronectin-like finger domain (F), which uPA lacks. The two-chain forms of both PAs are more efficient than their single-chain forms, but the single-chain PAs are still functional. Though both PAs perform similar functions, tPA is more common. "

Fibrinolysis can occur in two ways, or in combination

Internal fibrinolysis

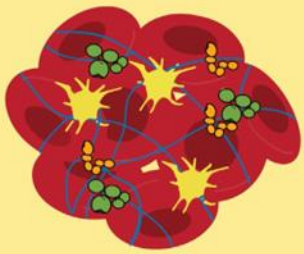

Physiological presence of lytic enzymes within a clot

External fibrinolysis

Exogenous delivery of lytic enzymes to a fully formed clot

tPA is a "clot buster" for clots that cannot be degraded on their own

Fibrinolysis inhibitors[40-59]

Below is each inhibitor's proposed mechanism of action

Plasminogen activator inhibitors (PAIs)[41-47]

PAIs inhibit lysis by binding PAs and impairing their ability to activate plasminogen into plasmin to cleave fibrin

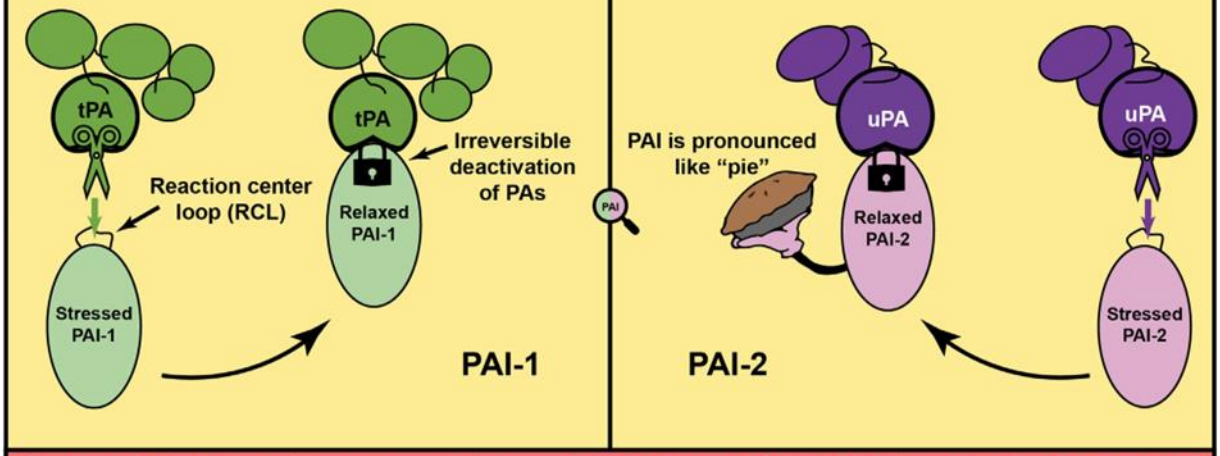

PAs cleave PAIs' RCLs and become covalently bound, thereby irreversibly inhibiting themselves in what is reffered to as a "suicide mechanism." There are two PAI isoforms: PAI-1 and PAI-2. While PAI-1 is more potent and efficient than PAI-2, tPA and uPA are affected by each PAI differently. PAI-1 is more potent for tPA than uPA, while PAI-2 is more potent for uPA than tPA. PAI-1 levels are elevated from obesity, cancer, and even pregnancy.

α2-Antiplasmin[48-52]

α2-AP limits lysis by binding to and inhibiting plasmin

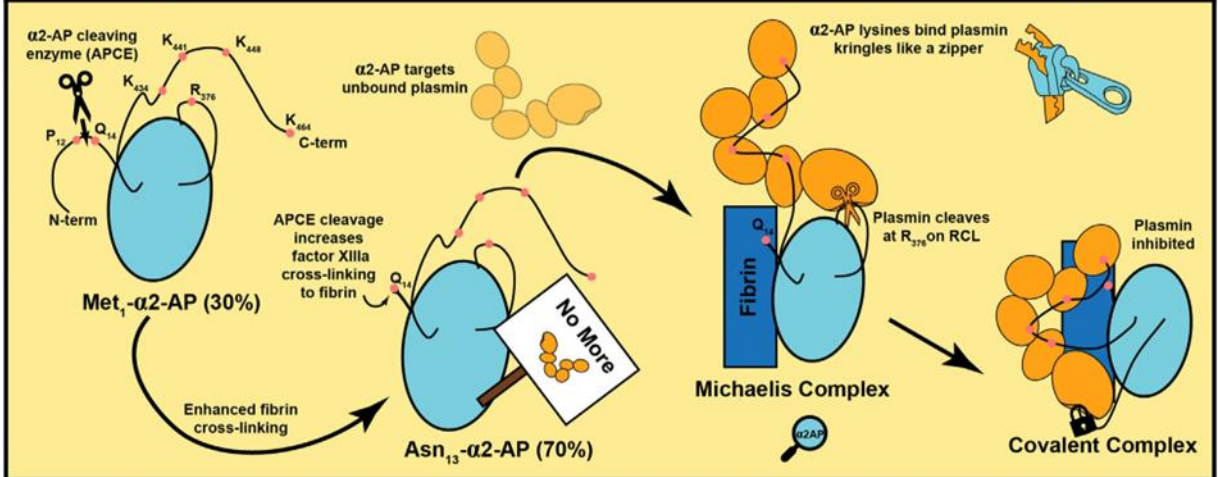

α2-AP is covalently linked to fibrin by factor XIIIa, and is involved in the inhibition of plasmin-mediated fibrinolysis. Incorporation of α2-AP into the fibrin network is increased (13 times faster) after APCE cleaves N-term residues of Met1-α2-AP (30% of α2-AP in blood) to give Asn13-α2-AP (70% of α2-AP in blood). Covalently linked to αC residue Lys 303, α2-AP is situated to grab unbound plasmin molecules and inhibit further fibrinolysis.

Thrombin activatable fibrinolysis inhibitor (TAFI)[52-58]

TAFI inhibits lysis by cleaving plasmin binding sites on fibrin

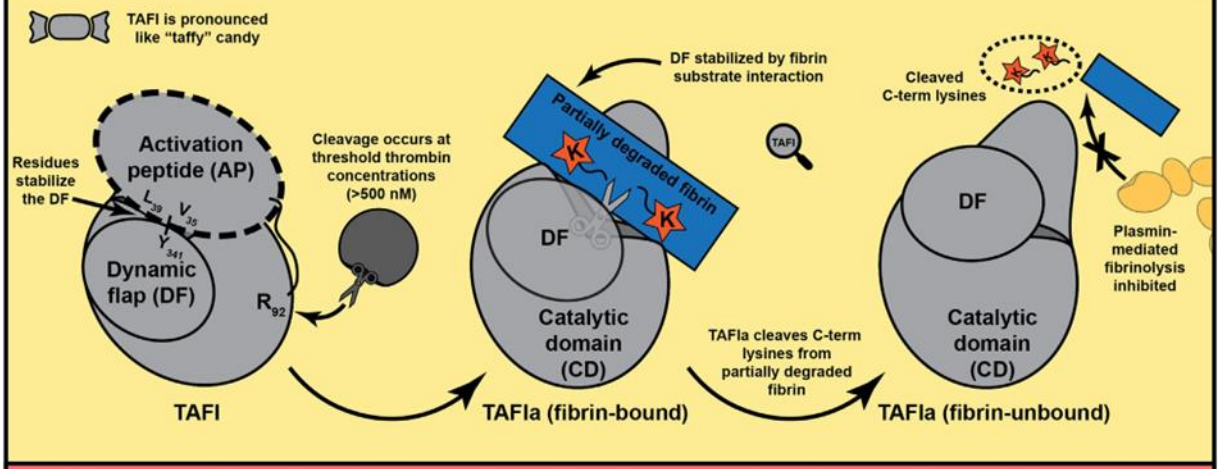

In TAFI's inactive form, the activation peptide stabilizes the dynamic flap. Cleavage of the activation peptide by thrombin at residue R 92 leads to dynamic flap destabilization and yields activated TAFI (TAFIa). Stability is returned as TAFIa binds partially degraded fibrin and cleaves C-term lysines. Since plasminogen and plasmin bind C-term lysines, TAFIa indirectly inhibits fibrinolysis by removing these sites.

Microscale overview of fibrinolysis[59]

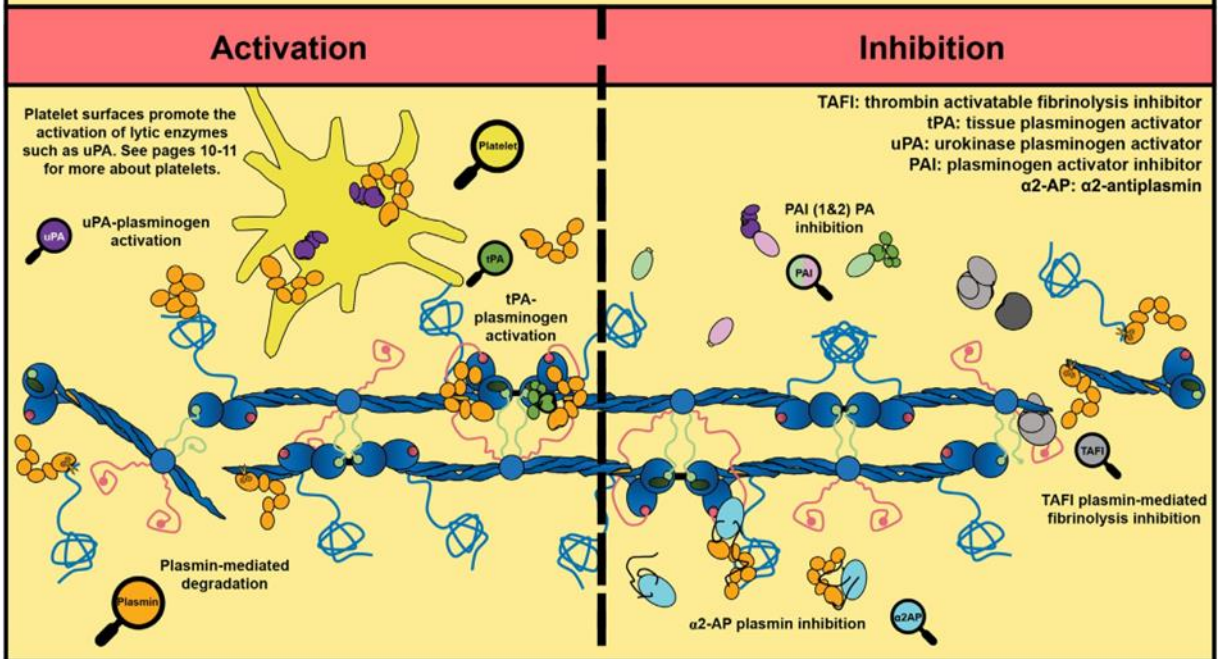

"As discussed on page 2, a balance of fibrinolytic activators and inhibitors are required to achieve hemostasis. The above graphic displays uPA, tPA, and plasmin in action to promote fibrinolysis (left) and PAIs, α2-AP, and TAFI interacting with the activators to inhibit fibrinolysis (right)."

Influence of fibrin network structure on fibrinolysis[60-72]

Fine/densely packed fibrin network with thin individual fibers

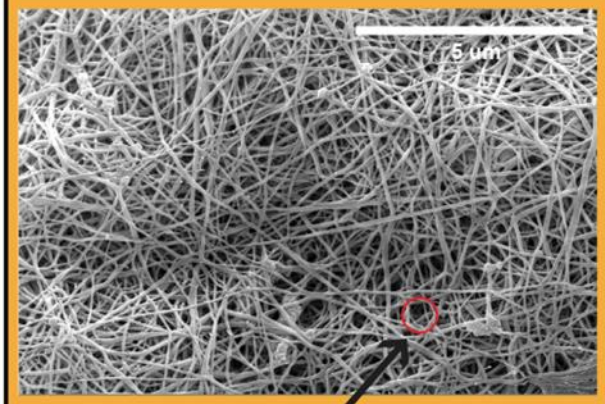

The pore size of the fibrin network is associated with network density. The lytic enzymes diffuse or perfuse through this space.

Coarse/loosely packed fibrin network with thick individual fibers*

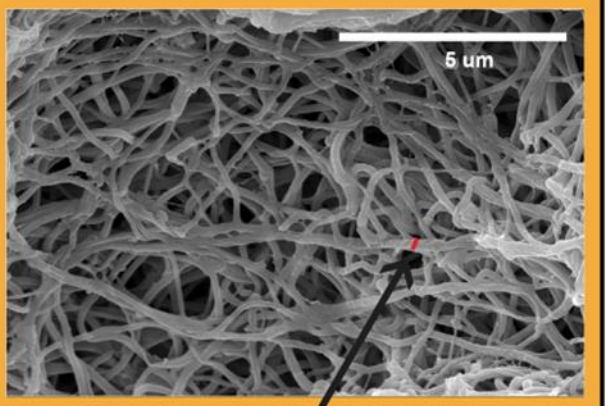

The diameter of the fibrin fiber is dependent on the lateral aggregation of protofibrils. Sometimes lateral aggregation occurs during the onset of lysis.

"Below, we represent fiber thickness by the width of the tree trunk and the packing density of the network by the number of trees that take up the same volume. The axe cutting down the trees is akin to plasmin lysing fibers."

Individual thin fibers lyse faster than individual thick fibers[60-63]

Thinner fibers have less width for plasmin/tPA to transversely cut.

Coarse clots lyse faster than fine clots* [60-62]

Fine clots have more fibers to break down

*There is conflicting evidence of this behavior, which supports the need for interdisciplinary studies (e.g., modeling)[15, 64]

Does tPA molecule to fiber ratio or tPA concentration govern rate of lysis?[25]

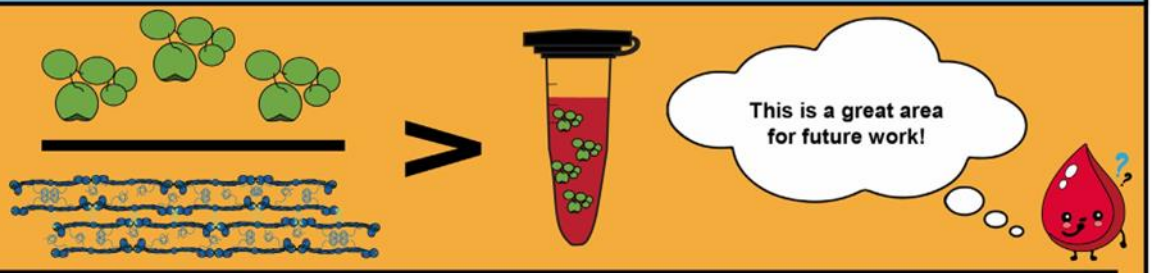

Modeling has shown the ratio is the dominant driver rather than the concentration. This relates to how tPA in the clinic is delivered to patients in a fixed concentration based on body weight, rather than considering personal concentrations of important factors, such as fibrinogen.

tPA: tissue plasminogen activator

Role of FXIIIa cross-linking[40, 46, 65-72]

FXIII, also known as fibrin stabilizing factor, is a blood protein that cross-links fibrin

Permeability

α-α and γ-γ cross-linking decreases the space between fibers and can limit permeability

α-α cross-linking leads to formation of higher molecular weight α polymers

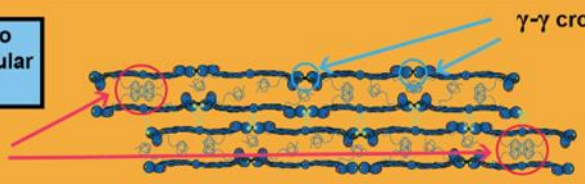

α2-AP and resistance to lysis

FXIIIa prevents α2-AP from being expelled from the network which makes the clot resistant to lysis. Below, we look at three scenarios with α2-AP and plasmin when there is FXIIIa cross-linking.

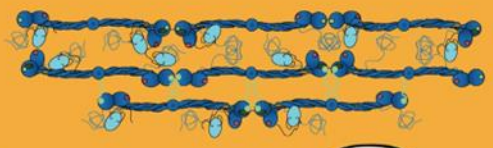

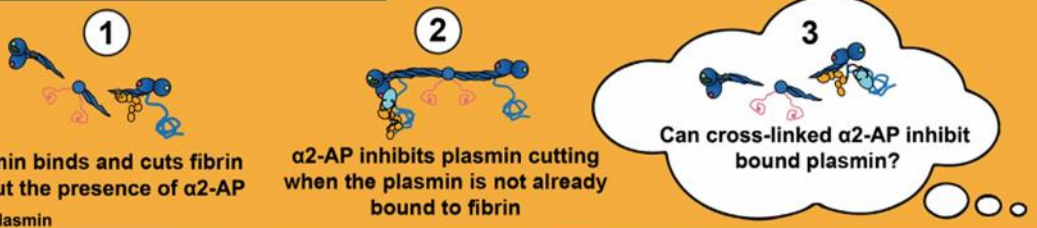

Plasmin binds and cuts fibrin without the presence of α2-AP

α2-AP inhibits plasmin cutting when the plasmin is not already bound to fibrin

α2-AP: α2-antiplasmin

Clot retraction

FXIIIa cross-linking and resulting clot retraction happens quickly and plays a large role in lysis inhibition

RBC retention

FXIIIa cross-linking aids in RBC retention, further limiting lysis

D-dimer production

D-dimers result from γ-γ cross-linking by FXIIIa.

Influence of platelets on fibrinolysis[73-87]

Platelet-activated clot contraction[63, 73-83]

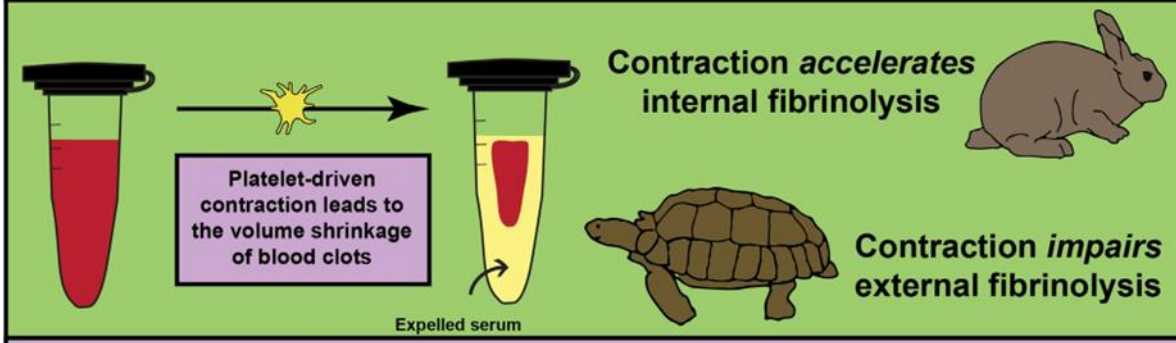

During clot contraction, platelets pull fibrin fibers together.
Clot contraction contradictorily modulates internal and external fibrinolysis.

Contraction reduces clot permeability[84]

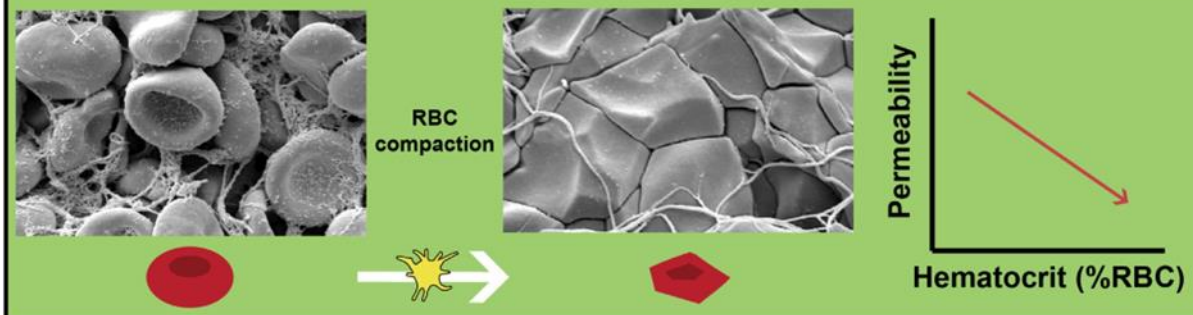

Red blood cells become densely packed in a tesselated polyhedral network during contraction, reducing the permeability of the clot and limiting lytic agent diffusion/perfusion

Platelets release fibrinolytic factors[85-87]

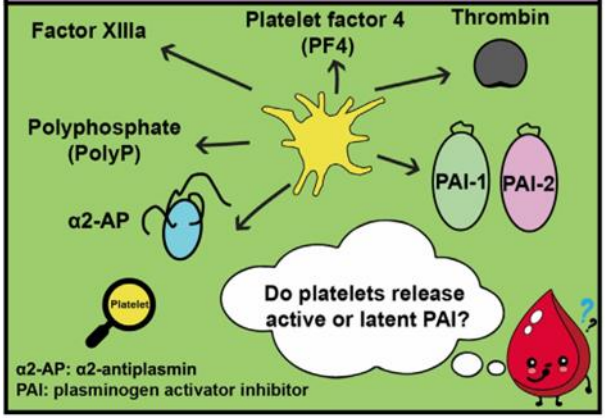

Platelets as activation sites[74, 76, 88]

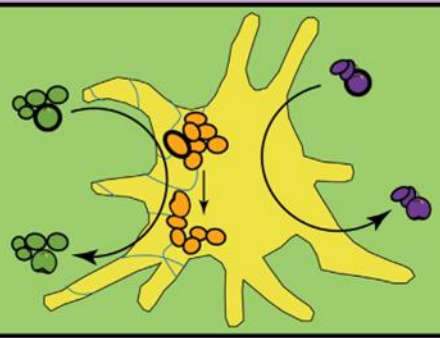

Platelet surfaces act as sites for activation of many fibrinolytic enzymes such as plasminogen and uPA

Platelets and fibrin-tension[89-95]

Platelets impact fiber tension and influence lysis

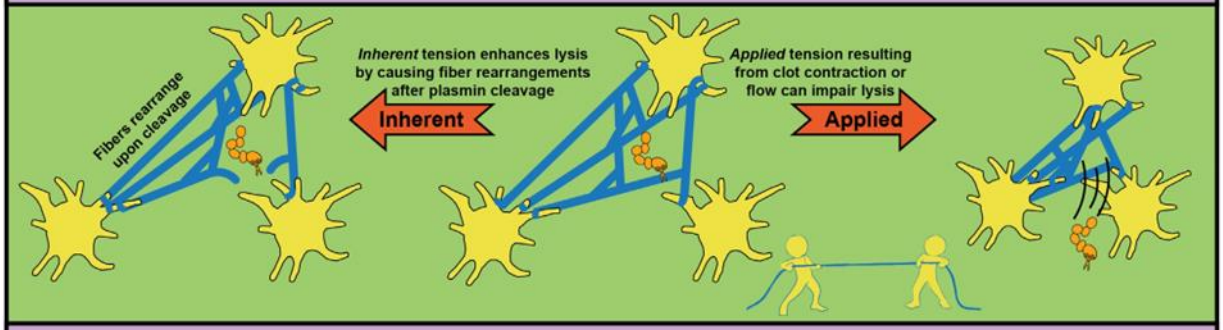

Fibers experience inherent tension upon polymerization and rearrange as select fibers are lysed (left), while platelets apply tension to a fibrin network by pulling and contracting a clot (right). Network shrinkage due to fiber rearrangements expels fibrinolytic molecules.

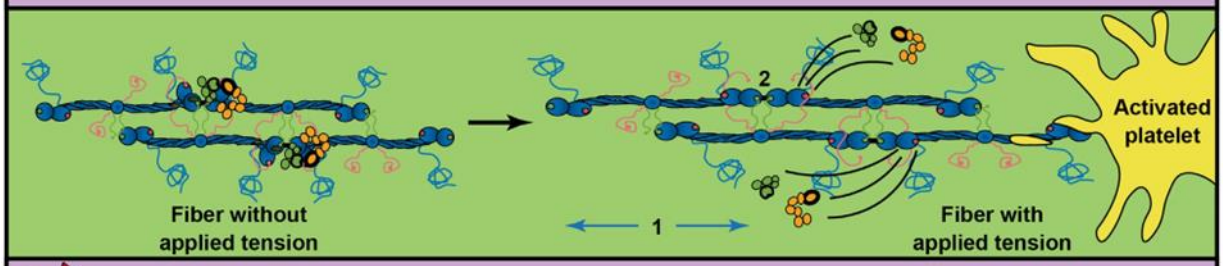

"Does molecular tension cause (1) elongation and/or (2) conformational change of D region that blocks plasminogen/tPA binding site?"

Does tension pull fibers apart during digestion?[7]

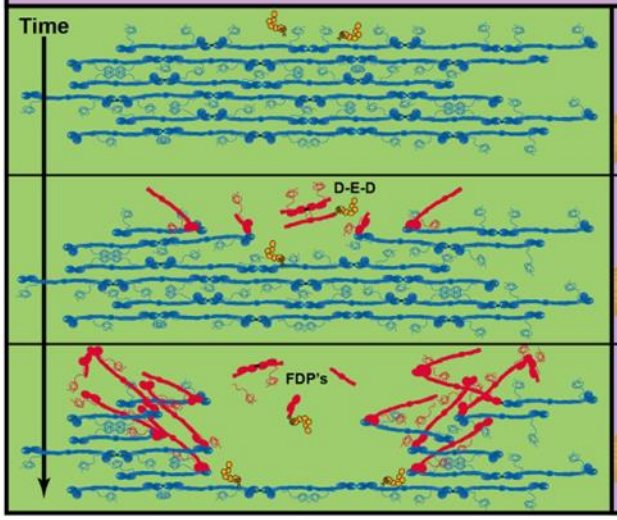

Protofibrils are under tension in a fiber, much like single strands experience strain in a rope.

It is hypothesized that as plasmin cleaves protofibrils, they splay backwards (red) like strands in a tensed rope.

Splaying backwards could expose buried binding sites and accelerate lysis.

Influence of red blood cells on fibrinolysis[96-100]

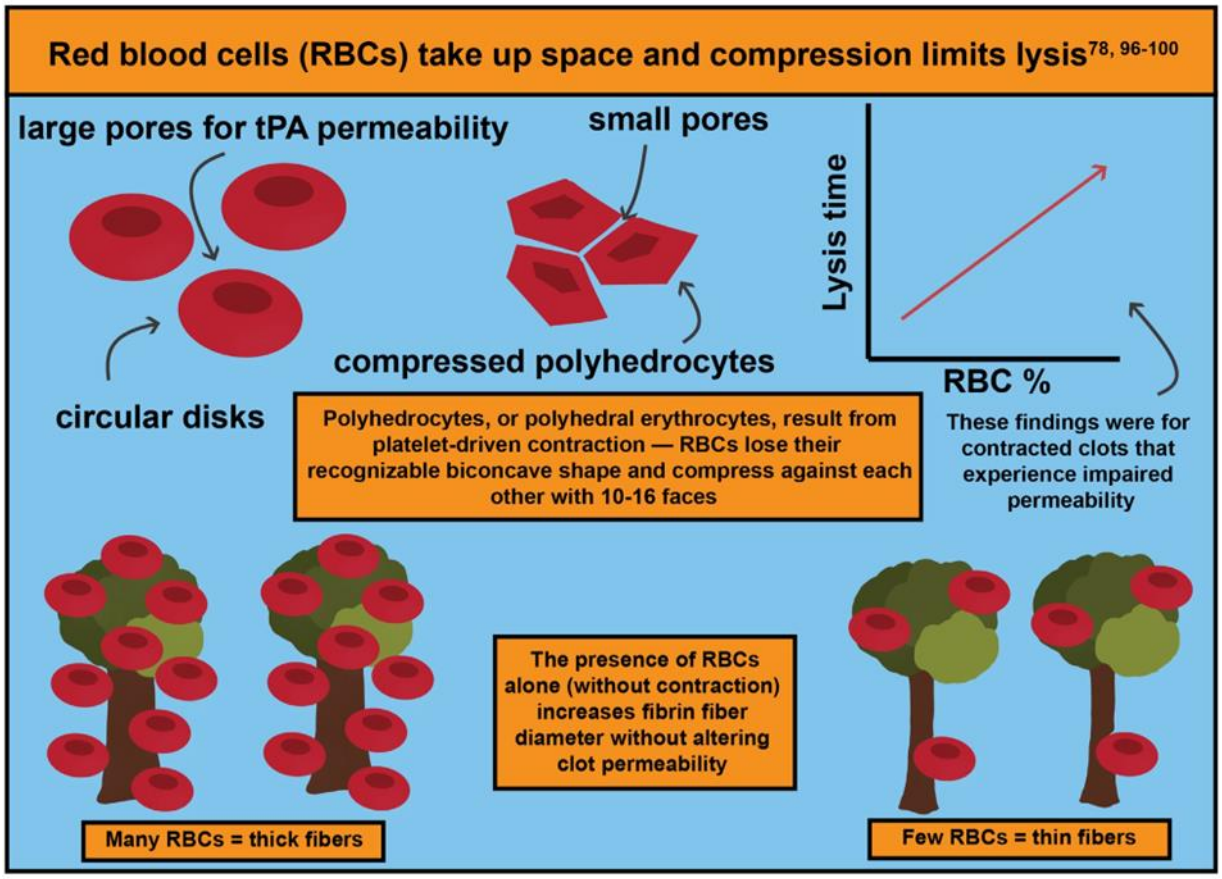

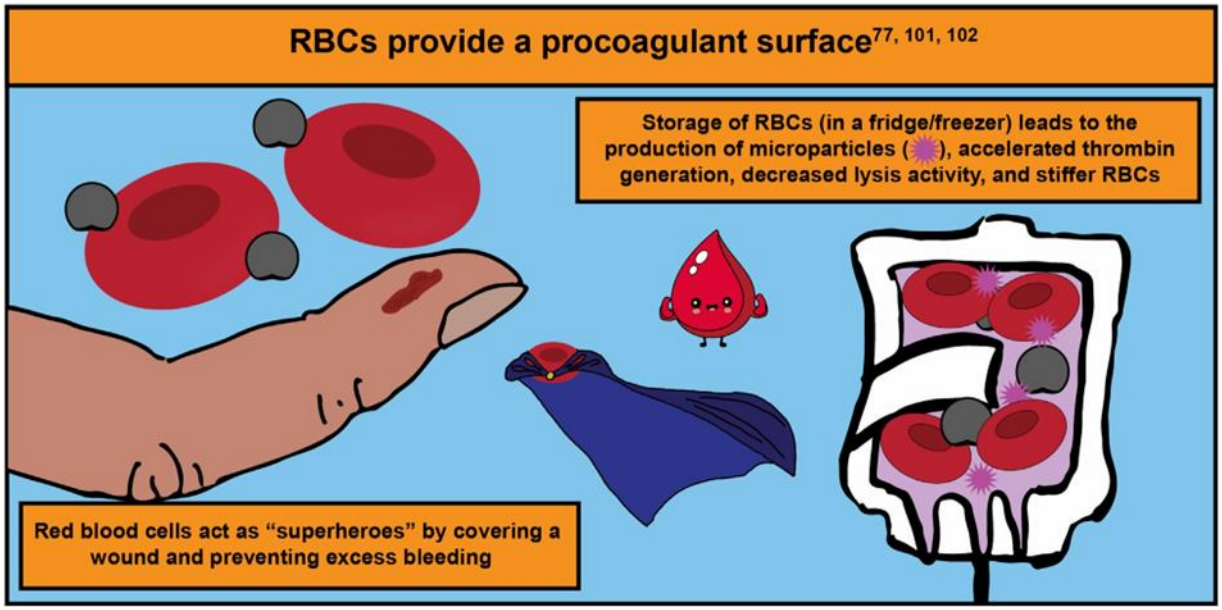

Laboratory techniques for analyzing fibrinolysis[103-119]

Turbidity[105-109]

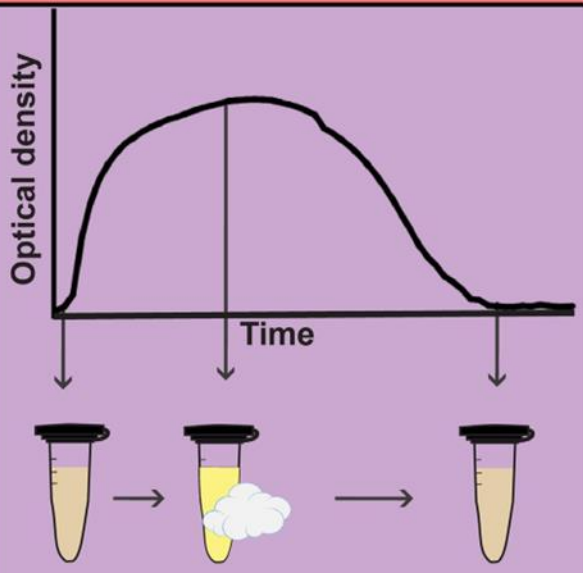

Transparent plasma becomes cloudy (or turbid) when a clot is formed. It turns back to transparent when lysed.

Fluorescent microscopy[25, 28, 110-112]

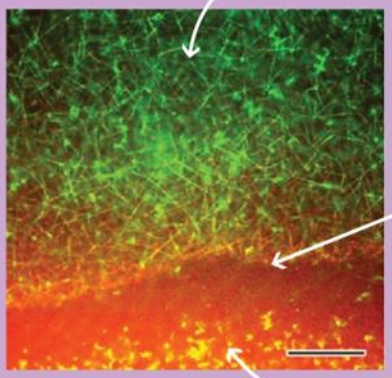

Confocal microscopy allows researchers to statically or kinetically visualize the 3-dimensional fibrin network

tPA: tissue plasminogen activator

Modeling[113, 114]

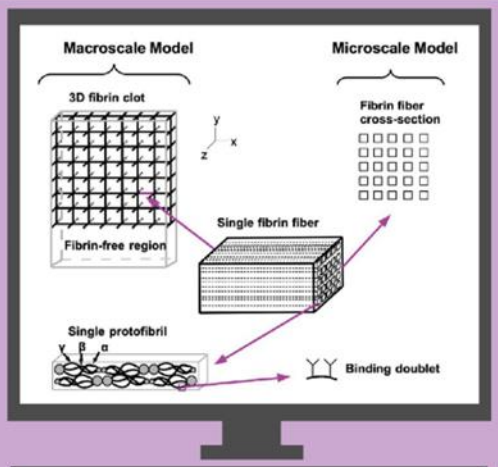

Modeling can vary parameters in a way that cannot be done experimentally.

Scanning electron microscopy (SEM)[111, 115]

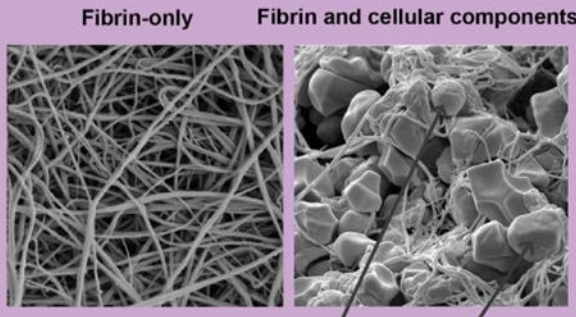

SEM clots are prepared through a number of dehydration steps. Lysis is initiated and immobilized before complete digestion.

Chandler loop[116]

A Chandler loop is an apparatus made of polymer tubes filled with circulating blood. This ex vivo model allows for testing of materials and lysis times with physiological blood flow.

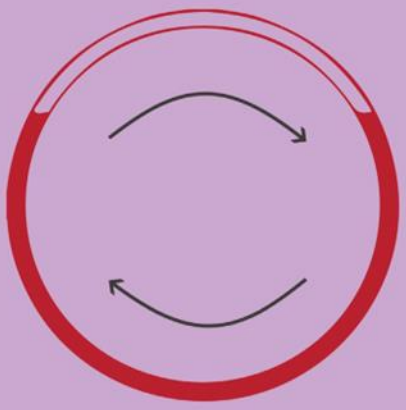

Viscoelastic mechanics[117-119]

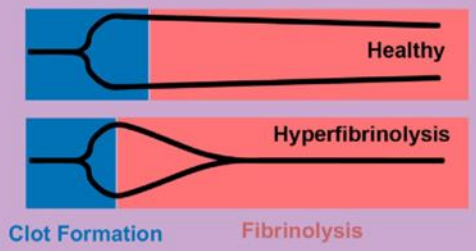

Thromboelastography (TEG) and rotational thrombolaseometry (ROTEM) are used clinically to assess global hemostasis which includes assessment of fibrinolysis. Learn more in RPTH's illustrated review on viscoelastical testing!

Immunoassays

Immunoassays are used experimentally and clinically. They can be used to measure concentrations of clotting or fibrinolytic factors or the enzyme activity. An enzyme-linked immunosorbent assay (ELISA) is a common technique that uses antigen/antibody cocktails to quantify amount of proteins (i.e., tPA), protein-complexes (i.e., PAI-1 and tPA), or active vs latent states.

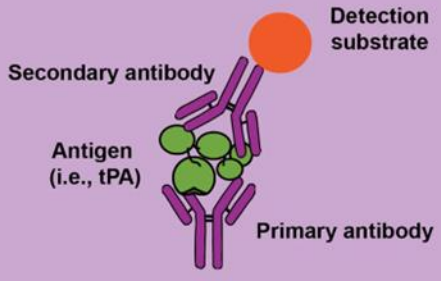

tPA: tissue plasminogen activator
uPA: urokinase plasminogen activator
PAI: plasminogen activator inhibitor

History of fibrinolytic development[120-126] [118-126]

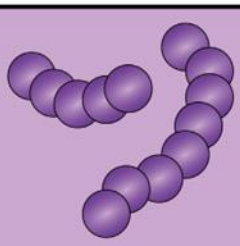

1933 — Tillet and Garner discover that streptococcus can dissolve a thrombus

1947 — First clinical use of streptokinase

1959 — Clot dissolution by plasmin *in vitro*

1960s — Tranexamic acid (TXA) identified as an antifibrinolytic. Learn more in RPTH's illustrated review on TXA!

mid - 1970s — CT scans available to visualize and locate clots

Right: Anthony P. Fletcher, Norma Alkjaersig, and Sol Sherry were key researchers in developing plasminogen activators for treatment of thromboembolic disorders

1984 — Zivin et al. discover the benefits of tPA in reducing neurological damage after embolism

1996 — The Food and Drug Administration (FDA) approves tPA for clinical use to treat acute ischemic stroke within a *three hour window*. See the right side about limitations of this discrete time window

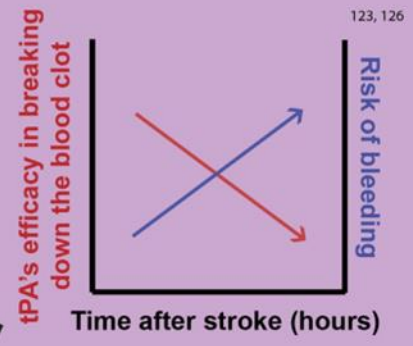

2000 — Genentech develops a generic tPA that has a higher specificity for fibrin

Is there a way to optimize tPA affinity for fibrin to improve efficacy?[106, 127, 128]

tPA: tissue plasminogen activator

See the following page for novel thrombolytics

New translational perspectives on fibrinolysis [127-133]

Recent advances in fibrinolytics have worked to improve delivery and efficacy. Check out RPTH's illustrated review that takes a closer look at two tPA thrombolytic agents used to treat ischemic stroke!

FDA approved thrombolytics/ fibrinolytics

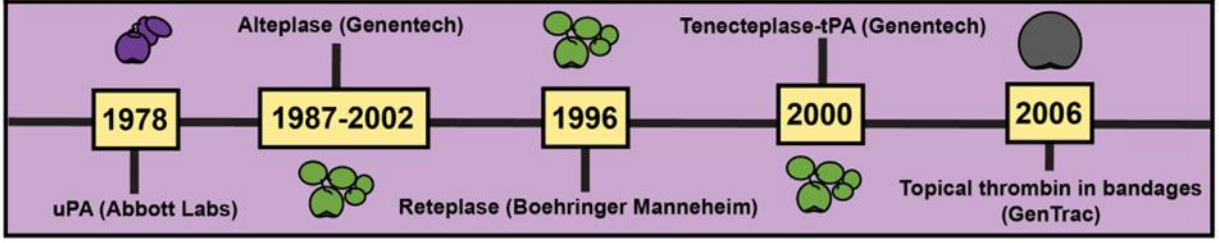

RBCs and nanoparticles as delivery agents for thrombolytics[129-132]

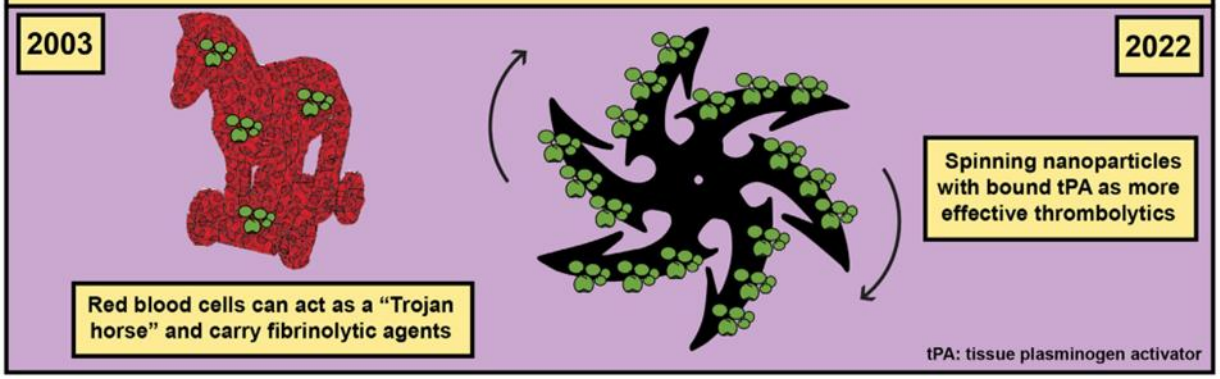

Novel thrombolytics[133]